ELSEVIER

Colloids and Surfaces
A: Physicochemical and Engineering Aspects 107 (1996) 1–56

COLLOIDS AND SURFACES A

Review

Colloid mobilization and transport in groundwater

Joseph N. Ryan [a,1], Menachem Elimelech [b,*]

[a] *Department of Civil, Environmental, and Architectural Engineering, University of Colorado, Campus Box 428, Boulder, CO 80309-0428, USA*

[b] *Department of Civil and Environmental Engineering, School of Engineering and Applied Science, University of California, Los Angeles, CA 90095-1593, USA*

Received 23 May 1995; accepted 31 July 1995

Abstract

Recent field and laboratory experiments have identified colloid-facilitated transport of contaminants as an important mechanism of contaminant migration through groundwater. For colloid-facilitated transport to be important, three criteria must be met: (1) colloids must be generated; (2) contaminants must associate with the colloids; and (3) colloids must be transported through the groundwater. Significant progress in the understanding of colloid generation (by mobilization of existing colloids) and transport (limited by deposition) in model colloid and collector systems has been made in the past few decades. This knowledge of the model systems, however, is inadequate for prediction of colloid behavior in natural groundwater systems. An understanding of colloid behavior in natural systems is essential for predicting the potential for colloid-facilitated transport in a given groundwater. This review presents theories describing colloid mobilization, deposition, and transport, laboratory experiments in model systems designed to test these theories, and applications of these theories to colloid mobilization and transport experiments in natural groundwater systems. Emphasis is placed on mobilization of existing colloids by chemical and physical perturbations, the kinetics and dynamics of colloid deposition (filtration) and the "blocking" effect, and the effect of surface chemical heterogeneities on colloid deposition and transport.

Keywords: Colloid deposition; Colloid filtration; Colloid mobilization; Colloid transport; Colloids; Contaminant transport; Facilitated transport; Groundwater; Particle deposition; Porous media

Table of contents

* Corresponding author. E-mail: elim@seas.ucla.edu

[1] E-mail: joeryan@spot.colorado.edu

SSDI 0927-7757(95)03384-X

1. Introduction

In recent years, the idea that colloids enhance the groundwater transport of low-solubility contaminants has gained widespread acceptance [1–3]. In notable field studies at hazardous waste sites, the unexpectedly rapid transport of cationic radionuclides (Pu, Am) and metals has been attributed to colloid-facilitated transport [4–8]. In addition, colloids have been implicated in the transport of U, Ra, and Th from natural uranium deposits [9–12]. Laboratory experiments testing colloid-facilitated transport have confirmed that colloids can accelerate the transport of cationic and anionic metals through porous and fractured media [13–16]. Some field studies showed that the inorganic colloids thought to be responsible for enhanced contaminant transport are composed of clay minerals, oxides, and carbonates in the 10 nm to a few micrometer size range. In most cases, these colloids appeared to have been generated in the aquifer by chemical and physical perturbations and to be potentially mobile.

Much attention has also been devoted to the role of "organic colloids", or natural and synthetic organic macromolecules, in enhancing contaminant transport. Field and laboratory studies have demonstrated that humic substances facilitate metal transport [17–22]. Laboratory studies have also demonstrated that humic substances and microbial exudates facilitate the transport of hydrophobic organic contaminants (HOCs) like polychlorinated biphenyls, pesticides, and polycyclic aromatic hydrocarbons [19, 23–31]; however, enhanced transport of HOCs in the field has not been observed. Although organic colloids also play an important role in enhanced transport, consideration of their transport behavior will be omitted from this review because the governing mechanisms for the transport of organic macromolecules are different than those for inorganic colloidal particles.

1.1. Colloid-facilitated transport

1.1.1. Predicting colloid-facilitated transport

When contaminants have appeared at distances far greater than those anticipated based on two-phase partitioning between solution and stationary sediment phases, colloid-facilitated transport has been invoked as a possible explanation. Greater migration distances are possible when the contami-

nants associate with a third phase, the mobile colloids. For example, Penrose et al. [6] detected colloid-associated Pu in a monitoring well downstream of a radioactive waste source in an alluvial deposit at Los Alamos National Laboratory. Based on simple two-phase partitioning, a tritium transport velocity of $v_{tritium} = 3.4$ km yr^{-1}, a bulk density to porosity ratio of $\rho_b/n = 8$, and a K_d value of 10^4 ml g^{-1} (measured for Pu interaction with the colloidal material), Pu is predicted to migrate at a velocity of only 4.2 cm yr^{-1} using the retardation formula in Fig. 1 [32]. The actual Pu transport velocity was measured at nearly 500 m yr^{-1}, nearly 1200 times greater than the predicted transport velocity. The enhanced Pu transport velocity may be attributed to local nonequilibrium or preferential flow paths, but the evidence collected by Penrose et al. [6] suggests that the Pu was transported with colloidal phases. A simple modification of the K_d approach to account for the presence of colloidal phases is designated as three-phase partitioning in Fig. 1. Interestingly, the addition of a mobile colloid phase into the retardation formula does not improve the prediction of Pu transport. Using 10 mg l^{-1} colloids and the same K_d value for Pu association with both the stationary and mobile sorbents, the predicted Pu transport velocity is only 4.7 cm yr^{-1}. Note that this simple model assumes that Pu adsorption to both the stationary sediments and the colloids is governed by the same K_d value while it is likely that the colloids will more effectively adsorb Pu owing to their high surface area.

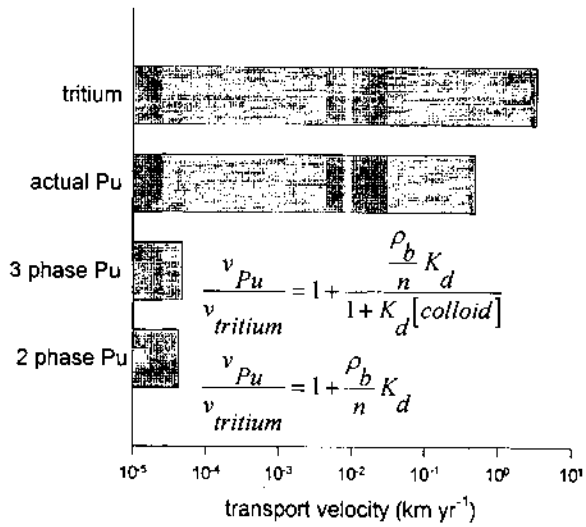

Fig. 1. The measured and estimated groundwater transport velocities for plutonium in the Mortendad Canyon alluvial aquifer at Los Alamos National Laboratory [6]. "Tritium" velocity represents conservative transport rate of tritiated water. "Actual Pu" velocity represents the measured transport rate of plutonium isotopes. "3 phase Pu" velocity represents the predicted plutonium transport rate in the presence of 10 mg l^{-1} colloids. "2 phase Pu" velocity represents the predicted plutonium transport rate in the absence of colloids. The same K_d value is used in the retardation expressions for adsorption of the plutonium to both the stationary aquifer sediments and the mobile colloids.

Even though this modification to the retardation formula assumes conservative transport of the colloids, the effect of colloids on Pu transport is predicted to be insignificant. According to classical colloid filtration theory, colloid transport in most aquifers will be limited to distances of meters to tens of meters under typical conditions [33–35]; therefore, assuming that colloid transport will be conservative is inadvisable. If colloid filtration is considered, the difference between the two-phase and three-phase Pu transport predictions will become even smaller. Gounaris et al. [36] used the three-phase retardation expression to account for the effect of colloids on contaminant transport in a landfill leachate plume. They obtained similar predictions — the presence of colloids at concentrations as high as a few hundred milligrams per liter would not significantly affect the transport of the contaminants. Based on this simple model of colloid-facilitated transport, how can the presence of colloids explain the unexpectedly large migration distances observed in the field studies?

This discrepancy between predicted and actual contaminant transport distances can be examined by evaluating the three criteria that must be met for inorganic colloids to facilitate the transport of contaminants: (1) colloids must be present; (2) contaminants must associate with the colloids; and (3) colloids and associated contaminants must be transported through the aquifer (Fig. 2). Only extremely low-solubility contaminants that sorb extensively to immobile aquifer solids will be affected by colloid-facilitated transport because only these contaminants can associate with colloids at significant levels owing to the generally low concentrations of colloidal phases in groundwater.

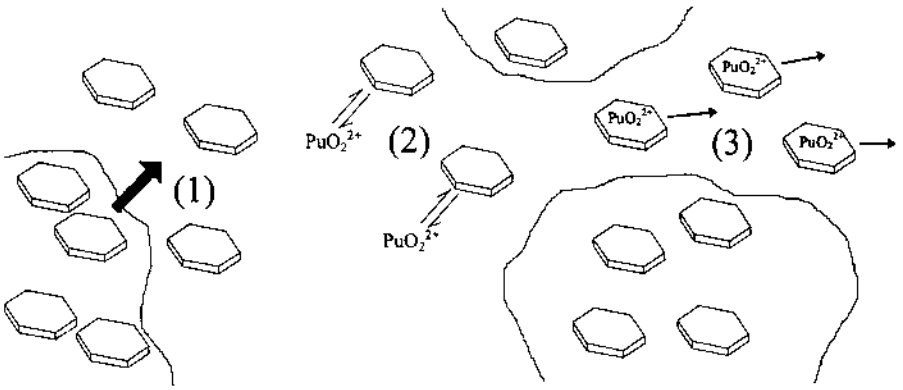

Fig. 2. The three criteria for colloid-facilitated transport: (1) colloids (shown as clay plates) must be generated; (2) contaminants (shown as PuO_2^{2+}) must associate with the colloids, and (3) the colloids must be transported through the porous media (shown as the large grains). Colloids are generated primarily by chemical and physical perturbations that mobilize existing colloids. Colloid transport is limited by deposition to (or filtration by) aquifer sediments.

1.1.2. Colloid generation

The first criterion that must be met for colloid-facilitated transport is that colloids must be present; however, field studies implicating colloids in contaminant transport rarely assess the source of the colloids. In addition, attempts to model the transport of colloids [37–42] have also ignored the generation of colloids in groundwater.

As McCarthy and Degueldre [43] concluded in their review of the nature and abundance of colloids in groundwater, "colloids appear to be ubiquitous" in groundwater. Colloids have been detected in groundwater samples taken from aquifers in a wide variety of geological and geochemical settings at concentrations as high as 100 mg l^{-1} [5,10,12,36,44–54]. McCarthy and Degueldre [43] also noted that colloid abundance was promoted by perturbations in the hydrogeochemistry of the aquifer system, particularly by waste disposal activities. Studies of colloid release in model systems clearly demonstrate that changes in solution chemistry that produce more repulsive interactions between attached colloids and collectors will mobilize colloids [55–57]; however, the effects of solution chemistry changes on colloid release can currently be predicted only qualitatively. Chemical perturbations that cause colloid mobilization commonly occur in contaminant plumes, thereby generating colloids in the midst of contaminants.

Perturbations in the aquifer hydraulics can also generate colloids. For example, rapid flow through fractures [48], rapid infiltration of rainfall [58,59], and increases in pumping rate during sampling [53,54,60] will produce higher colloid concentrations in groundwater as expected from theoretical and laboratory investigations of model systems [61–63].

1.1.3. Contaminant association with colloids

Current understanding of contaminant association with colloids allows accurate prediction of the extent of association, at least compared to current understanding and prediction of colloid mobilization and transport [64–66]. Most colloidal phases are effective sorbents of low-solubility contaminants because colloids, owing to their small size, have high surface area. Many of the inorganic colloids encountered in groundwater, like clays, metal oxides, and carbonates, are especially effective at adsorbing radionuclides and metals through ion exchange and surface complexation reactions. If the association of contaminants with colloids is not strong, the presence of mobile colloids will not guarantee that colloid-facilitated transport will occur. For example, the transport of pentachlorophenol [67] and simazine, a triazine pesticide [68], is not enhanced by the presence of organic colloids because these ionized compounds are not strongly sorbed by organic colloids. Colloid-associated contaminants may also be created by

homogeneous and heterogeneous precipitation of colloids containing contaminants. This scenario may be especially relevant in the near-field environment of nuclear waste repositories [69,70].

The strength of some of the contaminant–colloid associations is especially relevant for consideration of facilitated transport. As adsorbed contaminants are carried by colloids beyond the realm in which the dissolved and adsorbed contaminants are in equilibrium, the contaminant will desorb from the colloid to re-establish equilibrium between the dissolved and stationary sediment phases. As the strength of the contaminant–colloid association increases, the time to reach desorption equilibrium increases, resulting in increased distances for colloid-facilitated transport. For example, Vilks et al. [12] estimated that colloids emanating from the Cigar Lake uranium deposit in Canada have retained adsorbed U for as long as 8000 years based on radioisotope disequilibrium. The extremely slow desorption of contaminants from colloids is not accounted for in the three-phase retardation formula — the retardation formula assumes instantaneous, reversible equilibrium between the solution, colloid, and stationary sediment phases. Accounting for the irreversibility of contaminant association with colloids may explain the large discrepancy between predicted and actual Pu transport observed by Penrose et al. [6].

1.1.4. Colloid transport in groundwater

Transport of colloids over hundreds of meters to kilometers may be inferred from facilitated transport observations [5,6]. These studies, however, do not prove colloid transport — they only demonstrate that contaminants are associated with colloids at the monitoring locations. Given that the mobilization of colloids in concentrations sufficient to affect contaminant transport requires the kind of chemical perturbations occurring in a contaminant plume, it is unlikely that these colloid concentrations will be maintained beyond these plumes. Future studies of colloid-facilitated transport must include verification of colloid transport from waste source to monitoring points to prove that colloid-facilitated transport is responsible for enhanced contaminant migration.

Field observations and experiments have demonstrated that certain types of traceable colloids, such as bacteria, viruses, and polystyrene microspheres, are transported through aquifers at rates comparable to conservative solute tracers [71–77]. In both porous and fractured media, these traceable colloids typically suffer substantial attenuation over the short distances of these field tests (about 1–10 m). As Keswick et al. [78] noted in their review of the use of microorganisms as groundwater tracers, bacteria and virus transport over distances up to 1.6 km has been observed in fractured aquifers. Colloid transport is also commonly observed in the geologic record. The presence of clays recognized as "illuviated" provides evidence for colloidal transport through ancient soil layers [79–84].

Despite these instances of colloid transport, classical colloid filtration theory [85,86] predicts that colloid transport distances should be limited even for colloids that strenuously resist attachment to aquifer surfaces [33–35]. The release of radioactivity from the Chernobyl accident provided Von Gunten et al. [87] with an opportunity to demonstrate that meeting the first two criteria for colloid-facilitated transport, (1) the presence of colloids and (2) the association of the contaminant ^{137}Cs with the colloids, does not guarantee colloid-facilitated transport. Although Cs was predominantly associated with colloids in the River Glatt, it was not detected in the adjacent glacial outwash aquifer, suggesting that the colloids did not readily move from the River Glatt into the aquifer.

1.2. Scope of this review

This review will explore the current understanding of colloid generation and transport, two of the three criteria that must be met for colloid-facilitated transport of contaminants in groundwater. For colloid generation, this review will focus on the mobilization of existing colloids by chemical and physical perturbations. For colloid transport, this review will examine colloid deposition (filtration) theories, role of chemical heterogeneity in colloidal transport, and the dynamics of colloid deposition and transport. For both colloid mobilization and colloid transport and deposition in groundwater, field observations that have driven

investigations into these processes will be presented. These observations are, in some cases, accompanied by qualitative interpretations of the factors affecting colloid mobilization and transport. In most cases, however, the researchers have not attempted any quantitative analysis of these processes. Second, for both colloid mobilization and transport, the theories that define current understanding of these processes will be presented. Third, the laboratory studies (and, in some cases, field studies) that have attempted to rectify theory with observations of colloid mobilization and transport behavior will be assessed. Special emphasis will be placed on the ability of theoretical approaches to describe colloid mobilization and transport in natural systems.

2. Colloid mobilization: observations in the field

In this section, we will examine the major source of colloids in groundwater, mobilization of existing colloids, from the perspective of field observations. These field observations may be viewed as phenomena that drive investigation into the processes that govern colloid mobilization. Colloid mobilization is promoted by perturbations of the chemical and physical conditions of the aquifier system.

2.1. Sources of colloids in groundwater

Colloids in groundwater originate from two sources: (1) mobilization of existing colloid-sized minerals in the aquifer sediments and (2) *in situ* precipitation of supersaturated mineral phases. The majority of the colloids catalogued in McCarthy and Degueldre's [43] review may be attributed to mobilization of existing colloids by some perturbation of the ambient groundwater conditions. Groundwater chemical perturbations may also conspire to generate colloidal mineral phases by precipitation [44,46,88]. However, the formation of colloids by *in situ* precipitation appears to be relatively uncommon with the possible exception of the near-field environment in high-level radioactive waste repositories [69,70].

The majority of the colloids found in groundwater appear to be derived from existing mineral phases in the aquifer sediments. Existing minerals in the colloid size range can be mobilized by perturbations of groundwater chemical and physical conditions. Perturbations to groundwater chemical conditions, like a decrease in ionic strength accompanying the injection of recharge water to deep aquifers, mobilize existing colloids by increasing the repulsive electrostatic forces between colloids. Perturbations to groundwater physical conditions, like an increase in the groundwater velocity caused by pumping, mobilize existing colloids through additional hydrodynamic shear.

2.2. Colloid mobilization by chemical perturbations

Most of the colloids we find in groundwater appear to have been mobilized by changes in the solution chemistry of the groundwater [43]. These changes include decreasing ionic strength, increasing pH, or adsorption of ions and macromolecules that alter mineral surface charge. In some formations, colloid mobilization leads to hydraulic conductivity reductions and plugging as the mobilized colloids apparently deposit in narrow pore throats. Aquifers and geologic formations susceptible to such reductions in hydraulic conductivity are termed "water sensitive" [89–91].

2.2.1. Colloid mobilization by ionic strength changes

The most common change in groundwater chemistry is a decrease in ionic strength caused by infiltration of dilute precipitation water, irrigation by fresh water, or injection of fresh water for artificial recharge or secondary oil extraction. Many examples of colloid mobilization and formation plugging caused by infiltration of dilute waters can be found in the soil science literature [92–95]. Most of these experiments demonstrate that dilute solutions composed of monovalent ions are most effective at mobilizing colloids and reducing hydraulic conductivity in saturated soils and in flow-through columns. In contrast, these experiments showed that solutions of higher ionic strength and solutions containing bivalent ions do not mobilize colloids.

At a groundwater artificial recharge site called

Leaky Acres in California, Nightingale and Bianchi [96] documented a case of colloid mobilization during the infiltration of water of less than 50 μmho cm^{-1} specific conductance into aquifers containing water of about 150 μmho cm^{-1} conductance. When the specific conductance of the aquifer was reduced to about 100 μmho cm^{-1} (or about 1–2 mM ionic strength, depending on the dominant ions [97]), the turbidity of the groundwater started to rise, reaching values as high as nearly 50 NTU. Later, adjustment of the conductance of the infiltrating water to greater than 120 μmho cm^{-1} prevented mobilization of colloids. The mobilized colloids, which reached concentrations as high as 30 mg l^{-1}, did not lower recharge rates by plugging pores. In a similar effort in the coastal plains of Virginia, Brown and Silvey [98] observed that the injection of fresh water into a brackish aquifer resulted in decreases in hydraulic conductivity. Pretreatment of the aquifer with a 0.2 N $CaCl_2$ solution prior to introduction of the fresh water stabilized the hydraulic conductivity of the aquifer by lessening the repulsive electrostatic interactions between colloids.

Using column experiments to simulate the interface between fresh water and sea water in coastal aquifers, Goldenberg and colleagues [99–101] showed that the displacement of sea water by fresh water caused decreases in hydraulic conductivity of one to four orders of magnitude. The presence of montmorillonite, an expandable clay, produced much greater reductions in hydraulic conductivity than the presence of illite or kaolinite, leading Goldenberg and colleagues to assume that the permeability reduction was caused by clay swelling and gel formation. If clay swelling caused the clogging, the permeability reduction would be reversible by addition of salt solution. Instead, the clogging was largely irreversible upon re-introduction of the salt solution [101]. Clogging by clay dispersion, where mobilized particles are deposited in narrow pore throats, is irreversible without a change in flow direction [102]. Montmorillonite may have caused greater permeability reduction because its pH_{pzc} value is slightly lower than those of illite and kaolinite [103]. With the lower pH_{pzc} value, the montmorillonite may have been mobilized to a greater extent than illite and kaolinite owing to greater intersurface repulsion between the attached colloids. In a notable implication of this clogging effect, Goldenberg and colleagues speculated that attempts to repel the advance of the salt water by injecting fresh water may create an impermeable barrier that defeats the purpose of the fresh water injection.

The practice of secondary oil recovery is replete with examples of colloid mobilization because fresh water is often used to displace residual oil deposits in oil-bearing formations [89,90,104]. Typically, oil-bearing formation waters are quite saline to briny; therefore, introducing fresh water drastically lowers the ionic strength and increases interparticle repulsion.

2.2.2. Colloid mobilization by other chemical perturbations

Increases in the pH of infiltrating water (from pH 6–9) also decreased the hydraulic conductivity of soils through clay dispersion [105]. Muecke [89] noted that the practice of introducing surfactants to enhance oil recovery also increases colloid mobilization and formation plugging. Surfactant flushing for remediation of contaminated aquifers may cause colloid mobilization and permeability reductions that limit the effectiveness of this enhanced remediation technique [106,107]. Allred and Brown [107] measured permeability reductions of two orders of magnitude in a loamy soil subjected to injections of surfactants at concentrations typically used in remediation.

The infiltration of organic matter-rich groundwater from a swampy, intermittent stream caused colloid mobilization in a quartz sand coated mainly by goethite and kaolinite in the New Jersey Pine Barrens [49]. A detailed study of the sediments' elemental and mineralogical composition revealed that the infiltrating organic matter caused reducing conditions that led to the dissolution of the goethite [108]. Because clay concentrations in the sediments were lower where the goethite content was lowered by dissolution, it was hypothesized that the clay colloids observed in the groundwater had been mobilized by "decementation" of the coatings — the removal of the positively-charged goethite led to repulsive interactions between the negatively-charged kaolinite colloids and quartz

grains. Further study of the sediments in flow-through columns suggested that goethite dissolution was not necessary for colloid mobilization. A surfactant, dodecanoic acid, was capable of mobilizing the colloids without dissolving goethite and the infiltrating groundwater mobilized the kaolinite colloids more rapidly than it dissolved goethite [109]. These results suggest that the surfactant and the natural organic matter mobilized the kaolinite colloids by adsorbing to the goethite and reversing the surface charge.

2.3. Colloid mobilization by physical perturbations

In groundwater, the most common physical perturbation is an increase in the flow velocity by pumping. Usually, colloid mobilization by groundwater removal is a concern, particularly in obtaining groundwater samples that accurately represent the groundwater in the aquifer. Injection of groundwater, however, may also accelerate groundwater flow near wells. In the artificial recharge and secondary oil recovery examples noted above, colloid mobilization was attributed to chemical perturbations, but it is possible that the rapid injection of water produced hydrodynamic shear that mobilized colloids near the wells. This effect may be a concern in many small-scale field tests of colloid and biocolloid transport — the rapid addition of the injectate for the test may mobilize naturally immobile colloids or colloids injected and attached in previous tests.

2.3.1. Colloid mobilization during groundwater sampling

The effect of pumping is a major concern in the collection of representative groundwater samples. Above natural groundwater velocities, colloids are likely to be mobilized by hydrodynamic shear. Backhus et al. [110] first recommended that pumping rates be kept low (about 100 ml min^{-1}) to avoid mobilization of "artifactual" colloids. By comparing calculated shear rates based on estimates of groundwater velocity near sampling well intakes to shear rates known to be capable of mobilizing colloids from surfaces and disaggregating colloids, a maximum pumping rate of 100 ml min^{-1} was suggested by Ryan [111] for a sandy aquifer with a porosity of 0.4 and hydraulic conductivity of about 4×10^{-4} m s^{-1}. At a distance of 2.5 cm from a typical 5 cm-diameter monitoring well, pumping rates of 1 and 4 l min^{-1} produced shear rates that exceeded the shear rates necessary to mobilize spherical colloids and cells from flat surfaces, about 1 to 25 s^{-1} [61,112,113], while pumping at 100 ml min^{-1} did not. The distance of 2.5 cm from the well screen was chosen as the radial extent of the zone already disturbed by drilling. Recently, the United States Environmental Protection Agency (EPA) [114] suggested that the maximum pumping rate for groundwater sampling of colloids and colloid-associated contaminants be the maximum rate at which drawdown does not occur in the formation; therefore, higher pumping rates would be allowable in more porous or more permeable aquifers.

Field results from groundwater sampling in porous media suggest that high pumping rates mobilize "artifactual" colloids (colloids that would not be mobile at natural groundwater flow rates), but the effect has not been conclusively proven. Puls et al. [53] showed that increases in pumping rate from about 0.6 to 92 l min^{-1} increased the size of the colloids collected in groundwater samples at a metal-contaminated site in Globe, AZ. The highest pumping rate, achieved using a high capacity submersible turbine pump, produced colloids as large as 2.5 μm in diameter, while the lower pumping rates, achieved using a bladder pump and a low-capacity turbine pump, produced colloids of less than 1.5 μm in diameter. Interestingly, the colloid concentration decreased to approximately the same level after sufficient purging, about 2.5 mg l^{-1} (calibrated to the light scattered by kaolinite suspension standards). The colloid sizes in the samples were determined by dynamic light scattering (photon correlation spectroscopy), a particle-sizing technique that is useful for (1) submicrometer particles [115,116] and (2) "simple" particle size distributions (e.g. monomodal or bimodal). The larger colloids present in natural waters and the polydispersity of natural colloid size distributions stretch the limitations of dynamic light scattering; therefore, data reported using this technique for particle size distributions in natural waters must be viewed with caution.

Backhus et al. [54] presented data from two Atlantic Coastal Plain sites at which an increase in the pumping rate from about 100 ml min^{-1} to 1 l min^{-1} caused a temporary increase in the groundwater colloid concentration above the plateau achieved at 100 ml min^{-1}; however, pumping was not continued to determine the stable colloid concentration at the elevated rate. At a coal tar-contaminated site in New York, a similar increase in pumping rate was continued until the colloid concentration stabilized at the higher flow rate. The increase in pumping rate caused an increase in the stable colloid light scattering count rate of about 40 to 230 counts s^{-1}, equivalent to colloid concentrations of zero and 0.1 mg l^{-1} (based on kaolinite suspension standards). The removal of an equal number of well volumes by bailing, a technique that suddenly withdraws about 1 l of water from the wells each time the bailer is lowered into the well, produced light scattering count rates as high as 20000 counts s^{-1} (or about 10 mg l^{-1} of kaolinite colloids). Using a video camera lowered into the well (the "colloidal borescope"), Kearl et al. [60] confirmed directly that an increase in flow rate from 100 to 1450 ml min^{-1} caused increases in particle mass concentration, although they did not continue pumping to reach stable colloid concentrations. They noted that the increase in particle mass concentration was caused mainly by an increase in particle size, not particle number, similar to the observation made by Puls et al. [53].

2.3.2. Colloid mobilization by rapid infiltration

The rapid infiltration of water through soils also causes colloid mobilization by shear. Field observations, however, have not produced clear relationships between rainfall rate and the extent of colloid mobilization. Kaplan et al. [58] observed an apparent correlation between the flow rate of water through $3 \times 3 \times 1.5$ m^3 soil lysimeters and the colloid concentration produced; however, both flow rate and colloid concentration were also dependent on the elapsed time of the rainfall simulation. It is possible that most of the colloids were mobilized early in the test when flow rates were high, leaving no colloids to be mobilized later in the test when flow rates were low. Increases in flow rate also appeared to produce increases in the mean colloid size in the soil lysimeter effluent.

2.3.3. Colloid mobilization by fracture flow

Groundwater flow in fractured media may also produce velocities capable of causing colloid mobilization. The weathering of primary minerals in fractures produces colloid-sized secondary minerals (particularly clay minerals) that may be mobilized by the relatively high velocity flows occurring in fractures. Degueldre et al. [48] showed that fractures in granite at Switzerland's Grimsel Test Site produce steady quantities of colloids at concentrations of about 10^{10} l^{-1} in the 40 to 1000 nm size range, or about 0.2 mg l^{-1}. The elemental compositions of various colloids were dominated by Si, Ca, Mg, Sr, Ba, Fe, S, and probably Al, which was difficult to analyze. Colloids dominated by organic carbon were also detected.

A plot of $\log(dN/dd_p)$ vs. $\log d_p$ for the primary particle size distribution for one of the Grimsel samples gave a slope of about -3 to -3.5 [48,117], where N is the particle number concentration in a given size range and d_p is the particle diameter. For log–log plots of dN/dd_p vs. d_p, the slope is equal to $-(\beta^*+1)$ where β^* is defined by $N = kd_p^{-\beta^*}$ [118–120]; therefore, $\beta^* \approx 2$ to 2.5 for the Grimsel colloids. A value of $\beta^* = 3$ signifies equal particle volumes in logarithmically increasing size ranges. Values of $\beta^* > 3$ indicate that smaller particles dominate the volume distribution, while values of $\beta^* < 3$ indicate that the size distribution is enriched with particles of larger sizes. For many natural systems, the observed magnitude of β^* seems to be related to the vigor of mixing in the fluid medium; for the upper atmosphere, $\beta^* \approx 4$; for the ocean, $\beta^* \approx 2.7$ to 3.5 [121]. Theoretical values of β^* calculated using expressions for the kinetics of coagulation by Brownian motion, shear, and differential settling result in values of 1.5, 3.0, and 3.5 [121,122]. The β^* value of the Grimsel colloids may suggest that colloid mobilization by hydrodynamic shear boosts the abundance of larger particles. Size distribution measurements of colloids collected from soils containing macropores during rainfall simulations revealed β^* values of 0.9 to 1.3, suggesting that increases in the velocity of the water moving through the fracture or macro-

pore may increase the abundance in larger particle sizes, reflected in lower values of β^* [59].

3. Colloid mobilization: theory

In the following sections, theories describing colloid mobilization by chemical and physical perturbations will be presented to provide a framework for the analysis of processes affecting colloid mobilization. The emphasis in this section will be placed on the intersurface and hydrodynamic forces that promote colloid detachment from collector surfaces.

3.1. Theory of colloid mobilization by chemical perturbation

The mobilization of colloids by a change in solution chemistry depends on the alteration of the forces between the surfaces of colloids and the aquifer grains to which they are attached. These intersurface forces include double layer repulsion or attraction, London–van der Waals attraction, and poorly characterized short-range "non–DLVO" forces such as hydration and steric repulsion. The net effect of these attractive and repulsive forces on the interactions between surfaces is described by the DLVO theory [123,124]. For colloids to be mobilized, the change in solution chemistry must produce repulsive forces between attached colloids and grains that exceed the attractive forces. According to the energy barrier approach [125], the rate of colloid mobilization depends on the height of the barrier in DLVO potential energy that attached colloids must exceed.

3.1.1. Colloidal interactions and DLVO theory

The DLVO theory describes the attractive and repulsive forces between colloid and grain surfaces in profiles of the intersurface potential energy. The potential energy profile is constructed by summing the double layer, London–van der Waals, and short-range repulsive potential energies over the separation distance between the colloids and grains (Fig. 3). Changes in solution chemistry promote colloid mobilization mainly by altering the double

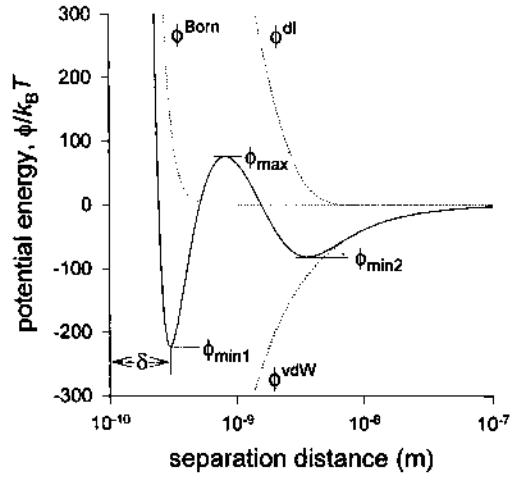

Fig. 3. DLVO potential energy as a function of separation distance between a colloid and collector. The total potential energy, ϕ^{tot} (solid curve), is the sum of (1) the double layer potential energy, ϕ^{dl}, shown here for repulsion between particles of similar charge, (2) the van der Waals potential energy, ϕ^{vdW}, and (3) the Born potential energy, ϕ^{Born}, the short-range repulsion energy. This typical total potential energy curve is characterized by a deep attractive well at a very small separation distance, the primary minimum (ϕ_{min1}), a repulsive energy barrier, the primary maximum (ϕ_{max}), and a shallow attractive well at a larger separation distance (ϕ_{min2}). The potential energy is normalized by k_BT.

layer potential energy. The attractive van der Waals forces are independent of changes in solution chemistry. Short-range (up to a few nanometers separation distance) repulsion forces may also be affected by changes in solution chemistry, but these forces are not yet understood well enough to assess their effects [126].

The double layer potential energy arises from the overlap of diffuse clouds of ions (double layers) that accumulate near charged surfaces to balance the surface charge. If the interacting surfaces are like-charged, the double layer potential energy will be repulsive. If the surfaces are oppositely charged, the double layer potential energy will be attractive. All formulations of the double layer potential energy are sensitive to variations in (1) the surface potentials of the colloid and collector, (2) the ionic strength of the solution, and (3) colloid size. While the dependence of the double layer potential energy on surface potentials and ionic strength has been demonstrated in coagulation and deposition

studies, the dependence on colloid size has not been verified [35,127–129].

The charge on colloid surfaces gives rise to surface potentials and diffuse double layers that extend out into the bulk solution [126,130]. Most minerals possess amphoteric surface charge. The surface charge is strongly dependent on solution pH because the minerals' surface functional groups exchange protons with the solution. In general, amphoteric minerals are positively charged at lower pH values and negatively charged at higher pH values. At some intermediate pH, the surface charge of amphoteric minerals is zero (the point of zero charge, pH_{pzc}, or the isoelectric point, pH_{iep}). For natural amphoteric oxide minerals, pH_{pzc} values range from about 2 for quartz to 9 for iron and aluminum oxyhydroxides [103,131]. Some minerals, like clay minerals, have "permanent" surface charge from isomorphic substitution on their faces and amphoteric surface charge on their edges [64,132]. The repulsive force between colloids and grains can be increased by increasing the surface charge, and hence the surface potentials, between like-charged surfaces. In addition, attractive double layer potentials between oppositely charged surfaces can be made repulsive if a change in solution chemistry reverses the surface charge of one of the surfaces.

Surface potentials cannot be measured directly, but they can be calculated using various models of the oxide–water interface [133,134] or approximated by zeta potentials derived from measurements of electrophoretic mobility or streaming potential [130]. Zeta potentials are frequently substituted for surface potentials in calculations of double layer potential energy. Because zeta potentials refer to the potential at some distance from the surface (known as the shear plane), the use of zeta potentials in double layer expressions should be accompanied by a minimum separation distance, x_0, between the colloid and collector, equal to twice the distance to the shear plane [35]. Experimental results report shear plane distances of 10–49 Å [135,136], but these values have been characterized as bearing little resemblance to reality [130,137].

Direct surface force measurements indicate that only the first few water layers are held immobile at mica surfaces [138,139], providing a better accepted estimate of the shear plane distance (about 5–6 Å). Advocates of the triple layer model of the oxide-water interface assume that measured zeta potentials are equal to the potential at the distance of the Stern plane, the origin of the diffuse layer [140–143]. Locating the shear plane at the thickness of the layer of specifically adsorbed ions in the Stern plane corresponds well to the shear plane location at the first few layers of adsorbed water. Proponents of the Gouy–Chapman double layer model propose that the shear plane distance is variable [134]. While no physical significance was assigned to this proposal, it is conceivable that the shear plane distance varies with solution chemistry. The viscosity of vicinal water is greater than that of bulk water [144,145], probably due to the orientation imposed in vicinal water by proximity to the charged surface. It is possible that changes in solution chemistry that alter the double layer potential may alter the shear plane distance by influencing the viscosity of the vicinal water. The adsorption of macromolecules and polymers also affects zeta potential measurements by displacing the shear plane away from the colloid surface [130,146].

The ionic strength of the solution controls the extent to which double layers extend from the surface into the bulk solution [130]. At high ionic strength, the surface charge can be balanced by a small ("thin") double layer because the ion concentration near the surface is high; conversely, low ionic strength will produce large ("thick") double layers. At high ionic strength, the double layers of approaching surfaces will overlap only at small separation distances and the double layer repulsion between the surfaces is reduced. At low ionic strength, the double layer repulsion is increased. The ionic strength effect plays an important role in coagulation of colloidal suspensions — high ionic strength enhances coagulation because the attractive van der Waals forces will dominate the potential energy profile when the repulsive double layers are compressed.

The attractive London–van der Waals interactions are long-range forces caused by instantaneous dipole-dipole interactions between surfaces [126,130]. The magnitude of the attraction

depends on the density and polarizability of the interacting surfaces and the medium, factors taken into account in the complex Hamaker constant. The effect of changes in the solution chemistry of water, the medium across which the dipole interactions are felt, are not considered in the Hamaker constant. At some separation distance, the magnitude of the van der Waals attraction will exceed the magnitude of the double layer repulsion because the van der Waals attraction decays with distance as x^{-1} and the double layer repulsion decays exponentially with distance. The excess van der Waals attraction results in the formation of a secondary minimum in the potential energy profile (Fig. 3). The depth of the secondary minimum increases with increasing ionic strength as the double layer repulsion at the corresponding separation distance decreases.

The short-range repulsive forces that are often attributed to some form of hydration or steric repulsion are not well understood currently [126,147–149]. Despite the lack of understanding, these forces most likely play an important role in colloid mobilization because they define a primary minimum of finite depth [125,150]. Without these short-range repulsive forces, the probability of colloid escape from the infinitely deep primary minimum would be zero. Surface force measurements between the surfaces of minerals like mica, clays, and silica have demonstrated the existence of very strong short-range repulsion at separation distances less than a few nanometers. At very small separation distances, less than a nanometer, the energy required to remove water of hydration appears to contribute to the large repulsion [35,138,151,152]. These experiments showed that higher solution concentrations of monovalent salts produced greater short-range repulsion owing to an increase in the concentration in hydrated ions between the surfaces. In addition, the presence of more strongly hydrated bivalent and trivalent ions augments the short-range repulsion [153,154]. In some cases, oscillations in the intersurface force within about 5 nm separation distance suggest that sequential removal of layers of water must occur to bring surfaces closer together [139,155]. At larger separation distances, anomalously high repulsive forces have been attributed to steric repulsion between adsorbed macromolecules [156–159]; in the case of silica, dendritic silica chains [160] that extend out to distances of 1–2 nm. Beyond this near-surface region, direct measurements of surface force by a variety of techniques agree well with the intersurface force predicted by double layer and van der Waals interactions [138,152,161–164].

The effect of short-range repulsion has been included in DLVO profiles in two ways: (1) designation of a minimum separation distance [165–168] corresponding to the shear plane distance and the thickness of the layers of water of hydration between surfaces; and (2) calculation of the Born potential energy [125,150]. Both means of representing short-range repulsion are derived from the modeling of interatomic potentials [169]. The minimum separation distance is analogous to a "hard" potential where the potential energy is infinitely repulsive at the colloid surface and zero beyond that. The Born potential is a "soft" potential derived from the same interatomic potential model used to generate the van der Waals potential, the Lennard-Jones 6–12 potential [126,170]. The application of either of these short-range potentials is highly speculative [126,169] given the complexity of the near-surface interactions. Inability to accurately estimate the short-range interactions precludes accurate estimation of the depth of the primary minimum. Therefore, continued advances in the direct measurement of surface forces is crucial to advances in understanding the mechanisms controlling colloid detachment.

3.1.2. Energy barrier approach to colloid detachment

In classical colloid filtration theory, colloid deposition on collector surfaces is modeled as an irreversible process [85,86]. Analyses predict that the rate of colloid deposition under unfavorable chemical conditions depends primarily on the magnitude of the DLVO energy barrier opposing deposition, the primary maximum [171–173] (Fig. 3). The assumption that colloid deposition is irreversible stems from the infinitely deep primary minimum produced by calculating the intersurface potential energy with only the double layer and van der Waals potential energies. The attractive

van der Waals potential energy dominates the DLVO profile at very small separation distances. An infinitely deep primary minimum implies that the probability of colloid transport back over the primary maximum is zero.

As Hamaker [174], Verwey and Overbeek [124], and Frens and Overbeek [165] noticed for reversibility of colloid coagulation, Ruckenstein and Prieve [125] recognized that a primary minimum of finite depth would be necessary to allow colloid detachment from the primary minimum. To achieve a primary minimum of finite depth, Ruckenstein and Prieve added Born repulsion to the DLVO potential energy profile. With the primary minimum of finite depth, the DLVO profile provides an estimate of the energy barrier to detachment of colloids (Fig. 4). In the near-surface region where the transport of colloids is dominated by diffusion, colloids approaching the collector grain must possess sufficient thermal energy to overcome the energy barrier to deposition, ϕ_{max}, to attach in the primary minimum. Likewise, colloids attached in the primary minimum must possess sufficient energy to overcome the energy barrier to detachment, $(\phi_{max} - \phi_{min1})$. At equilibrium, the colloids are expected to form a Boltzmann distribution on either side of the energy barrier depending on the relative potential energy of the primary minimum and the bulk solution (where $\phi^{tot} = 0$). Through an analysis of the particle flux through the interaction boundary layer (δ_ϕ), Ruckenstein and Prieve showed that the rate coefficients of attachment (k_{att}) and detachment (k_{det}) should decrease exponentially as the height of the corresponding energy barriers increases:

$$k_{att} \propto \exp\left(-\frac{|\phi_{max}|}{k_B T}\right) \tag{3.1}$$

$$k_{det} \propto \exp\left(-\frac{|\phi_{max} - \phi_{min1}|}{k_B T}\right) \tag{3.2}$$

where k_B is Boltzmann's constant and T is the absolute temperature. These rate coefficients have an Arrhenius form, with the energy barriers serving as the activation energies for attachment and detachment, giving the expression for colloid transport across the energy barrier the same form as a first-order, reversible, heterogeneous reaction [125,165].

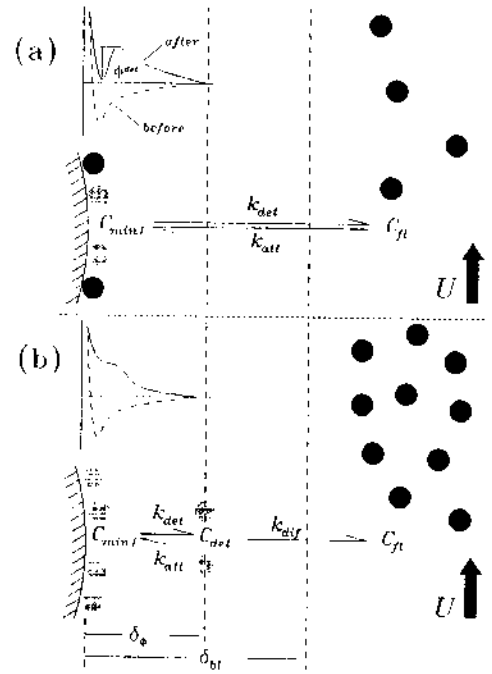

Fig. 4. The kinetics of colloid release from collector surfaces. (a) Following the Ruckenstein and Prieve [125] model, colloid deposition and release are controlled by diffusional transport over energy barriers (Eqs. (3.1) and (3.2)). The height of the detachment energy barrier is represented by ϕ^{det}. The DLVO curves pertaining to the solution chemistry conditions "before" and "after" a perturbation in solution chemistry conditions that caused colloid release are shown above. The first-order mass transfer showing the exchange of particles attached in the primary minimum, C_{min1}, with particles in the bulk fluid, C_f, is shown below. (b) If the solution chemistry perturbation produces a DLVO curve without an energy barrier to detachment, colloid detachment from the surface is fast and colloid diffusion to the bulk fluid is the rate-limiting step. The mass transfer is now a two-step process where the second step, the diffusion of detached particles, C_{det}, across the diffusion boundary layer of thickness δ_{bl}, to the bulk fluid, is the rate-limiting step.

The analysis by Ruckenstein and Prieve [125] assumed that the colloids were affected only by intersurface forces. Dahneke [175] provided an analysis that includes inertial forces on the colloids (relevant for larger particles and high velocity fluid flows) by solving the more general Fokker–Plank equation of convective diffusion in a force field [176]. Dahneke's result displays the same expo-

nential dependence of the detachment rate coefficient on the height of the energy barrier. Note that both of these analyses assume that the energy barrier to detachment is present, i.e. a quasi-stationary distribution of colloids exists in the attached and detached state. This assumption limits the application of these expressions to case (a) in Fig. 4, where the detachment energy barrier is still present.

3.1.3. Diffusion-controlled colloid release

When perturbations in solution chemistry produce DLVO potential energy profiles without energy barriers to detachment (case (b) in Fig. 4), colloid release should no longer be limited by diffusion over the energy barrier and the models of Ruckenstein and Prieve [125] and Dahneke [175] are inapplicable. Without an energy barrier, the rate of colloid release will be controlled by diffusion across the diffusion boundary layer. The diffusion boundary layer is defined as the near-surface region in which colloid transport is dominated by diffusion (δ_{bl} in Fig. 4). The rate of colloid transport across the boundary layer is controlled by the colloid diffusion coefficient, the colloid concentration gradient, and the thickness of the boundary layer, which is controlled primarily by the velocity of the advecting fluid. The thickness of the boundary layer around a single spherical collector in laminar flow may be estimated by [172,177]:

$$\delta_{bl} \approx a_c \left(\frac{D_\infty}{V a_c}\right)^{1/3} \tag{3.3}$$

where a_c is the radius of the spherical collector, D_∞ is the bulk particle diffusion coefficient, and V is the pore velocity of the bulk fluid. Given that the distance traveled by a diffusing particle can be estimated as $(2D_\infty t_{dif})^{1/2}$ [178], where t_{dif} is the characteristic time of diffusion, the rate coefficient for colloid diffusion across the boundary layer, k_{dif} (Fig. 4), can be estimated by inserting δ_{bl} as the diffusion distance and solving for the reciprocal of time [179]:

$$k_{dif} = t_{dif}^{-1} = \frac{2D_\infty}{\delta_{bl}^2} \tag{3.4}$$

Beyond the diffusion boundary layer, colloid transport is controlled by advection of the bulk fluid.

3.2. Theory of colloid mobilization by physical perturbation

Theories describing colloid mobilization by physical perturbations are based on a balance of torques on a particle adhered to a flat surface in a moving fluid where detachment is initiated by rolling [61,180]. The torque balance on the attached particle includes (1) an adhesive force operating normal to the surface, (2) a drag force operating tangential to the surface, and (3) a lift force operating normal to the surface (Fig. 5a). The adhesive force binds the particle to the surface and the lift and drag forces attempt to mobilize the particle.

The adhesive force, F_A, can be calculated as the sum of the van der Waals and double layer forces acting on the particle [61,62,181]; thus, the mobilization of colloids by physical perturbations, like an increase in the groundwater flow rate, does not depend solely on physical parameters. Variations in solution chemistry will affect the mobilization of colloids by hydrodynamic shear.

The drag force F_D operating on a spherical particle of radius a_p in contact with a plane wall in a slow, linear shear flow has been calculated by Goldman et al. [182] and O'Neill [183]:

$$F_D = (1.7009)(6\pi\mu a_p U_x) \tag{3.5}$$

where μ is the fluid viscosity and U_x is the fluid velocity at the center of the attached particle (i.e. at a distance a_p from the wall). The fluid velocity U_x is given by [62]

$$U_x = 6\frac{Q_f a_p}{Al}\left(1 - \frac{a_p}{l}\right) \tag{3.6}$$

where Q_f is the flow rate, A is the cross-sectional area, and l is the thickness of the flow area (normal to the plane wall). To adapt these flow parameters to porous media, Q_f/A could be approximated as the pore velocity and l as the pore diameter. By combining Eqs. (3.5) and (3.6), it is clear that the drag force depends primarily on the radius of the attached particles. Large particles will be subjected

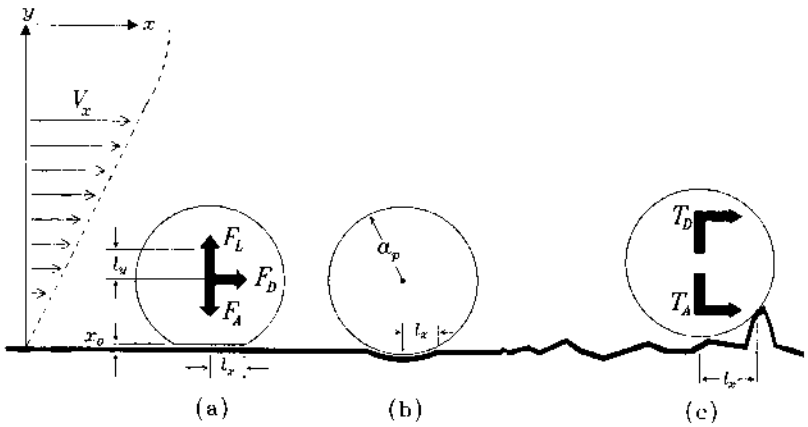

Fig. 5. The torque balance on spherical particles attached to collector surfaces. Hydrodynamic shear is the result of the Poiseuille velocity profile producing the height-dependent velocity, V_x. The drag torque, T_D, is caused by the drag force, F_D, operating on the lever arm l_y. The adhesive torque, T_A, is caused by the adhesive force, F_A, operating on the lever arm l_x. Different models of particle attachment to the collector surface determine the appropriate lever arm l_x: (a) a deformable particle (separated from the surface by the minimum separation distance, x_0); (b) a deformable surface; and (c) a rough surface. In most cases, the lift force, F_L, is negligible compared to the adhesive force.

to much greater drag force than smaller particles and, hence, large particles will be mobilized before small particles as velocity increases (Fig. 5).

The lift force on a spherical particle can be calculated using [184]:

$$F_L = \frac{81.2 a_p^2 \mu \omega^{0.5} U_x}{\nu^{0.5}} \tag{3.7}$$

where ω is the velocity gradient at the plane wall and ν is the kinematic viscosity of the fluid. The lift force for Brownian particles is negligible compared to the opposing adhesive force [180] and is often omitted from the torque balance [62,63].

The torque due to drag on the attached particle, T_D, has been presented as [182,183]:

$$T_D = l_y F_D = 1.399 a_p F_D \tag{3.8}$$

Owing to the increase in velocity with distance from the plane wall, the drag force effectively acts on the attached particle at a height of $1.399 \times a_p$; thus, the drag force creates torque by acting on a lever arm of $l_y = 0.399 a_p$ (Fig. 5a). For detachment, the hydrodynamic torque must exceed the adhesive torque, which is represented as the net attractive force acting on a lever arm of l_x:

$$T_A = F_A l_x \tag{3.9}$$

For the case of deformable particles or deformable surfaces (Figs. 5a and 5b), the lever arm l_x is equal to the radius of contact [180]. The concept of a contact region is a concept not considered in the theory of colloid mobilization by chemical perturbations because there is no need to assess torques — the attractive and repulsive forces affecting colloid detachment in the absence of hydrodynamic shear operate in the same direction. Electron microscopy revealed that the extended contact area does indeed occur [185]. Visser [186] presented a slightly different picture explaining the extended contact area. Instead of a deformable colloid, a deformable surface was envisioned that provides regions within which colloids may reach the minimum separation distance at more than one point (Fig. 5b).

By combining Eqs. (3.5), (3.8) and (3.9), a critical velocity for detachment can be identified:

$$U_x^{crit} = \frac{F_A l_x}{(1.399 \times 1.7009)(6\pi\mu a_p^2)} \tag{3.10}$$

With experimental measurements of the critical velocity, Eq. (3.10) can be used to estimate the adhesive force binding colloids to collector surfaces.

In contrast to this approach considering deform-

able particles and surfaces, Hubbe [61,187] postulated that surface roughness plays the dominant role in colloid detachment by hydrodynamic shear. Rather than the deformation of the colloid or surface producing the lever arm by which the adhesive force restrains the rolling colloid, Hubbe conjectured that surface asperities define the lever arm (Fig. 5c). In this case, the lever arm l_x is a function of the surface roughness of the collector surface and the particle. Current interpretation of the effect of surface roughness on hydrodynamic detachment will be explored in the next section.

4. Colloid mobilization: testing theories in the laboratory

In the following sections, experiments in model systems testing the theories of colloid mobilization will be examined. First, for colloid mobilization by chemical perturbations, the effects of changing pH, ionic strength, and surfactant concentration will be discussed. Second, for colloid mobilization by physical perturbations, the effect of increasing velocity and changing solution chemistry will be explored.

4.1. Colloid mobilization by chemical perturbations

Testing the energy barrier approach to colloid mobilization usually involves two steps: (1) attachment of colloids to collector grains under attractive DLVO conditions; and (2) release of colloids from the grains by changing pH, ionic strength, or the concentration of some aqueous species that alters the surface charge of the colloids or grains. The first set of experiments examined here were performed in model systems of well-characterized colloids and grains. The second set of experiments considered attempted to apply the energy barrier model to colloid release from natural sediments by flushing with solutions of varying chemistry.

4.1.1. Colloid mobilization by increasing pH: model systems

Kallay et al. [55] summarized a series of experiments by Matijević and colleagues that explored the effects of solution chemistry alterations on colloid release from surfaces. Using packed column techniques similar to those developed by Clayfield and Lumb [188], Matijević and colleagues attempted to relate the rate of colloid release from porous media surfaces to the DLVO potential energy between the colloids and grains.

In the first paper in the series "Particle Adhesion and Removal in Model Systems", Kolakowski and Matijević [166] measured the release rate of chromium hydroxide ($Cr(OH)_3$) colloids from glass beads. The chromium hydroxide colloids were attached to the glass beads at low pH values that produced oppositely charged colloid and bead surfaces; therefore, the colloids were attached in the primary minimum. The rate of colloid release increased as the pH of the release solution was increased from 9.6 to 11.5; however, at pH 12.6, the release rate declined to an intermediate value. When the rates were compared with DLVO profiles calculated using only the double layer and van der Waals potential energy (producing a primary minimum of infinite depth), it appeared that the magnitude of the barrier to detachment increased as the rate of release increased. To explain this apparent contradiction, Kolakowski and Matijević [166] employed a minimum separation distance, x_0, that increased as pH increased. The increases in x_0 prevented attached particles from residing in the deepest part of the primary minimum, thereby decreasing the size of the detachment energy barrier. To estimate the increase in x_0 with pH, the calculated release rate coefficients [175] were matched to the measured rates of colloid release by varying x_0 to produce detachment energy barriers that corresponded to the trends observed in the data. By this analysis, x_0 varied from 6.3 to 9.5 Å. The minimum separation distance was also sensitive to the pH of attachment and the aging of the attached particles. Interestingly, aging times of about 1 day and 1 week resulted in increases in the fitted minimum separation distances to the higher end of the range.

Kuo and Matijević [167,168] performed similar analyses with model colloid–collector systems consisting of chromium hydroxide–steel and hematite–steel. The chromium hydroxide and ferric oxide have similar pH_{pzc} values and the pH_{pzc} value of

the stainless steel grains was about 5. Comparison of the release rates in both systems to the height of the detachment energy barriers again produced contradictions to the trends predicted by theory until variations in x_0 were invoked [167]. The introduction of an alternative expression for the double layer potential energy [189], in place of the commonly-used Hogg et al. [190] expression, lessened the size of the energy barriers opposing detachment [168], producing better agreement between measured and predicted release rates. The observed decrease in release rate observed at very high pH (>12), also observed by Kolakowski and Matijević [167], was explained with a decrease in x_0. It is more likely, however, that the decrease in the release rate was caused by an increase in ionic strength from NaOH addition. The solutions used in these experiments were not buffered against changes in ionic strength. In addition, zeta potentials used to calculate double layer potentials were not measured for all solution chemistry conditions, possibly explaining the lack of agreement between the measured and predicted release rates.

In all of these experiments, increases in pH cause increases in the release rate and increases in the total amount of particles released. The increase in the extent of particle release was attributed to a decrease in the retention of particles in surface heterogeneities on the collectors. In the steel collector experiments [167,168], scanning electron microscopy (SEM) revealed that colloid aggregates were retained in the crenulate surface of the steel beads following flushing by release solutions. Recognition of these surface heterogeneities led Matijević and colleagues to adopt two-population and continuous distribution models of attached colloids [55,191–194]. In the two-population model, one population of colloids was released from the surface quickly after the high pH release solution was added and the other population was considered to be permanently bound following lateral translation to sites of lower energy [192].

In summary, the model system experiments by Matijević and colleagues confirmed that increases in pH produce repulsive forces that drive colloid release; however, prediction of the release rates was not entirely satisfactory. To fit the measured release rates, adjustments in the minimum separation distance were required without any physical basis for the mechanisms causing the variations in minimum separation distance.

4.1.2. Colloid mobilization by increasing pH: natural sediments

More recent studies of the effect of pH on colloid mobilization from natural sediments in laboratory columns have produced similar results, that is, an increase in pH causes an increase in colloid mobilization [195–198]. In these systems, colloid mobilization was measured indirectly, as a decrease in the hydraulic conductivity. Kia et al. [195] identified a "critical pH" of 4.8 below which colloid mobilization did not occur in Berea sandstone, a reference porous medium in the oil and gas industry that contains about 8% dispersible clay colloids and calcite cement. Because colloid release was measured indirectly, the possibility that the low pH solution promoted colloid release via dissolution of the calcite cement ("decementation") was not observed. These authors all attempted to relate the occurrence of formation plugging to critical pH values; however, their representations of the DLVO profiles corresponding to the critical conditions for colloid mobilization did not follow the accepted models of colloid detachment [125,175].

A dramatic increase in the rate of clay colloid release was observed when the pH of a solution passing through an iron oxide-coated sand exceeded the pH_{pzc} value of typical iron oxides, about pH 7–8 [109]. At $pH > pH_{pzc}$, the surface charge of the predominantly goethite cement binding the kaolinite colloids to the quartz grains was reversed, resulting in repulsive conditions and rapid colloid release. The increase in release rate was qualitatively related to the increase in detachment energy barrier height. The energy barriers for these experiments were calculated by assuming a minimum separation distance of 10 Å, which resulted in the appearance of energy barriers under all tested conditions. For calculation of the DLVO potential energy, Ryan and Gschwend [109] assumed that released colloids were detaching from the kaolinite–goethite coating and not directly from the quartz grains because only a small amount of the total colloid content was released in these experiments. The double layer potential

energy was calculated using zeta potentials of colloids appearing in the effluent.

4.1.3. Colloid mobilization by decreasing ionic strength: model systems

Many of the studies summarized by Kallay et al. [55] also investigated the effect of ionic strength on colloid mobilization. According to colloid release theory, a decrease in ionic strength will allow expansion of the diffuse layers between colloids and grains, increase the repulsive interactions, and promote colloid detachment. Most experimental results obtained by Matijević and colleagues demonstrate that this is qualitatively correct [166,167,193]. Kallay et al. [199], however, observed that more hematite colloids were released from glass beads at 10^{-2} M sodium nitrate than at 10^{-3} M. This counterintuitive behavior was justified by agreement of the observations with trends in the energy barrier height calculated using constant potential (corresponding to relaxed double layers) of the double layer interaction. Kallay et al. [55] also suggest that enhanced opportunities for particle redeposition following detachment existed in the packed bed columns.

Ryan and Gschwend [57] investigated the effect of ionic strength in a similar system containing hematite colloids and quartz sand grains. In this system, decreases in ionic strength promoted increases in colloid release rate and extent; however, the energy barrier size predicted with the constant potential double layer expression still predicted the opposite trend. Reasoning that the intersurface forces between colloids and grains are poorly known at the very short separation distances at which colloids are attached, Ryan and Gschwend [57] adjusted the Born collision parameter, σ, by increasing it until the DLVO profiles for the attached colloids were repulsive at all separation distances. Under conditions promoting release, pH 11 and 0.1–0.001 M sodium nitrate, this is a reasonable assumption because both the hematite and quartz surfaces are highly negatively charged. This adjustment of the Born collision parameter is essentially equivalent to adjusting the minimum separation distance as done by Matijević and colleagues.

Even in the absence of the detachment energy barriers, the measured release rates were still dependent on the ionic strength [57]. The release rates increased as the magnitude of the repulsive force existing at x_0 increased following the decrease in ionic strength, suggesting that the decrease in ionic strength "pushed" the colloids away from the surface. The problem of zeta potential measurements not providing an adequate representation of surface potentials over the entire range of ionic strengths used in the experiments was circumvented by calculating the surface potentials using a surface complexation/double layer model [134]. A similar examination of the $Cr(OH)_3$–glass system studied by Kolakowski and Matijević [166] showed a similar trend, with the slight differences attributed to the greater size and slower diffusion of the $Cr(OH)_3$ colloids [57].

The increase in the extent of colloid release with decreasing ionic strength may have been caused by double layer repulsion between adjacent colloids, as Johnson and Elimelech [200] and Liu et al. [201] found in studies on the effect of ionic strength on blocking and colloid deposition dynamics. As the ionic strength decreases, colloids, which were attached to small, favorable regions of the surface grains under high ionic strength conditions, begin to push each other off the surface because of the lateral repulsion caused by expanding double layers.

Assuming that colloid detachment was relatively rapid in the absence of detachment energy barriers, Ryan and Gschwend [57] tested the effect of altering the diffusion boundary layer thickness on colloid release rates. They found that an increase in the flow rate, which causes a decrease in the thickness of the boundary layer, increased the colloid release rate. The measured relationship between release rate and flow velocity agreed fairly well with the relationship predicted from Eqs. (3.3) and (3.4). Calculations of the drag and lift forces on these 150 nm colloids indicated that shear was not responsible for the increase in release rate.

McDowell-Boyer [56] examined the mobilization of polystyrene latex (PSL) colloids deposited on sand grains and observed the usual increase in colloid release rate and extent with decreasing ionic strength. Based on the DLVO potential energy profiles generated with zeta potentials of

the colloids and sand grains, McDowell-Boyer [56] concluded that the particles were deposited in, and mobilized from, the secondary minimum. Under the experimental conditions, the depth of the secondary minimum was calculated to be 6.7 k_BT. This shallow secondary minimum would not be expected to effectively retain particles, yet attached particles were not removed from the column after the column influent was switched from the particle suspension to a particle-free solution of the same ionic strength. The lack of particle detachment into the particle-free solution may suggest that the particles were deposited in a much deeper primary minimum.

4.1.4. Colloid mobilization by decreasing ionic strength: natural sediments

In contrast to studies in which colloid mobilization and permeability reduction from the clay-containing Berea Sandstone were quite sensitive to changes in ionic strength [195,198,202], changes of ionic strength over four orders of magnitude (from 0.5 M to 5×10^{-4} M) produced only a slight increase in the colloid release rate from an iron oxide-coated sand [109]. This result suggests that the change in ionic strength did not affect the ability of the positively charged goethite cement to bind the negatively charged clay colloids. Changes in solution chemistry that reversed the surface charge of the goethite cement were required to initiate colloid release. Interestingly, the height of the DLVO detachment energy barrier, calculated using the constant potential formula, increased with decreasing ionic strength, similar to DLVO energy barriers calculated for model systems [57,166].

When the goethite cement was removed by reductive dissolution of the goethite by ascorbic acid, a decrease in ionic strength produced a rapid pulse of colloid release. The amount of colloids mobilized in the pulse was related to the concentration of ascorbic acid used in the previous dissolution step and to the amount of dissolved Fe released from the column by the reductive dissolution. The addition of ascorbic acid alone produced a slight increase in the colloid release at low ascorbic acid concentrations (10^{-4}–10^{-3} M). High concentrations of ascorbic acid (10^{-2}–10^{-1} M) did not increase the colloid release even though the Fe release rate continued to increase owing to the high ionic strength of these solutions.

4.1.5. Colloid mobilization by surfactants: model systems

The adsorption of surfactants to colloid and grain surfaces will alter the surface charge. Surfactant adsorption, even in the case where specific surface complexation is not important, can reverse the surface charge of mineral surfaces [203,204]. In a model system consisting of carbon black colloids, glass beads, and surfactants with a variety of functional groups, Clayfield and Smith [205] measured the extent of colloid release from a packed column through which the aqueous solutions flowed by gravity. The extent of colloid release increased with the concentration of surfactant and varied with the type of surfactant. The increase in colloid release with surfactant concentration was attributed to a decrease in the depth of the secondary minimum. The carbon black colloids were deposited in a KCl-surfactant solution originally and their release in the same solution (with a minimum of hydrodynamic disturbance) indicates that they were not deposited in the primary minimum. Dodecyl sulfate was much more effective at releasing the colloids than was the surfactant undecane-3-sulfate [205]. On dodecyl sulfate, the anionic group is located on the end of the molecule, while on undecane-3-sulfate, the anionic group is located on the interior of the surfactant chain. Assuming that adsorption of the surfactants results in orientation of the anionic groups toward the surface and the hydrophobic chains away from the surface, these results suggest that the dodecyl sulfate was more effective at promoting release because its surfactant chain extends further into solution and "pushes" the electrokinetic shear plane further away from the surfaces. In this way, the dodecyl sulfate produced greater repulsive force between the surfaces.

4.1.6. Colloid mobilization by surfactants: natural sediments

Ryan and Gschwend [109] tested the effect of dodecanoic acid and natural organic matter on the mobilization of colloids from an iron oxide-coated

sand. Concentrations of dodecanoic acid of about 16–48 μM, in the expected range of hemimicelle formation, caused a dramatic increase in the colloid release rate. The formation of hemimicelles on the goethite surfaces would result in a reversal of surface charge and rapid colloid release. Higher concentrations of dodecanoic acid further accelerated the release rate. The release rates qualitatively fit the trend in the predicted height of the DLVO detachment energy barrier. Compared to other solution chemistry changes, the surfactants produced greater release rates for energy barriers of the same height, suggesting that the presence of adsorbed surfactants resulted in increases in repulsive energy that could not be measured electrokinetically. In effect, surfactant adsorption may cause colloid release by some "non-DLVO" force like steric repulsion.

Subsequent experiments examining the effect of natural organic matter (NOM) on colloid mobilization from the iron oxide-coated sand revealed that the NOM mobilized clay more rapidly than it dissolved Fe, suggesting that the NOM caused clay mobilization in the same manner as the dodecanoic acid. In fact, for a given clay release rate, the dodecanoic acid and the NOM solutions contained approximately the same concentration of ionized carboxyl functional groups. Field studies of the conditions leading to the presence of colloids in this iron oxide-coated sand [49,108] led to the hypothesis that the colloids were mobilized by decementation, or the dissolution of the goethite cement. The experiments of Ryan and Gschwend [109], however, suggest that charge reversal by adsorption of NOM was the major cause of colloid mobilization.

4.2. Colloid mobilization by physical perturbations

Most tests of the theory of colloid mobilization by hydrodynamic shear have been limited to very simple model systems of colloids attached to flat surfaces. While this experimental arrangement allows for accurate testing of the theories, the resulting information is probably of very little applicability to natural systems.

4.2.1. Colloid mobilization by hydrodynamic detachment: model systems

The first detailed experiments on particle detachment by hydrodynamic forces were conducted by Krupp and colleagues [206,207] and Visser [180,186]. These experiments, examining detachment of polystyrene and carbon-black particles from glass and deformable cellulose and cellophane surfaces, tested variations in solution and surface chemistry, particle size, and shear force, and displayed qualitative agreement with the theory of hydrodynamic detachment.

Hubbe [61,112,208,209] presented a comprehensive test of the mechanisms controlling colloid detachment by fluid shear. Using an apparatus similar to that devised by Visser [186] in which spherical titania colloids ($pH_{pzc} \approx 4$–5) attached to a flat window composed of cellulose film ($pH_{pzc} \approx 3.5$) or glass ($pH_{pzc} \approx 2.5$) were exposed to turbulent shear flow, Hubbe [61] determined that the rate-determining step in detachment is the initiation of rolling. The window allowed visualization and quantification of the retained particles. The critical velocity corresponding to release was found to be in fair agreement with the net adhesive force predicted by DLVO theory and the characteristic length of the region of contact (Eq. (3.10)).

Later experiments involving colloids of varying composition (titania, alumina, and chromium hydroxide) probed the adhesive force between the attached colloids and the cellulose and glass windows [208]. These experiments showed that the adhesive force could be described by considering DLVO forces; however, adjustments of the minimum separation distance and the Hamaker constant were required to match the predicted shear thresholds required for release with the observed thresholds. To match the experimental data, the minimum separation distance was varied from 6–31 Å using both constant potential and constant charge double layer calculations. Hubbe [208] pointed out that the constant charge formulation provided better fits of release data for surfaces of similar pH_{pzc} (e.g. titania on cellulose), while the constant potential formulation better fits release data for surfaces of different pH_{pzc} (e.g. alumina on glass). The constancy of charge or potential is related to rate of relaxation of the double layer

relative to the speed at which the colloids move away from the surface [210–214].

Finally, Hubbe [209] examined the effect of surface charge modification by cationic polyelectrolytes on colloid detachment by shear. The adsorption of the polyelectrolytes increased the adhesion force by a factor of 30, presumably due to polymeric bridging between the cellulose and glass surfaces and the titania colloids. Attempting to calculate the adhesion force by DLVO theory initially led to the prediction that the presence of the polyelectrolytes would decrease the adhesive force and the shear rate required for detachment because the adsorbed polyelectrolytes would increase the separation distance between the attached colloids and the surface. Instead, Hubbe [209] concluded that the adsorbed polyelectrolytes were forming strong bonds between the surfaces and colloids. It was hypothesized that the formation of these bonds resulted in colloids that were "tethered" to surfaces by the polyelectrolytes. The "tethers" increased the lever arm on which the adhesive force acts, resulting in colloids more resistant to hydrodynamic detachment.

In a notable departure from many of the experiments described above, Gotoh and colleagues [215,216] measured the kinetics of nylon ($pH_{pzc} \approx 5$) particle detachment from a quartz plate. In these experiments, the shear impinging on the attached particles was the result of laminar electro-osmotic flow produced in a microelectrophoresis cell. While the rate at which particles were mobilized increased with increasing flow velocity, the release rate increased rapidly in one small velocity range and slowly over the remainder of the velocities tested, suggesting that a threshold shear force existed for the particles. In contrast to the effects of cationic polyelectrolytes observed by Hubbe [209], Gotoh et al. [216] observed that addition of the surfactant sodium dodecyl sulfate (SDS) reduced the adhesive force between the nylon particles and quartz surface. Gotoh et al. [215] observed that nylon particle detachment occurred when the hydrodynamic force exceeded the DLVO adhesive force for particles attached in the secondary minimum by a factor of 50–140. The hydrodynamic forces produced by these relatively low velocities may have affected particle release by altering the boundary layer thickness over which the detached particles diffuse rather than by shear forces on the attached particles.

Recent work on hydrodynamic detachment has confirmed the theoretical and empirical approach laid out by Hubbe [61]. Sharma et al. [62] tested the effects of flow rate, particle size, particle deformability, and solution chemistry (pH and ionic strength) on particle detachment in flow cell and centrifuge experiments. They found good agreement between the predicted and measured critical hydrodynamic force required for detachment and concluded that the essential physics of the problem had been captured for these model systems. In a fluidized bed system, Amirtharajah and Raveendran [217] observed that decreases in ionic strength allowed higher detachment efficiency for polystyrene latex particles on glass beads. Das et al. [63] explored the effect of surface roughness and deformation on hydrodynamic detachment, finding that surface roughness is a critical parameter in allowing particle rolling to initiate detachment. Recognition of the sensitivity of hydrodynamic detachment to surface roughness indicates that development of a more accurate deterministic approach to this problem may not be attainable. Rather, a probabilistic approach based on characterization of surface heterogeneity may be necessary to predict hydrodynamic detachment.

The biomedical field has delved into cell adhesion to, and hydrodynamic detachment from, biological and prosthetic materials. Shiga et al. [113] showed that addition of plasma proteins and plasma decreased the shear rate required to rapidly detach red blood cells from polymethylmethacrylate plates in a cone-plate viscometer. The addition of 0.1–0.5 μM fibrinogen reduced the shear rate necessary for detachment of 50% of the red blood cells from about $600\ s^{-1}$ to $20\ s^{-1}$. Truskey and colleagues [218–220] examined the hydrodynamic detachment of fibroblast cells from glass and fibronectin-modified surfaces. Truskey and Proulx [218] confirmed that increases in the cell contact area that occur following initial attachment of cells to surfaces increase the shear force required for cell release. The adsorption of fibronectin, an adhesion protein, to the glass surface increased the

critical shear stress required for fibroblast detachment from 5 to $\geqslant 140$ dyne cm^{-2} [220]. Truskey and Proulx [219] observed that smaller fibroblast cells were preferentially detached from glass and fibronectin-modified surfaces at shear stresses of less than 30 dyne cm^{-2}, while shear stresses above 30 dyne cm^{-2} preferentially detached larger cells. This result suggests that diffusion controlled cell release at the low shear stresses and hydrodynamic detachment controlled cell release at the high shear stresses.

4.2.2. Colloid mobilization by hydrodynamic detachment: natural sediments

Only one study in natural porous media has attempted to relate the amount and size of mobilized particles to the interstitial flow velocity. Kaplan et al. [58] characterized the particles mobilized by water infiltrating through soil horizons from the Savannah River Plant in Georgia. First, the soil characterized by high pH (6.9) and conductivity (23 $\mu S\ cm^{-1}$) produced the highest particle concentrations when subjected to 10.2 cm of "rain" (tap water, pH 6.1, 6 $\mu S\ cm^{-1}$) over two hours. Kaplan et al. [58] reported that the abundance of mobilized particles (measured by turbidity) and the size of the mobilized particles (measured by dynamic light scattering) both increased with increasing flow rate during the rainfall simulation, as expected from hydrodynamic detachment theory. The electrophoretic mobility of the mobilized particles, which was negative for all particles, was inversely related to flow rate. High flow rates mobilized particles of the lowest zeta potential, while the particles with the highest zeta potentials were mobilized by the lowest flow rates. This behavior also corresponds qualitatively to hydrodynamic detachment theory. Higher flow rates would be required to mobilize particles of lower zeta potential because these particles are bound by a greater adhesive force assuming that the surface to which they are bound is also negatively charged.

Despite these encouraging results, there may be some systematic bias in the data collected by Kaplan et al. [58]. The high flow rates, high particle concentrations, and large mean particle sizes all occurred at the onset of rainfall simulation. It is possible that the high concentrations of large particles that were correlated with high flow rates were mobilized by the initial surge of infiltrating water. It could be anticipated that the initial surge of water would produce very high particle concentrations regardless of flow rate. Furthermore, the use of dynamic light scattering for particle size analysis in these experiments is not appropriate. Dynamic light scattering is ill-suited for size measurement of supramicrometer particles and polydisperse particle size distributions. It is likely that the infiltrating water mobilized soil particles that spanned a wide size range. For example, Ryan et al. [59] observed particle sizes as large as 50 μm in samples collected from zero-tension samplers during rainfall simulation.

5. Colloid transport and deposition (filtration): field observations

In this section, we will review field observations and tests of colloid transport that have driven investigations of colloid transport and deposition phenomena. The most valuable studies described in this section are those that utilized traceable colloids to measure colloid transport behavior. In contrast, some reports of colloid transport as measured by the appearance of a colloid-associated tracer are less reliable because continued association of the tracer cannot be assured. For example, experiments testing colloid-facilitated transport of contaminants suggest, but do not prove, colloid transport. Experiments designed to test colloid deposition (filtration) theory will be described separately in Section 7.

5.1. Colloid transport and deposition (filtration): field experiments

Studies of colloid transport in natural aquifers are limited by the ability to detect the injected colloids in downstream monitoring wells. Owing to this difficulty, much of our knowledge of colloid transport in groundwater comes from experiments testing the mobility of "biocolloids", viruses and bacteria, in aquifers. The factors controlling the transport of biocolloids in porous media have been reviewed by Keswick and Gerba [221], Keswick

et al. [78], Harvey [222,223], and Bitton and Harvey [224]. Many of these studies of bacteria and virus transport have included co-injections of polystyrene latex microspheres, which can be detected in samples by epifluorescence microscopy.

In the only study tracing the transport of inorganic colloids injected into an aquifer, Higgo et al. [74] injected 25 nm silica colloids into a sandy, iron oxide-coated aquifer at Drigg, Cumbria, UK. The silica colloids were detected by light scattering. Over nearly 2 m of transport, only 12% of the silica colloids were lost by deposition to the aquifer material. Silica breakthrough was approximately coincident with a tritiated water tracer.

The remainder of the studies discussed here focus on transport of bacteria and viruses, along with co-injections of microspheres. Harvey et al. [72] monitored the transport of indigenous bacteria and fluorescent polystyrene latex microspheres through a sandy glacial outwash aquifer on Cape Cod, MA. In forced- and natural-gradient tests, the bacteria, stained with a DNA-specific fluorochrome, traveled about 1.25 times faster than the bromide tracer. The more rapid breakthrough of the bacteria, which measured about 0.5–0.7 μm in diameter, was attributed to size exclusion chromatography [225–229]. Size exclusion refers to the exclusion of the bacteria from many of the smaller pore spaces and more tortuous flow paths. Carboxylated microspheres of diameters 0.2, 0.7, and 1.2 μm also broke through before the bromide tracer. Wood and Erlich [71] observed similar results for the transport of *Saccharomyces cerevisiae* (baker's yeast) and bromide and iodide through a heterogeneous aquifer; however, they determined that bromide and iodide were sorbed to the aquifer material. These halide tracers are probably reversibly sorbed by ion exchange into the double layers of positively charged mineral surfaces.

In the natural-gradient tracer test, microspheres of different size and surface functional groups were injected and monitored for 32 days of transport by Harvey et al. [72]. In this test, carboxylated microspheres of 1.35 μm diameter broke through about 1.25 times faster than carboxylated spheres of 0.23, 0.53, and 0.91 μm diameter; however, the breakthrough of all of the carboxylated microspheres slightly lagged the bromide breakthrough in the natural-gradient experiment (RB = 1.1 for the 1.35 μm microspheres versus RB = 1.4 for the others, where RB is the relative breakthrough calculated as the ratio of the integrated concentration histories of the colloids and the tracer [72]). Microspheres described as uncharged (which probably contained some residual sulfonate functional groups) broke through coincidentally with the chloride tracer in the natural-gradient test (RB ≈ 1.0), while microspheres with polyacrolein (>C=O) functional groups broke through slightly ahead (RB = 1.3) of the carboxylated microspheres of similar size.

In another natural-gradient field test at Cape Cod, Harvey and Garabedian [73] injected indigenous bacteria into an aquifer and observed that the bacteria traveled about 30% faster in the sewage-contaminated zone of the aquifer than in the pristine zone. The groundwater in the contaminated zone is near-neutral, suboxic to anoxic, and high in conductivity and organic matter, while the pristine groundwater above the sewage plume is slightly acidic, oxic, dilute, and low in organic matter. Apparently, the effects of the pH and organic matter increase within the plume outweigh the effect of increased ionic strength, resulting in a net increase in repulsive interactions within the plume. In an accompanying experiment, Harvey and Garabedian [73] noted an increase in mean bacterial cell size from about 0.46 to 0.71 μm over a transport distance of 640 m from the sewage infiltration beds at the source of the plume. The increase in mean bacteria size was attributed to enhanced removal of the smaller bacteria by diffusion-driven attachment.

Harvey et al. [230] explored the transport of flagellated protozoa in a natural-gradient test in the Cape Cod aquifer. The transport of the natural protozoa (2–3 μm diameter) was quite similar to the transport of 2 μm carboxylated microspheres co-injected with the protozoa: the breakthrough of both significantly lagged behind that of the bromide tracer (RB from 2–6) and attenuated (approximately one log-order reduction of bacteria concentration per meter of transport).

The transport of viruses through aquifers has also been investigated owing to concern over the spread of pathogens to drinking water supplies.

Viruses have also been used as tracers of groundwater flow. McKay and colleagues [75,76] used two bacteriophages to trace groundwater flow through fractures in a clay-rich glacial deposit. The bacteriophages broke through only 1–2 days after injection; in contrast, the bromide tracer required about 150 days for breakthrough. The large difference in breakthrough was attributed to the restriction of the bacteriophages to fracture flow and the diffusion of the bromide into the clay matrix. McKay et al. [75] noticed that the bacteriophage transport was attenuated by a factor of about one log-order per meter of travel. The attenuation was attributed to attachment to fracture walls. Rossi et al. [77] measured the transport of two bacteriophages in a fluvial deposit with layered heterogeneities at Wilerwald, Switzerland. The bacteriophages followed paths of preferential flow through gravel channels mapped by radio-magneto-tellury.

5.2. *Colloid transport and deposition: field observations*

Colloid transport plays a significant role in the deposition of clay in sediments. In geology and soil science, clays transported to a sediment layer after deposition are referred to as "illuviated" or "infiltrated" clays. Illuviated clays are often considered to be indicative of ancient soil layers through which infiltrating water has carried the clay colloids to greater depths [79–84]. These clays appear characteristically as disorganized coatings on framework aquifer grains. In most cases, the transport of illuviated clays is thought to be limited by deposition near the water table, where the velocity of the infiltrating water decreases. In one notable case where a transport distance may be estimated, Owens et al. [80] detected the presence of halloysite, a hydrated form of kaolinite, in the Cohansey Sand, NJ. Halloysite appears in the Cohansey Sand only where it is overlain by the Bridgeton Formation, which contains abundant halloysite. Using the average thickness of the Bridgeton as an indicator of transport distance, the halloysite colloids have been transported over distances of about 15–20 m vertically. The Bridgeton Formation was deposited in the Miocene period, approximately 20 million years ago, so the rate of colloid transport is quite slow.

Interaction of colloids with soil layers rich in oxide minerals appears to limit illuviation [231–233]. The appearance of periodically spaced clay lamellae in soils has prompted explanations based on the deposition of iron oxide-rich layers at depths where infiltrating organic matter carrying adsorbed Fe is degraded and the Fe is released. As these iron oxide-rich layers form, they accumulate infiltrating clay particles.

The detection of suspended colloids in saturated aquifers unaffected by anthropogenic alterations [44,47,49] suggests that emplacement of infiltrated clays need not be indicative only of ancient soils [108]. The studies cited above all link illuviated clay with the vertical transport of colloids through soils in areas with arid climates and deep water tables. The associated leaching environments have been used to explain the formation of red beds, sediments stained by iron oxide coatings. The studies by Postma and Brockenhuus-Schack [47] and Ryan and Gschwend [108] suggest that the process that produces red beds, the intrastratal alteration of Fe-bearing primary minerals, can occur below the water table and in temperate climates. These findings are significant because infiltrated clays are often associated with red bed formation.

6. Theories of colloid deposition and filtration kinetics

Theoretical approaches to calculate particle deposition rates onto stationary surfaces from flowing suspensions are described in this section. As described earlier, particle deposition is the primary factor controlling the transport of colloids in groundwater. Hence, a thorough understanding of colloid deposition is essential for prediction of colloidal transport in natural porous media. Emphasis is given to "filtration theories", that is, theories for calculating the initial particle deposition rate in granular porous media. Approximate analytical expressions for calculating the initial particle deposition rate under favorable and

unfavorable chemical conditions are presented along with a discussion of their limitations.

6.1. Theoretical approaches

There are two theoretical approaches for calculating the particle deposition rate onto model collectors from flowing suspensions, namely Lagrangian and Eulerian [35,234–237]. These methods are described briefly below. We will focus on the Eulerian approach which is widely used in filtration theories for Brownian and non-Brownian particles.

6.1.1. Lagrangian versus Eulerian approach

Lagrangian methods describe the trajectory of a particle as it approaches the collector surface, whereas Eulerian methods describe the particle concentration in time and space. The Lagrangian description of particle motion focuses on a single particle trajectory that is governed by Newton's second law. Inclusion of a thermal random force (Brownian effects) in the equation of motion leads to a Langevin-type equation, the solution of which results in stochastic trajectories [236,238,239]. In the Eulerian approach, the difficulty of accounting for Brownian effects is eliminated. In addition, this approach is more amenable to numerical or approximate analytical solutions than Lagrangian methods.

Eulerian methods are concerned with obtaining the concentration distribution (or probability density) of particles in space, as well as the orientation distribution for non-spherical particles. Such distributions are described by a set of coupled ordinary differential equations termed the Fokker–Plank equations [176,234,237,240]. In dilute suspensions of spherical particles where interparticle interactions can be neglected, the Fokker–Plank equations reduce to the common continuity equation. For situations involving particle transport and deposition in fluids, the continuity equation is often called the convective diffusion equation [177,235].

Extensive discussions of these methods as applied to particle deposition can be found elsewhere [234,237,241–243]. Both methods have been successfully used to describe particle deposition in granular porous media [35,241,244,245].

6.1.2. The convective diffusion equation

The convective diffusion equation in its general form is given by [234,235,242]

$$\frac{\partial C}{\partial t} + \nabla \cdot \boldsymbol{J} = Q \tag{6.1}$$

where C is the particle number concentration, t is the time, $\boldsymbol{J}$ is the particle flux vector, and Q is a source term. The particle flux vector is given by

$$\boldsymbol{J} = -\boldsymbol{D}\cdot\nabla C + \boldsymbol{u}C + \frac{\boldsymbol{D}\cdot\boldsymbol{F}}{k_B T}C \tag{6.2}$$

Here, $\boldsymbol{D}$ is the particle diffusion tensor, $\boldsymbol{u}$ is the particle velocity induced by the fluid flow, k_B is the Boltzmann constant, T is the absolute temperature, and $\boldsymbol{F}$ is the external force vector. The terms on the right-hand side of Eq. (6.2) describe the transport of particles by diffusion, convection, and external forces respectively.

For particle deposition in aquatic systems, the relevant external forces are colloidal and gravitational, that is

$$\boldsymbol{F} = \boldsymbol{F}_{col} + \boldsymbol{F}_G \tag{6.3}$$

where $\boldsymbol{F}_{col}$ represents the colloidal forces acting between suspended colloids and collector surfaces and $\boldsymbol{F}_G$ is the gravitational force. The colloidal force can be obtained from the total interaction potential, ϕ_T, as follows:

$$\boldsymbol{F}_{col} = -\nabla\phi^{tot} \tag{6.4}$$

Within the framework of the classical DLVO theory, ϕ^{tot} is the sum of van der Waals and electrical double layer interactions. In principle, other non-DLVO colloidal interactions can be included in the ϕ^{tot} term; however, no analytical expressions for such interactions are available at the present time.

Substituting Eq. (6.2) in Eq. (6.1), and assuming no source term, reduces the convective diffusion equation to

$$\frac{\partial C}{\partial t} + \nabla\cdot(\boldsymbol{u}C) = \nabla\cdot(\boldsymbol{D}\cdot\nabla C) - \nabla\cdot\left(\frac{\boldsymbol{D}\cdot\boldsymbol{F}}{k_B T}C\right) \tag{6.5}$$

When Eq. (6.5) is applied to coagulation [137] or deposition [246] phenomena, a steady state is established within a period of time that is much smaller than the time scales pertaining to most particle deposition problems. Hence, Eq. (6.5) simplifies to the familiar steady state form:

$$\nabla\cdot(\boldsymbol{u}C)=\nabla\cdot(\boldsymbol{D}\cdot\nabla C)-\nabla\cdot\left(\frac{\boldsymbol{D}\cdot\boldsymbol{F}}{k_BT}C\right) \tag{6.6}$$

This equation provides the basis for several colloid deposition models, such as the Smoluchowski–Levich and the interaction force boundary layer approximations discussed later.

6.2. Boundary conditions at the collector surface

To calculate the particle deposition rate from the convective diffusion equation, proper boundary conditions pertaining to the collector surface must be specified. With these boundary conditions, Eq. (6.6) can be solved for the particle concentration distribution from which the local and average deposition rates can be calculated. Because of insufficient detailed knowledge about chemical and physical conditions at the collector surface, simplifying assumptions have to be made when specifying boundary conditions. Two different models for boundary conditions at the collector surface are discussed below: the perfect sink model and the non-penetration boundary condition.

6.2.1. The perfect sink model

The most commonly used boundary condition at the collector surface is the so-called perfect sink model [234,245,247]. In this model, it is assumed that all particles arriving at the collector surface are irreversibly consumed by a very fast immobilization reaction [234,248]. In other words, it is assumed that particles are captured in an infinite energy sink and disappear from the system.

This perfect sink boundary condition is stated mathematically as

$$C=0 \quad \text{at} \quad h=0 \tag{6.7}$$

where h is the surface-to-surface separation distance between particle and collector. Several investigators [249–252] express the perfect sink boundary condition as

$$C=0 \quad \text{at} \quad h=\delta \tag{6.8}$$

where δ is the primary minimum distance (Fig. 3). This expression states that all particles arriving at a distance sufficiently close to the collector surface (the primary minimum distance) are irreversibly captured. All classical analytical solutions for particle deposition, such as the Smoluchowski–Levich approximation [177,234] and the interaction force boundary layer approximation [171,172] were obtained using the perfect sink model (Fig. 6).

Song and Elimelech [247] have shown that the particle migration (drift) flux component (i.e. the flux induced by colloidal interactions) dominates very close to the collector surface. They also demonstrated that the perfect sink boundary condition is equivalent to a constant migration flux boundary condition. The latter is more convenient for numerical solution of the convective diffusion equation when repulsive double layer interactions predominate. The constant migration flux boundary condition is given by

$$\left.\frac{\mathrm{d}(uC)}{\mathrm{d}h}\right|_{h=\Delta}=0 \tag{6.9}$$

where u is the particle velocity component perpendicular to the surface and Δ is an arbitrary point beyond the energy barrier (toward the collector surface) where the migration particle flux is the dominant flux component. The utility of this boundary condition and the limitations of the usual perfect sink model shown by Eqs. (6.7) or (6.8) were discussed in detail by Song and Elimelech [247].

6.2.2. Non-penetration boundary condition

A major disadvantage of the perfect sink model is that it completely neglects the accumulation of immobilized particles at the collector interface. In addition, this model does not consider the possibility of a finite rate of colloid immobilization at the collector surface. To overcome these difficulties, Adamczyk et al. [234] and Adamczyk and van de Ven [250] proposed the non-penetration boundary condition. In this model, it is no longer assumed that particles disappear at the collector surface;

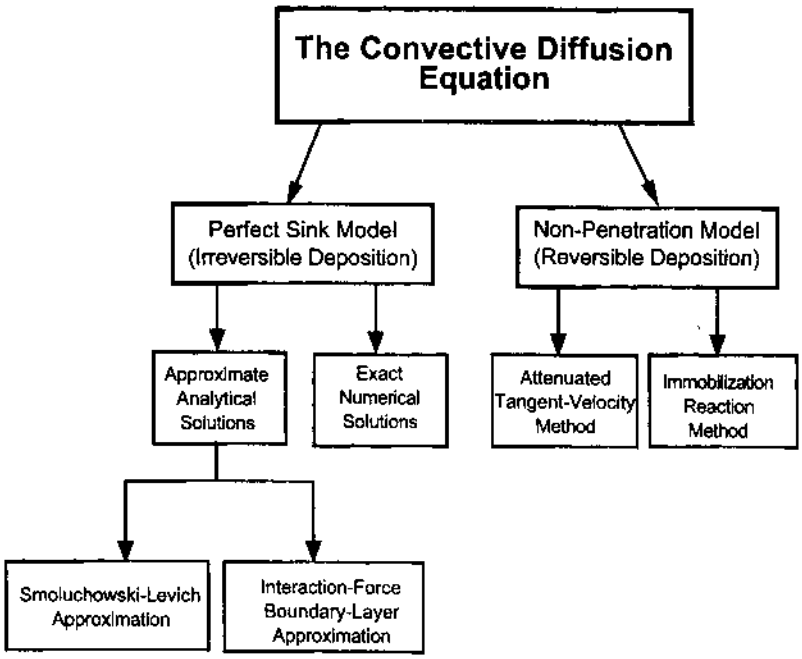

Fig. 6. Theoretical methods for calculating the rate of particle deposition based on the convective diffusion equation (Eulerian approach). The perfect sink model is the widely-used method, but other approaches such as the non-penetration model are more realistic (see text and cited references for more details on the non-penetration model). With the perfect sink model, approximate analytical solutions are available for favorable deposition (Smoluchowski–Levich approximation) and for unfavorable deposition (IFBL approximation). Adapted from Adamczyk et al. [234] and Elimelech et al. [35].

instead, it is assumed that particles cannot penetrate the collector solid surface. Mathematically, the non-penetration boundary condition states that the perpendicular particle flux at the collector surface $J_\perp$ vanishes, i.e.

$$J_\perp = 0 \quad \text{at} \quad h = 0 \tag{6.10}$$

In the non-penetration model, mass balance equations are formulated for the dispersed (mobile) and stationary (immobile) phases. Furthermore, the source term Q in the convective diffusion equation (Eq. (6.1)) is used to account for the complex "specific interactions" at the collector surface which are responsible for particle attachment (immobilization) and release reactions. Adamczyk et al. [234] attribute the "specific interactions" at the collector surface to physical and chemical heterogeneities and to steric and hydration forces which exist at small separations from the collector surface. These poorly known interactions cause the total interaction potential to possess components tangential to the collector surface in addition to the usual perpendicular components.

The non-penetration boundary condition model can also be used to quantify the amount of particles dynamically accumulated within primary and secondary minima, so that, in principle, the release rate of particles can be calculated. The model, however, is rather general and cannot be applied directly to particle deposition because the "specific interactions" at the collector surface are not explicitly known.

6.3. Colloid filtration theories

Two useful analytical expressions for calculating the initial deposition rate of suspended particles in granular porous media are described in this section. These include the interaction force boundary layer (IFBL) approximation and Rajagopalan and Tien's correlation equation. Prior to presenting

these approximations, the principles of the microscopic approach to model particle removal in granular filtration are discussed.

6.3.1. The fundamental (microscopic) approach for filtration

The fundamental (microscopic) filtration theories describe the deposition of particles during the initial stage of filtration (the so-called "clean-bed removal") based on fundamental concepts of mass transfer, hydrodynamics, and colloid and surface chemistry. In this approach, the filter bed is modeled as an assemblage of single or unit collectors having a known geometry. The fluid flow field around or through this geometry is described analytically using theories based on low-Reynolds-number hydrodynamics [241,242,253,254].

In the fundamental approach, deposition of particles is represented by a single or a unit collector removal efficiency, usually denoted as η. The unit collector efficiency is defined as the ratio of the overall particle deposition rate onto the collector to the convective transport of upstream particles toward the projected area of the collector. For an isolated spherical collector, the single collector removal efficiency is [85]

$$\eta = \frac{I}{UC_0\pi a_c^2} \tag{6.11}$$

where C_0 is the bulk concentration, U is the fluid approach velocity, and I is the actual deposition rate on a collector with radius a_c. The single collector efficiency is then related to the removal efficiency of the entire granular filter medium through a simple mass balance. For a granular filter composed of uniform spheres, the result is [35,85]

$$\ln(C/C_0) = -\frac{3}{4}\frac{(1-\epsilon)\eta L}{a_c} \tag{6.12}$$

Here ϵ is the porosity and L is the depth of the granular medium in the filter. This expression can also be viewed as the logarithmic attenuation in concentration of suspended particles traveling a distance L in porous medium. Hence, Eq. (6.12) can be used to estimate the travel distance of colloids in saturated porous media such as groundwater aquifers [34,35].

The goal of the fundamental filtration theories is to predict η for a given suspension under known physical and chemical conditions. However, as will be discussed later in this paper, current theories fail to predict η when repulsive double layer interactions predominate. As a result, it is necessary to combine an empirical factor in predicting η. In this approach, we multiply the single collector efficiency, η_0, determined from physical considerations, by an empirical collision (attachment) efficiency, α, which describes the fraction of collisions with filter grains that result in attachment [35,129,255–258]. Thus, the overall single collector removal efficiency is

$$\eta = \alpha\eta_0 \tag{6.13}$$

Here η_0 is the calculated single collector removal efficiency without the inclusion of electric double layer interaction in the calculations. The collision efficiency, α, for a given colloidal suspension, solution chemistry, and filter medium can be determined from column experiments and is usually in the range 10^{-3}–1 [35,129,256,258].

6.3.2. Idealized porous (filter) medium

In a granular medium, the flow field around an individual spherical collector is influenced by neighboring collectors. Hence, a flow model for granular porous media must be used to account for the disturbance of the flow field around the individual collectors. Various theoretical models describing the flow field in a packed bed of spherical collectors are available [259–261]. An excellent summary of these models has been given by Tien [241]. Of these models, Happel's sphere-in-cell model [260] is the most commonly used in filtration studies.

In Happel's model, the porous medium is treated as an assemblage of identical spherical collectors, each of which is enveloped in a shell of fluid (Fig. 7). The thickness of the shell, b, is determined so that the overall porosity of the granular medium is maintained for the single collector:

$$b = a_c(1-\epsilon)^{-1/3} \tag{6.14}$$

Happel's model has been successfully applied to

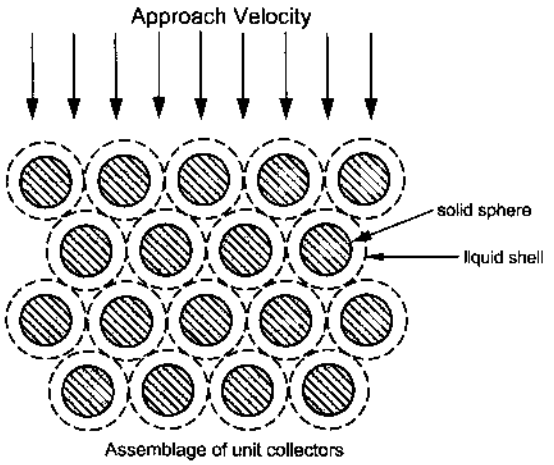

Fig. 7. Schematic description of a granular porous medium based on the sphere-in-cell model. In this model, the porous medium is described as an assemblage of identical spherical collectors. Each collector has a fluid envelope around it to form a so-called "cell". The thickness of the liquid envelope with relation to the solid sphere is determined by the porosity of the medium.

numerous particle deposition and filtration studies [86,129,258,262–264]. It has also been used in column studies dealing with the transport of colloidal particles and biocolloids in natural porous media [73,265–267]. Some of the limitations of the Happel sphere-in-cell model were discussed by Payatakes et al. [268] and Song and Elimelech [269].

6.3.3. IFBL approximation

The deposition (capture) rate of suspended colloidal particles in a porous medium can be found from a numerical solution of the convective diffusion equation (the Eulerian approach) or the trajectory equation (the Lagrangian approach). The single collector removal efficiency η is then obtained from the calculated deposition (capture) rate using Eq. (6.11). Extensive discussions of these methods as applied to deposition (filtration) in packed beds are given by Tien [241], Elimelech [242], and Elimelech et al. [35].

A major disadvantage of the numerical methods is the lack of an explicit expression for calculating colloid deposition rate. An elegant approximate analytical solution for calculating colloid deposition rate in the presence of repulsive double layer interactions was developed independently by Ruckenstein and Prieve [171] and Spielman and Friedlander [172]. This method, known as the IFBL approximation, is used for predicting the deposition rate of Brownian particles in the presence of repulsive energy barriers. The IFBL approximation has been used in numerous investigations of colloid deposition under unfavorable chemical conditions [129,258,270–275].

The premise of the IFBL approximation is that colloidal interaction forces operate over very short distances from the collector surface (usually up to several tens of nanometers) where convective transport is negligible. Hence, it is possible to identify two regions adjacent to the collector surface, characterized by the relative magnitude of the colloidal interaction forces. In the inner region, in the vicinity of the collector surface, colloidal interaction forces predominate while convective transport is negligible. This region is referred to as the IFBL (or surface interaction boundary layer), and is taken to be on the order of the double layer thickness (characterized by the Debye length). In the outer region, colloidal interaction forces vanish while convective transport becomes important. The thickness of this region is taken to be on the order of the diffusion boundary layer [172], described earlier by Eq. (3.3).

Following the classical solution of Spielman and Friedlander [172], the single collector removal efficiency for a porous medium is given by [172,276]

$$\eta = 4.0 A_S^{1/3} \left(\frac{D_\infty}{2a_c U}\right)^{2/3} \left(\frac{\beta}{1+\beta}\right) S(\beta) \tag{6.15}$$

$$\beta = \frac{1}{3}(2)^{1/3}\Gamma\left(\frac{1}{3}\right) A_S^{-1/3} \left(\frac{D_\infty}{U a_c}\right)^{1/3} \left(\frac{k_F a_c}{D_\infty}\right) \tag{6.16}$$

Here A_S is a porosity dependent parameter of Happel's model, D_∞ is the colloid bulk diffusion coefficient, k_F is a pseudo-first-order rate constant which implicitly accounts for the retarding effect of double layer repulsion on deposition rate, and $S(\beta)$ is a slowly varying function of β with tabulated numerical values given by Spielman and Friedlander [172].

The assumptions used in the derivation of the IFBL approximation and some of its limitations are worth mentioning. The IFBL approximation is limited to [171,277]:

(1) Small, Brownian colloids for which gravitational forces are negligible.

(2) Situations where the double layer repulsion is sufficiently strong.

(3) Situations where the secondary minimum is sufficiently shallow.

Furthermore, the model assumes that:

(1) Hydrodynamic (viscous) interaction is partially included (through its effect on the diffusion coefficient but not on the particle flow field).

(2) Interception does not play a role in the capture of particles (i.e. point size particles).

Inspection of the terms found in Eqs. (6.15) and (6.16) reveals that, in the absence of colloidal and hydrodynamic interactions, $\beta \rightarrow \infty$ whereas $S(\beta) \rightarrow 1$. Hence, the single collector efficiency is reduced to the familiar Smoluchowski–Levich approximation for capture of small, Brownian colloids in a porous medium [85,177,234]:

$$\eta = 4.0 A_S^{1/3} \left(\frac{D_\infty}{2 a_c U} \right)^{2/3} \tag{6.17}$$

It follows from Eqs. (6.13) and (6.15)–(6.17) that the theoretical collision (attachment) efficiency is simply

$$\alpha = \left(\frac{\beta}{1+\beta} \right) S(\beta) \tag{6.18}$$

As will be discussed later in this review, serious discrepancies exist between collision efficiencies calculated from Eq. (6.18) and experimentally measured collision efficiencies.

6.3.4. Rajagopalan and Tien's correlation equation

Based on numerical results obtained from a solution of the trajectory equation under various physical conditions (in the absence of double layer interaction), Rajagopalan and Tien [86] proposed a correlating equation for η_0. This equation accounts for the effects of hydrodynamic (viscous) interaction (retardation) and van der Waals attraction on colloid deposition rate. It is given by [86,278,279]

$$\eta_0 = 4.0 A_S^{1/3} \left(\frac{D_\infty}{d_c U} \right)^{2/3} + A_S N_{LO}^{1/8} N_R^{15/8} + 3.38 \times 10^{-3} A_S N_G^{1.2} N_R^{-0.4} \tag{6.19}$$

where A_S is a porosity-dependent parameter of the Happel sphere-in-cell model [260], and N_{LO}, N_R, and N_G are dimensionless parameters. The term N_{LO} characterizes the van der Waals attraction and is defined as

$$N_{LO} = \frac{4 A_{123}}{9 \pi \mu d_p^2 U} \tag{6.20}$$

where A_{123} is the Hamaker constant of the interacting media and d_p is the particle diameter. N_R is an aspect ratio given by

$$N_R = \frac{d_p}{d_c} \tag{6.21}$$

with d_c being the diameter of the collector. Lastly, N_G is a gravitational force number given by

$$N_G = \frac{(\rho_p - \rho) g d_p^2}{18 \mu U} \tag{6.22}$$

Here, g is the gravitational acceleration, μ is the fluid viscosity, and ρ_p and ρ are the density of particles and fluid respectively.

It should be noted that only the second and third terms on the right-hand side of Eq. (6.19) were obtained from Rajagopalan and Tien's correlation. The first term on the right-hand side, which accounts for transport by diffusion, was added by Rajagopalan and Tien to their derived equation with the assumption that the transport mechanisms are additive. This term is identical to the Smoluchowski–Levich approximation given by Eq. (6.17) and, therefore, does not account for the effect of hydrodynamic interaction on the capture rate of Brownian particles.

Another form of the correlation equation of Rajagopalan and Tien is obtained when the removal rate of particles by a unit collector is normalized by the convective flux of particles toward the projected area of the sphere-in-cell envelope (i.e. use of b rather than a_c). In this case, each term on the right-hand side of Eq. (6.19) is

modified by a factor of $(1-\epsilon)^{2/3}$ to yield [35,278,279]

$$\eta_0 = (1-\epsilon)^{2/3}\left\{4.0A_S^{1/3}\left(\frac{D_\infty}{d_c U}\right)^{2/3} + A_S N_{LO}^{1/8} N_R^{15/8} + 3.38\times 10^{-3} A_S N_G^{1.2} N_R^{-0.4}\right\} \quad (6.23)$$

When Eq. (6.23) is used to calculate the dimensionless particle deposition rate by a unit collector of the filter, the following equation should be used to calculate the attenuation of the particle number concentration as particles travel a distance L in the granular filter medium [35,279]:

$$\ln(C/C_0) = -\frac{3}{4}\frac{(1-\epsilon)^{1/3}\eta L}{a_c} \quad (6.24)$$

This equation is obtained from a mass balance over a packed bed composed of unit collectors with a radius $b = a_c(1-\epsilon)^{-1/3}$. When used appropriately, identical particle removal efficiencies (or attenuation) should be obtained from (1) Eq. (6.12) along with Eqs. (6.13) and (6.19), and (2) Eq. (6.24) along with Eqs. (6.13) and (6.23). This subject has been a source of confusion in the filtration literature because the original equation published by Rajagopalan and Tien [86] contained an error which was later clarified by Rajagopalan et al. [278].

It should be emphasized that Eq. (6.19) (or Eq. (6.23)) provides an approximate value for η_0. The correlation equation was obtained from numerical calculations with the trajectory equation over a wide range of parameters usually encountered in water filtration. Since groundwater velocities are much smaller than those encountered in granular filtration, the applicability of this equation to low velocities should be verified. Furthermore, the correlation equation does not include corrections for hydrodynamic interaction for Brownian particles (the first term on the right-hand side of Eq. (6.19)). Although hydrodynamic interaction is much more significant for non-Brownian particles [241,262,280], deviations by a factor of two from exact numerical solution of the convective diffusion equation are expected for Brownian particles when Eq. (6.19) is used [245,264,281].

Lastly it should be noted that Eq. (6.19) may yield single collector efficiencies greater than one for small, Brownian colloids when fluid velocities are very small (as in groundwater). It is physically impossible, however, to obtain single collector efficiencies greater than unity because a collector cannot remove more particles than those supplied by convection [269]. For this case, Song and Elimelech [269] modified the boundary conditions for the problem of particle deposition with the sphere-in-cell model. They further showed that, with the modified boundary conditions, the single collector efficiency approaches unity as the Peclet number becomes very small.

7. The success and failure of colloid deposition (filtration) theories

In this section, we discuss the adequacy of current filtration theories to predict the deposition rate of colloids in porous media. Discrepancies between theoretical predictions and experimental observations are described and possible explanations for these discrepancies are discussed.

7.1. General observations

Colloid deposition (filtration) theories can be tested by conducting column experiments with model colloids and collectors under controlled chemical and physical conditions. For convenience, two types of colloid deposition are recognized [35,257,282]. The first is colloid deposition in the presence of repulsive interactions (usually double layer repulsion), the so-called "unfavorable" deposition. For unfavorable deposition conditions, colloidal interactions control the rate of particle deposition. The second condition, referred to as "favorable" deposition, involves colloid deposition in the absence of repulsive energy barriers or in the presence of attractive double layer interactions. In this case, colloidal transport to the vicinity of the solid surface is the rate controlling step.

In this section, we will focus on unfavorable colloid deposition, as it applies to most groundwater colloidal transport problems of interest. Furthermore, the discussion will be limited to the initial deposition rate onto "clean" solid surfaces

before retained particles start to influence the subsequent deposition of colloidal particles. The role played by retained particles in the dynamic (transient) behavior of colloid deposition is discussed later in Section 9.

7.1.1. Deposition under unfavorable chemical conditions

Several well-defined studies dealing with deposition of Brownian and non-Brownian particles in granular porous media under unfavorable chemical conditions are reported in the literature. Some of these studies are summarized in Table 1. They will be used to demonstrate the main features observed in particle deposition kinetics.

A common feature of the investigations summarized in Table 1 is the large discrepancy between theoretical predictions and experimental observations when repulsive double layer interactions predominate. This is also demonstrated in Fig. 8 which compares predicted and measured initial deposition rates (expressed as collision efficiencies) of Brownian colloids as a function of ionic strength. Colloid deposition rate and collision efficiency calculated from current particle deposition models which incorporate the DLVO theory are many orders of magnitude smaller than those observed experimentally. Experimentally determined collision efficiencies are sensitive to the ionic strength of the solution and to the electrokinetic (zeta) potentials of particles and collectors but not to the large extent predicted by theory.

Another serious discrepancy between theory and experiments is noted for the effect of particle size on particle deposition rate. Particle deposition models based on the DLVO theory predict that collision efficiencies and critical deposition concentrations are dependent on particle size. Experimentally determined collision efficiencies and critical deposition concentrations, however, are virtually independent of particle size, as shown in Fig. 8.

The discrepancies discussed above are universal since they were obtained from studies involving a wide array of colloids and collector surfaces. These include Brownian and non-Brownian particles, particles of different surface chemistries (e.g. synthetic latex particles and metal oxides), collectors of various geometries (planar and curved surfaces), and collectors of different chemical compositions (e.g. glass, silica sand, mica, and steel).

7.1.2. Deposition under favorable chemical conditions

In contrast to particle deposition under unfavorable chemical conditions, a relatively good agreement is observed between theoretical predictions and experimental observations in particle deposition under favorable chemical conditions (i.e. when double layer repulsion is negligible [129,258,263] or in the presence of attractive double layers [264,281,286]). For instance, when attractive double layer interactions develop for oppositely charged particles and collector surfaces, particle deposition models within the framework of the DLVO theory are satisfactory in predicting the effect of solution ionic strength, fluid velocity, and particle size [264,281,286]. Favorable chemical conditions for particle deposition may develop in groundwaters with high levels of hardness and ionic strength. Particle deposition will also be favorable for aquifer surfaces (or patches on solid surfaces) which are positively charged due to iron, aluminum, or manganese oxide coatings [65,108,201,287]. Extensive discussions on colloidal deposition in porous media under favorable chemical conditions can be found elsewhere [35,241].

7.2. Proposed explanations for observed discrepancies in unfavorable deposition

Two major discrepancies between theory and experiments in particle deposition kinetics in the presence of repulsive electric double layer interactions were described above. These discrepancies are (1) experimental collision efficiencies are many orders of magnitude larger than predicted values, and (2) experimental collision efficiencies and critical deposition concentrations are independent of particle size. Elimelech et al. [35] have recently presented an extensive discussion on possible explanations for these discrepancies. These explanations are summarized briefly below. Assessment of discrepancies with regard to colloidal transport

Table 1
Summary of representative controlled particle deposition studies in model porous media and their main conclusions

Reference	Granular medium	Particles	Solution chemistry	Findings and conclusions
Gregory and Wishart [271]	Alumina fibers	Polystyrene latex particles Diameter: 172 nm	pH was controlled by acid or base Ionic strength was controlled by a buffer solution	Large discrepancy between theory and observations when particles and collectors are similarly charged Good agreement with mass transfer theories when particles and collectors are oppositely charged Discrepancy was attributed to collector surface charge heterogeneity
Kallay et al. [283]	Stainless steel spheres	Hematite particles Diameter: 150 nm	$NaNO_3$ electrolyte	Large discrepancy between theory and observations when repulsive double layer interactions are significant
Elimelech and O'Melia [129,258]	Glass beads	Polystyrene latex particles Diameters: 46, 121, 378 and 753 nm	KCl electrolyte $CaCl_2$ electrolyte	Poor agreement between theory and observations when repulsive double layer interactions predominate Observed collision efficiencies are insensitive to particle size Several explanations for observed discrepancies are suggested and discussed
FitzPatrick and Spielman [284]	Glass beads	Latex particles Diameters: nine suspensions in the range 0.71–21.0 μm	HNO_3 to vary the pH NaCl electrolyte $CaCl_2$ electrolyte	No discussion is given for agreement between theory and observations when repulsive double layer interactions predominate
Tobiason and O'Melia [256]	Glass beads	Polystyrene latex particles Diameters: 4 and 12 μm	$NaNO_3$ electrolyte $NaNO_3$ and $Ca(NO_3)_2$ Acid or base to vary the pH	Poor agreement between theory and observations Several explanations for this discrepancy are suggested and discussed
Vaidyanathan and Tien [285]	Glass beads	Latex particles Diameters: five suspensions in the range 4.2–25.7 μm	NaCl electrolyte Acid or base to vary the pH	Poor agreement between theory and observations when repulsive double layer forces predominate A model for surface charge heterogeneity was proposed; this model narrows the gap between theory and observations

and deposition in groundwater will follow this discussion.

7.2.1. Distribution of surface and physical properties

Colloidal particles and solid surfaces in natural and engineered systems usually exhibit a distribution in measured physical and chemical properties, such as zeta potential and particle size [243,288–290]. It is well known from DLVO theory that particle deposition rate and collision efficiency are sensitive to the surface (or zeta) potentials of particles and collector grains and to the particle size of the suspension. Hence, a distribution in these properties will influence the predicted collision efficiencies.

The effect of a distribution in surface potentials and size of particles on the rate of Brownian coagulation has been investigated by Prieve and Ruckenstein [291] and more recently by Ofoli [292]. An approach similar to that of Prieve and Ruckenstein for coagulation was used to investigate the effect of a distribution in surface (zeta)

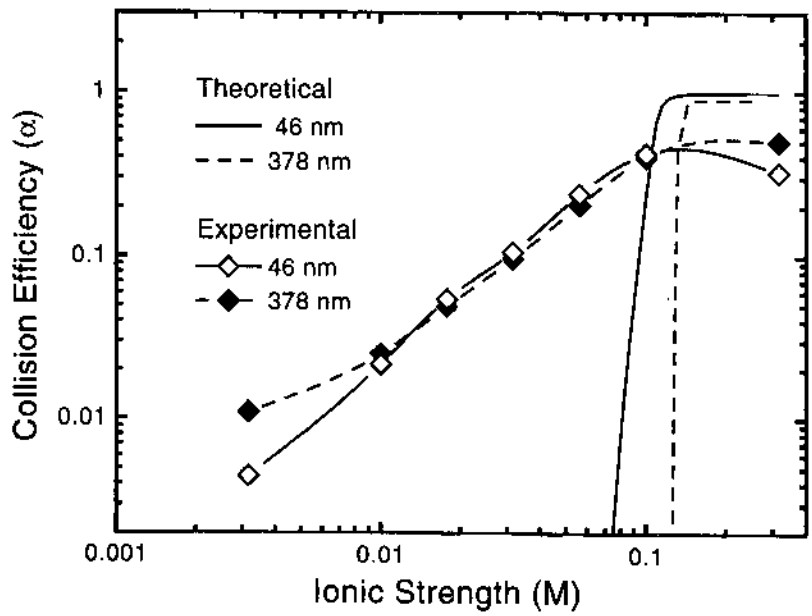

Fig. 8. Comparison of theoretical and experimental collision efficiencies of two different suspensions of Brownian, polystyrene latex colloids (after Elimelech and O'Melia [129]). The diameters of the particles are indicated. Under unfavorable chemical conditions (ionic strengths smaller than about 0.1 M for this case), theoretical predictions underestimate experimental results by many orders of magnitude.

potentials of particles and collectors on the kinetics of deposition of non-Brownian [279,293] and Brownian [129] particles in porous media. The results demonstrate that a distribution in surface potentials tends to decrease the discrepancy between theoretical deposition rates and experimental results. However, these studies demonstrated that unreasonably large distributions of surface potentials of particles and collector grains have to be invoked to explain experimental observations. As will be discussed below, it is more reasonable to assume large distributions in local surface properties, such as the local surface potential of collector grains, rather than a large distribution in the overall (mean) surface potential of particles and collectors.

7.2.2. Surface charge heterogeneity of solids

Most solid surfaces in aqueous media are heterogeneously charged at the microscopic (molecular) and macroscopic levels. Surface charge heterogeneity is attributed to the complexity of the crystalline structure of solids and to their variable chemical composition [64,65,294–296]. Surface-bound impurities may be an additional source of charge heterogeneity [251,275,287]. A separate discussion on the source of charge heterogeneity of solid surfaces in soils and groundwater is presented later in Section 8.1.

The significant role of surface charge heterogeneity in particle deposition kinetics under unfavorable chemical conditions has been noted for some time. Hull and Kitchener [297], Bowen and Epstein [298], and Gregory and Wishart [271] reported the results of controlled colloid deposition experiments under unfavorable chemical conditions. They observed that experimental deposition rates were many orders of magnitude higher than theoretical predictions based on the classic DLVO theory. The discrepancy was attributed to inherent physical and electrochemical heterogeneities of collector surfaces. They further proposed that particle deposition occurs preferentially onto favorable sites, resulting in initial deposition rates much higher than those predicted based on the average collector surface potential.

The role of surface charge heterogeneity in the kinetics of coagulation has also been investigated by Kihira and Matijević [299,300]. They concluded that the discrepancy between theoretical predictions and experimental stability ratios of homocoagulation and heterocoagulation can be rectified if the discrete nature of surface charge is considered.

Song et al. [287] developed a general theoretical approach for the calculation of colloid deposition rate onto heterogeneously charged surfaces (described in Sections 8.2 and 8.3). Patchwise and random (continuous) distribution models were used to quantitatively describe surface charge heterogeneity and its effect on the kinetics of colloid deposition. It was shown that minor degrees of charge heterogeneity of collector surfaces results in particle deposition rates that are orders of magnitude larger than similar surfaces having no charge heterogeneity. It was further demonstrated by Song et al. [287] that the sensitivity of particle deposition rate to solution ionic strength decreases markedly as the degree of surface charge heterogeneity increases.

7.2.3. Physical heterogeneity (surface roughness)

The classical DLVO theory of colloidal stability assumes that colloids and solid surfaces are perfectly smooth at the molecular level. In real systems, however, surface irregularities always exist and an assumption of ideal smooth surfaces breaks down. Consideration of surface roughness is of particular importance for solids and colloidal particles in the subsurface aquatic environment because of inherent physical heterogeneities at the molecular, colloidal, and granular scales. Physical as well as chemical heterogeneities of solid surfaces produce tangential forces which immobilize colloidal particles on solid surfaces [234]. Furthermore, when a colloidal particle is in the close vicinity of a surface having irregularities (i.e. roughness), the interaction can no longer be described by a single value of interaction energy; rather, a distribution of interaction energies should be considered [234,298,301].

The discrepancy with respect to the effect of particle size on the kinetics of particle coagulation was originally attributed to the effect of surface roughness [127,302]. Reerink and Overbeek [302] suggested that the total interaction energy between two particles may be determined by the radius of curvature of protrusions (surface irregularities) rather than by the curvature of the interacting particles. More recently, Shulepov and Frens [303] proposed a model for the effect of surface roughness on the stability ratio in slow, Brownian coagulation. Their analysis shows that the insensitivity of observed stability ratios to particle size can be attributed to surface roughness. The analysis of Shulepov and Frens, however, neglects other factors, such as surface charge heterogeneity, that strongly influence coagulation kinetics.

Several investigators have attributed the poor agreement between observations and theory in studies concerned with particle deposition kinetics to the roughness of collector surfaces [297,304]. Elimelech and O'Melia [258] showed that the slopes of the stability curves should be much less sensitive to particle size (compared to predictions with smooth collectors) when considering surface roughness. However, at the present time, no complete theories are available that enable prediction of colloid deposition rate onto real, rough surfaces.

7.2.4. Interfacial electrodynamics

Dukhin and Lyklema [305] and van Leeuwen and Lyklema [306] have suggested that some basis for the apparent insensitivity of colloidal stability to particle size may be found by considering the interfacial dynamics of interacting double layers. Those studies found that the extent of lateral adjustment of charge during interaction is dominated by hydrodynamic drag. It was postulated that the drag force may counteract the effect of particle size on the collision efficiency in particle coagulation and deposition because it depends on particle size.

Dukhin and Lyklema [307] treated the dynamics of double layer interaction semi-quantitatively by considering transient double layer disequilibration of interacting spherical particles. In their derivation, they considered desorption-adsorption disequilibrium of charge determining ions as the origin of relaxation-determined retardation. An expression for the stability ratio of coagulating spheres, which includes

an additional resistance term accounting for relaxation, has been derived. Their calculations showed that, under conditions where the relaxation retardation dominates, stability ratios become independent of particle size. Hence, this analysis can resolve the discrepancy with respect to particle size in particle–particle interaction phenomena. However, the resistance due to relaxation increases the stability ratios in coagulation (or decreases collision efficiencies in deposition), making agreement between theory and experiment poorer.

Kiljstra and van Leeuwen [214] argued that double layer dynamics can explain the discrepancy with respect to particle size only if the time scale for encounter is strongly dependent on the height of the energy barrier. Their theoretical analysis, however, indicates that this condition is unlikely to be satisfied in particle coagulation and deposition phenomena.

In a more recent study, Shulepov et al. [308] extended the analysis of Dukhin and Lyklema [307] described above. They showed that the transient disequilibration of double layers can be quantified by the rate of desorption of charge-determining ions from the interfacial region of interacting particles. Their rigorous quantitative analysis showed that the stability ratio in coagulation does not increase with increasing particle radius when the dynamic aspects of double layers are considered. These authors stated: "There are indications that the experimentally observed insensitivity of the stability ratio W to particle radius may have a dynamic origin".

The actual effect of double layer interaction dynamics on colloidal stability and collision efficiency may be further complicated by the coupling between surface roughness, surface charge heterogeneities, and interfacial electrodynamics. These complex factors may have a profound effect on colloidal stability, but, at the present time, there are no adequate theories to quantitatively assess their role.

7.2.5. *Deposition in secondary minima*

Secondary minima in the total DLVO interaction energy profile can be found at large to moderate separation distances (usually larger than several nanometers as shown in Fig. 3). Under given chemical conditions, the depth of the secondary minimum increases with increasing particle size and the Hamaker constant of the interacting media. The secondary minimum for a given suspension is also dependent on the solution ionic strength; deeper secondary minima occur at higher ionic strength.

In principle, coagulation of colloidal particles in secondary minima is possible, if the resultant of the forces of the thermal energy of particles and the fluid drag is insufficient to drive the particles out of the secondary minima. Indirect evidence for this phenomenon in coagulation has been reported by several investigators [243,309–311]. Wiese and Healy [312], and later other investigators [128,313,314], argued that the apparent independence of stability ratios on particle size in Brownian coagulation can be related to coagulation in secondary minima. Arguments against coagulation in secondary minima, however, were presented by Prieve and Ruckenstein [291]. They argued that the secondary minimum will be saturated with colloids after a very short relaxation time and that steady state coagulation will occur only in the primary minimum.

While some evidence exists for coagulation in secondary minima, there is no clear evidence at the present time for particle deposition from flowing suspensions in secondary minima. Several arguments against significant particle deposition on spherical collectors in secondary minima have been discussed by Tobiason [279] and Elimelech and O'Melia [129]. In a more recent study [315], however, it was argued that fast, transport-controlled deposition of particles in secondary minima and subsequent escape of captured particles may determine the deposition rate when a significant electrostatic barrier exists.

7.3. *Assessment of discrepancies with relation colloid transport in groundwater*

With the exception of interfacial electrodynamics, all explanations discussed in the previous section have been shown to narrow the gap between theoretical predictions and experimental observations in particle deposition kinetics under unfavorable chemical conditions. Moreover, some of these

factors (e.g. surface roughness, charge heterogeneity, and interfacial electrodynamics), are probably interrelated (coupled), thus making fundamental theoretical analyses of this subject extremely difficult. For practical situations involving unfavorable colloidal deposition in engineered or natural systems, it is of utmost importance to isolate the controlling factor(s) for colloid deposition.

Song et al. [287] showed that colloid deposition rates onto solids with only minor amounts of surface charge heterogeneity are orders of magnitude larger than those for similar surfaces having no charge heterogeneity. Even "ideal" collector surfaces used in controlled laboratory experiments, such as soda-lime glass beads, contain bulk chemical impurities (Al_2O_3 and Fe_2O_3) that give rise to favorable deposition sites [275,287]. The investigation of Song et al. [287] demonstrates that the initial deposition rate onto heterogeneously charged surfaces under unfavorable chemical conditions is ultimately controlled by the degree of surface charge heterogeneity. Recent experiments using anionic surfactants to mask favorable deposition sites have indeed achieved much better agreement between predicted and measured deposition rates [316]; however, "non-DLVO" repulsive forces that might develop due to adsorbed surfactant molecules were not considered.

Because solids in the subsurface aquatic environment have much higher degrees of surface heterogeneities than clean collectors used in laboratory experiments, it appears that surface charge heterogeneity is the key factor to consider when dealing with colloidal transport in groundwater. The large degree of surface charge heterogeneity will dominate the particle deposition behavior under unfavorable chemical conditions and the contributions of all other factors discussed in Section 7.2 to particle deposition are expected to be relatively insignificant. Hence, proper characterization of surface heterogeneities of aquifer solids may lead to improvements in our ability to predict deposition rates based on solution and surface chemistry. In the following section, we review current approaches to quantify surface charge heterogeneity and its effect on colloid deposition rate under unfavorable chemical conditions.

8. Colloid deposition kinetics in heterogeneously charged porous media

In the previous section, it was suggested that surface charge heterogeneity is the key factor controlling the deposition rate of colloids onto mineral surfaces in groundwater. In this section, we briefly discuss the main sources of surface charge heterogeneity of solids in the subsurface aquatic environment. We also discuss mathematical approaches to model the charge heterogeneity of solid surfaces and to calculate colloid deposition rate onto heterogeneously charged surfaces.

8.1. The heterogeneity of solids in the subsurface aquatic environment

Solid phases in subsurface environments (e.g. soil and aquifer sediments) exhibit both physical and chemical heterogeneity. Silicates and aluminosilicates are the dominant primary minerals in the stationary solid phase, especially quartz, feldspar, micas, and clays [64,65]. In addition, carbonates and the oxides of iron, aluminum, and manganese represent an important group of accessory minerals that are often present as coatings on the primary minerals and as intergranular cement [64,65,108,317,318]. Aquifer sediments also contain a heterogeneous variety of complex organic molecules characterized by a wide range of molecular weights and compositions [120,319]. These organic molecules are found attached to mineral surfaces as organic coatings or organic particulate matter occupying the interstitial regions of the stationary matrix.

The surfaces of all silicate and metal oxide minerals are covered with hydroxyl surface functional groups [64,65,320]. However, not all surface hydroxyl groups are chemically identical to one another, which leads to chemical heterogeneity of mineral surfaces [285,295,296,321,322]. Crystal morphology influences the reactivity of surface functional groups by controlling their geometric relation to the underlying crystalline lattice. Different ionic arrangements along adjacent crystal faces give rise to variations in the coordination of surface functional groups with the underlying ionic framework. As a consequence, the reactivity of

hydroxyl groups will vary according to the orientation of the crystal face in relation to the crystalline framework.

Due to the presence of physical and chemical heterogeneities, most natural surfaces have an uneven, or heterogeneous charge distribution. Surface charge heterogeneities can be classified in terms of scale as either macroscopic or microscopic. For deposition of colloidal particles onto heterogeneous surfaces, microscopic charge heterogeneity describes charge variations on a molecular level, whereas macroscopic charge heterogeneity refers to variations on the scale of colloidal particle dimensions or more. Microscopic charge heterogeneities arise from the regular arrangement of oppositely charged ions in the crystalline lattice, as well as from molecular-level structural defects such as kinks and screw dislocations [64,295,296, 321–324]. Macroscopic charge heterogeneity on natural surfaces may result from chemical anisotropy between adjacent crystal faces, the presence of surface impurities, and bulk chemical impurities [65,108,162,295,296].

8.2. *Models for charge heterogeneity of solid surfaces*

Song et al. [287] have introduced the concept of nominal surface potential as a means of calculating the double layer interaction energy between a particle and heterogeneous collector surfaces with the use of the current DLVO theory. The nominal surface potential of a heterogeneous surface is equivalent to the potential of a homogeneous surface which would produce the same double layer interaction with a particle as the heterogeneous surface at an identical separation distance. The nominal potential represents the homogeneous analog of a heterogeneously charged surface [325]. By replacing the actual surface potential with a nominal surface potential, double layer interaction energies can be calculated between heterogeneous surfaces by using the available expressions developed for interaction between ideal, homogeneously charged surfaces.

Surface charge heterogeneity can be characterized by the distribution of local potential on the surface. Generally, it is not possible to assign exact values for variations in potential over the entire surface. However, a probability distribution of nominal potentials may be assigned according to a priori knowledge or assumptions about surface characteristics. Song et al. [287] proposed two models to describe surface charge heterogeneity, namely the patchwise and random distribution models which are described below. These models are extensions of studies on the adsorption of dissolved species [294,325] or gases [294,326] onto solid surfaces.

Patchwise heterogeneity implies that surface sites of equal potential are grouped together in macroscopic patches, each of which can be treated as a homogeneous surface [287,325]. When considering large patches ($\kappa R > 1$, with κ being the inverse Debye length and R the size of the patch), it may be assumed that each patch behaves as a homogeneous, isolated surface in equilibrium with the bulk solution and that the interactions at patch boundaries can be neglected. In groundwater aquifers, macroscopic surface heterogeneities such as iron, aluminum, or manganese oxide patches on minerals are representative of large patchwise heterogeneities [108].

In the patchwise model, the ratio of each type of patch to the entire area of the collector surface, denoted as p_i or as a probability density function $p(\psi_i)$, is given by [287]

$$p_i = p(\psi_i) = \lambda_i \qquad i = 1, 2, \ldots, n \tag{8.1}$$

where ψ_i and λ_i are the surface potential and the surface fractions of patches of type i respectively, and n is the number of patch types. In cases where the heterogeneity of surface charge originates from one type of patch interspersed throughout a surface of otherwise uniform potential, the patches are conventionally taken to be the sites which are more favorable for particle deposition.

Random (continuous) heterogeneity indicates that sites of equipotential are randomly distributed over the entire surface. The random distribution model may be applied to collectors whose surfaces do not have an obvious patchwise arrangement of charge distribution, such as glasses and other amorphous substances. Because there is often no information available on the distribution of surface potentials, a normal distribution is generally

assumed [287]:

$$p(\psi) = \frac{1}{\sigma\,(2\pi)^{1/2}} \exp\left[-\frac{(\psi - \psi_0)^2}{2\sigma^2} \right] \tag{8.2}$$

where ψ_0 and σ are the mean and standard deviation of the potential respectively.

The patchwise and random distribution models should be regarded as mathematical representations of surface charge heterogeneity because, at the present time, there are no available methods to characterize actual charge site distribution of natural grain surfaces. Despite their limited nature, however, these models are useful means of describing the characteristics of surface charge heterogeneity as applied to particle deposition and transport.

8.3. Calculation of particle deposition rate onto heterogeneously charged surfaces

The overall particle deposition rate is the average of local particle deposition occurring over the entire collector surface. Generally, the kinetics of particle deposition onto collectors with surface charge heterogeneity can be described by the overall particle deposition rate [287]:

$$\eta = \int_S \eta(\psi) p(\psi) d\psi \tag{8.3}$$

Here η and $\eta(\psi)$ are the overall and local particle deposition rates (expressed as single collector efficiencies) respectively, ψ is the nominal surface potential, S is the range of possible variations of nominal potential, and $p(\psi)$ is the probability density function of the potential ψ. In cases where the patch model is used, Eq. (8.3) simplifies to

$$\eta = \sum_{i=1}^{n} \lambda_i \eta_i \tag{8.4}$$

where η_i is the particle deposition rate onto patches of type i, and λ_i is the surface fraction of patches of type i (i.e. the ratio of total area of patches of type i to the entire collector surface).

When only one kind of favorable patch exists on an otherwise homogeneous surface which is unfavorable for particle deposition, Eq. (8.4) can be further simplified to

$$\eta = \lambda \eta_P + (1 - \lambda)\eta_R \tag{8.5}$$

where η_P and η_R represent the particle deposition rates onto the patches and the rest of the collector surface respectively, and λ and $(1 - \lambda)$ are the area fractions of the patches and the rest of the collector surface respectively. When surface charge heterogeneity originates from positively (or uncharged) patches on an otherwise unfavorable negatively charged surface, the overall particle deposition rate may be approximated by

$$\eta = \lambda \eta_P \tag{8.6}$$

This simple expression shows that the deposition rate in the later case is ultimately controlled by the surface fraction of patches. Song et al. [287] showed that λ values on the order of 1% or less are sufficient to explain experimental unfavorable colloid deposition rates with the framework of the DLVO theory.

In cases where the Gaussian distribution model is used, Eq. (8.3) becomes

$$\eta = \int_{-\infty}^{\infty} \frac{\eta(\psi)}{\sigma\,(2\pi)^{1/2}} \exp\left[-\frac{(\psi - \psi_0)^2}{2\sigma^2} \right] d\psi \tag{8.7}$$

The average value of the surface potential of the collector ψ_0 cannot be used to exclusively determine the kinetics of particle deposition. The other necessary parameter is the standard deviation of the potential distribution σ, which represents the degree of surface charge heterogeneity.

Results based on the above theoretical models show that particle deposition rate under unfavorable chemical conditions is extremely sensitive to surface charge heterogeneities [287]. While small degrees of surface charge heterogeneity have a marked effect on colloidal deposition rate, this should not affect the average surface (or zeta) potential of the collector surface. The average surface potential of the collector surface is determined by the chemical characteristics of the unfavorable surface fraction because $\lambda \ll 1$. This important aspect has not been addressed in colloidal transport and deposition studies where the mean surface potential of collectors is used to

calculate the theoretical deposition rates under unfavorable chemical conditions.

9. Dynamic (transient) aspects of colloidal transport and deposition

In the previous section, we described filtration theories for calculating particle deposition rate in granular porous media. Because particle deposition is a dynamic (transient) process, the theories presented earlier are valid only for the initial stage of particle deposition. This section summarizes several aspects pertaining to the dynamics of particle deposition and transport in granular porous media. The role of the so-called "blocking" phenomenon in particle deposition dynamics is discussed and a quantitative approach for incorporating blocking in colloidal transport models is presented.

9.1. The blocking phenomenon

Particle deposition from aqueous suspensions onto stationary surfaces is a dynamic phenomenon characterized by a transient, or time-dependent, rate of deposition. As particles deposit on collector surfaces, the deposition rate will either decrease or increase, depending on the nature of particle–collector and particle–particle interactions [241,288,327–334]. A declining deposition rate results when particle–particle interactions are repulsive, so that collector surfaces become progressively occluded as particles accumulate. This surface exclusion phenomenon is termed blocking [200,234,332]. Blocking restricts particle density on collector surfaces to a single monolayer in thickness and may prevail in groundwaters having low ionic strength and reduced levels of hardness. In the absence of an electrostatic energy barrier, particle–particle interactions are favorable so that deposited particles enhance the rate of deposition by acting as additional collectors [85,241,335]. This dynamic phenomenon is known as ripening, and leads to a rather complex multilayer coverage of collector surfaces [241,328,335–343]. Ripening may occur in groundwaters having elevated levels of dissolved solids or hardness.

Because the majority of the available surface area of solids in groundwater has chemical characteristics unfavorable for particle deposition, colloidal deposition in groundwater is thought to be largely restricted to the minor surface fraction having energetically favorable charge characteristics [287,344–347]. These favorable sites, resulting from surface charge heterogeneity, are often manifested as positively-charged patches on the surface of negatively-charged mineral grains [108,287,318,348]. Patchwise charge heterogeneities are general to all aqueous geologic settings, originating from inherent differences in the surface properties of adjacent crystal faces on mineral grains [295,296,323,349], and from minerals having bulk- or surface-bound chemical impurities [109,287]. As discussed previously in this paper, the oxides of iron, aluminum, and manganese are the most common source of surface charge heterogeneity in the groundwater environment. These oxides carry a positive surface charge at near neutral pH, and are generally present in minor amounts as surface coatings on mineral grains [318,350,351]. Evidence for the important role played by oxide coatings in particle deposition and transport can be found in the experimental studies of colloid transport [318,334], bacterial transport [344,348,352,353], and virus transport [347] through porous media.

The dynamics of particle deposition in natural aquatic environments are thought to be largely determined by the rate at which favorable surface patches are blocked by deposited particles [287,346]. As favorable deposition sites are being blocked, the deposition rate falls off quickly with time at surface coverages which are characteristically very small. This behavior of declining deposition rate with the coverage (or blocking) of favorable deposition sites is schematically illustrated in Fig. 9.

9.2. Previous studies on the dynamics of blocking in colloid deposition

There are several systematic studies dealing with blocking and its influence on particle deposition dynamics in granular porous media [200,201,288,330,331,345]. These investigations point to the paramount importance of ionic

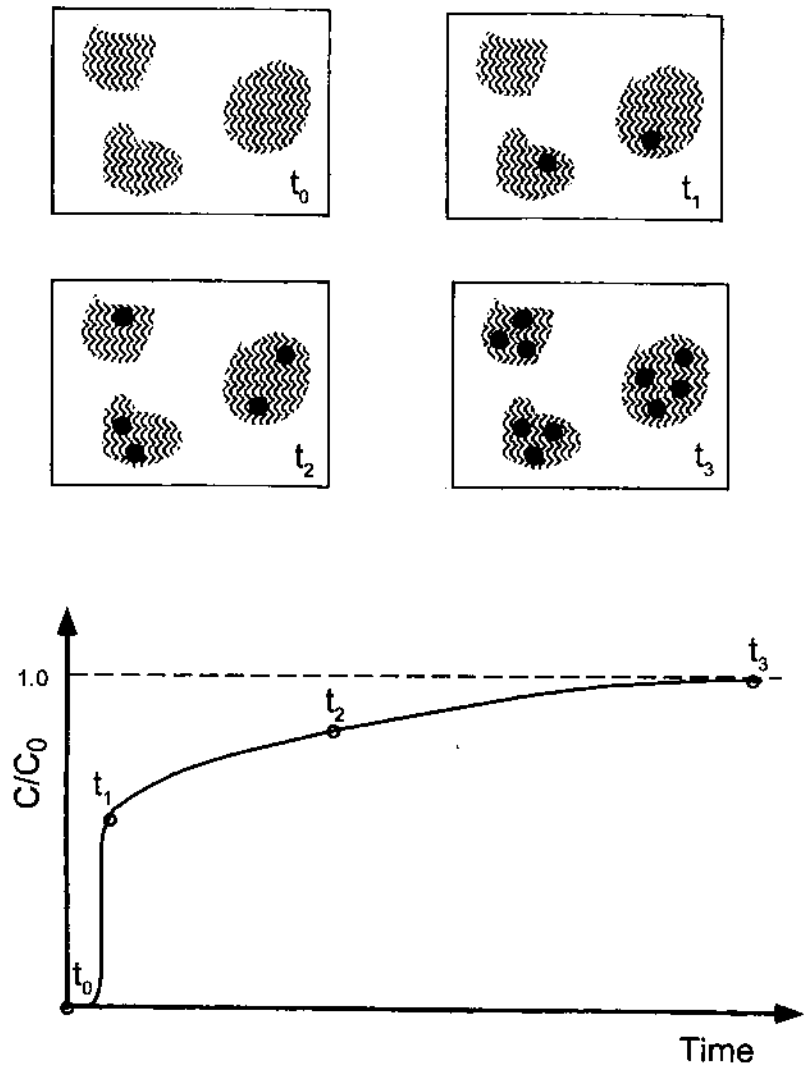

Fig. 9. Schematic illustration of the process of blocking of favorable patches in colloid flow through heterogeneously charged porous media and the resulting effect on the particle breakthrough curve of a short packed column. Patches (favorable for deposition) are denoted by the shaded areas and deposited colloidal particles are denoted by dark spheres. The time t_0 represents the porous medium before the flow of particles through the column. The time t_1 corresponds to "clean bed" removal, that is, before deposited particles influence the subsequent deposition of particles. For patchwise heterogeneity, the rate of deposition at this stage is proportional to the fraction of favorable patches (see Eq. (8.6)). As time progresses, favorable patches are being blocked by deposited particles and the rate of deposition decreases (i.e. more particles are being eluted from the column as represented by time t_2). When all patches are blocked by deposited particles, the deposition rate drops to zero and $C/C_0 \rightarrow 1.0$ (represented as t_3).

strength in controlling the area of collector surface that is excluded by deposited particles. Rajagopalan and Chu [288] and Song and Elimelech [331] demonstrated that colloids in aqueous solutions of low ionic strength deposit as "soft" particles having an expanded double layer and an excluded area several times larger than their projected area. An inverse relationship between ionic strength and blocking was exhibited in the experimental results of Ryde et al. [330], where a reduction in electrolyte concentration resulted in an enlargement of the excluded area.

More recently, Johnson and Elimelech [200] have shown that colloid blocking dynamics may be described using random sequential adsorption (RSA) mechanics. Liu et al. [201] presented experimental breakthrough curves under various chemical conditions to study the role of solution chemistry in colloid deposition dynamics. Calculated values of the excluded area were determined from the particle breakthrough curves for both Brownian and non-Brownian particles. Liu et al. [201] demonstrated that the excluded area for non-Brownian particles at low ionic strength is greater than that of Brownian particles and that a complete blocking of the collector surface can be attained at relatively low surface fractional coverages.

The effect of blocking on colloid transport in porous media is demonstrated in Figs. 10 and 11. In these Figures, the breakthrough curves of aluminum oxide colloids flowing through a packed column of quartz sand are displayed. Under the experimental conditions described in the Figures, the aluminum oxide particles are positively charged

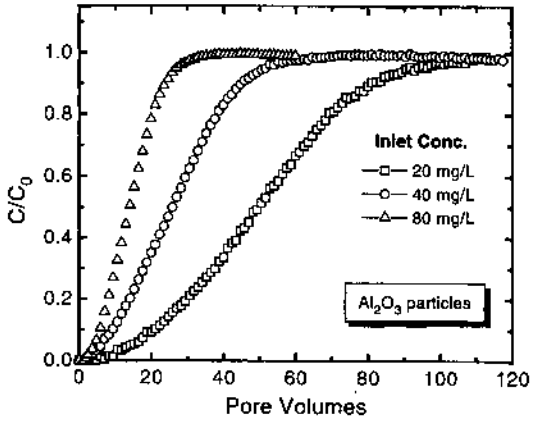

Fig. 10. Particle breakthrough curves for colloidal alumina depositing onto quartz sand grains. The curves are shown for various inlet colloid concentrations as indicated. The results demonstrate the effect of particle concentration on the rate of blocking. As particle concentration increases, the rate of blocking increases and particles break through the column at an earlier time. Experimental conditions were as follows: solution ionic strength, 10^{-3} M KCl; approach velocity, 0.1 cm s^{-1}; bed depth, 14.2 cm; particle diameter, 0.12 μm; grain diameter, 0.21 mm; pH, 5.6; temperature, 25°C. Data were taken from Liu [354].

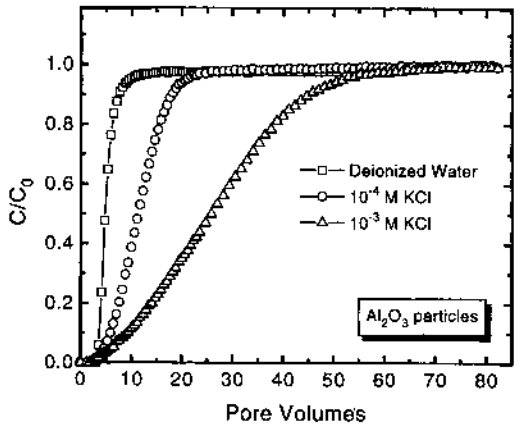

Fig. 11. Particle breakthrough curves for colloidal alumina depositing onto quartz sand grains. The curves are shown for different ionic strengths and fixed inlet particle concentration. The results demonstrate the effect of ionic strength on the rate of blocking. At low ionic strengths, the rate of blocking increases because of expanded double layers of particles, so that particles break through the column at an earlier time. Experimental conditions were as follows: particle concentration, 40 mg l^{-1}; approach velocity, 0.1 cm s^{-1}; bed depth, 14.2 cm; particle diameter, 0.12 μm; grain diameter, 0.21 mm; pH, 5.6; temperature, 25°C. Data were taken from Liu [354].

and the sand grains are negatively charged. This results in favorable particle–grain interaction, but the particle–particle and particle–retained particle interactions are unfavorable. The alumina breakthrough curves demonstrate the expected deposition dynamics encountered when blocking dominates, with a more pronounced rate of blocking observed for higher particle concentrations (Fig. 10) and reduced ionic strengths (Fig. 11) [354]. The dramatic role of solution ionic strength in controlling the rate of blocking and the subsequent shape of the colloid breakthrough curves is clearly demonstrated in Fig. 11. For the physical and chemical conditions employed, a complete removal of particles is achieved initially ($C/C_0 \approx 0$), and the deposition rate is transport limited. However, as particles deposit onto the bare grains, blocking progresses until the rate of particle deposition drops to zero (i.e. $C/C_0 = 1$). Johnson and Elimelech [200] showed that the sigmoidal shape of the breakthrough curves is predominately attributed to the irreversible deposition and blocking occurring on the sand grains.

For particle deposition in a porous medium composed of spherical collector grains, hydrodynamic flow conditions must be considered in addition to solution chemistry when evaluating the excluded area of a deposited particle. Adamczyk et al. [332,355] showed that the excluded area is position-dependent for non-planar collector geometries and non-stagnation point flow conditions. Their work is based on the so-called "hydrodynamic scattering" principle of Dabros and van de Ven [356], which predicts a coupling between repulsive electrostatic forces and shearing hydrodynamic flow. Because of hydrodynamic scattering, the excluded area associated with particle deposition on spherical collectors will change according to the position of a deposited particle on the collector surface due to variations in the intensity of the fluid shear component. Extensive discussions of this subject are given by Adamczyk et al. [332] and Johnson and Elimelech [200].

9.3. *Quantitative description of colloidal transport*

The concentration of particles in a dilute suspension flowing through a porous medium, where irreversible deposition of particles onto stationary media surfaces takes place, is governed by the advection–dispersion–deposition equation [345]:

$$\frac{\partial C}{\partial t} = \nabla\cdot(\boldsymbol{D}_h\cdot\nabla C) - \nabla\cdot(\boldsymbol{V}C) - \frac{f}{\epsilon}RC \qquad (9.1)$$

Here C is the particle number concentration, t is the time, $\boldsymbol{V}$ is the interstitial fluid velocity vector, $\boldsymbol{D}$ is the particle hydrodynamic dispersion tensor, f is the specific surface area of stationary media (area per unit volume), ϵ is the porosity, and R is the overall particle transfer rate (i.e. the product RC is the overall particle deposition rate). As will be shown later, the particle transfer rate R determines the dynamic (transient) behavior of particle deposition and transport in porous media. Because particle deposition in the subsurface aquatic environment is believed to occur mostly on favorable patches, the assumption of irreversible particle deposition is quite reasonable [264,271,298,345].

Equation (9.2) is in principle similar to the advection dispersion equation used to describe the transport of colloids [38,243,267,357,358], bacteria [359–361], or viruses [265,362] in columns and groundwater systems. These studies, however, did not properly address the role of blocking and excluded area effects in particle transport. Furthermore, none of the above mentioned studies addressed the relation between surface charge heterogeneity and particle blocking dynamics. A more fundamental approach for colloidal transport in heterogeneously charged porous media has been recently presented by Song and Elimelech [345]. The principles of this approach are given in the following paragraphs.

The overall particle transfer rate in a representative elementary volume (REV) of the porous medium can be written in its most general form as [345]

$$R = \frac{1}{S}\int_S K(\xi)g(F_0)d\xi \qquad (9.2)$$

where S is the total surface area in the REV and $K(\xi)$ is the local particle transfer rate coefficient to the "clean" (uncovered) area element $d\xi$. The term F_0 denotes the local bare fraction of the surface, which depends on the location ξ; that is, $1 - F_0$ is the local fraction of the surface which is covered with deposited particles. The function $g(F_0)$ accounts for the effect of retained particles on the local particle transfer rate. It is defined as the ratio of the particle transfer rate at surface coverage $(1 - F_0)$ to the particle transfer rate onto a clean, uncovered collector. This function is, in principle, similar to the dynamic blocking function discussed later in the next section. The local particle transfer rate $K(\xi)$ is calculated from a microscopic model of particle deposition from dilute flowing suspensions, for the given chemical and physical conditions [247,331,345]. Variations in local deposition rate originate from random surface heterogeneities [287,345] or the fluid flow field pattern around an individual spherical grain [331].

The REV requires dimensions large enough to overcome microscopic-scale fluctuations in the properties of the porous medium. This is accomplished by including a sufficient number of grains (collectors) or pores to allow a meaningful statisti-

cal average as required in the continuum approach. Conversely, the REV must be much smaller than the size of the entire flow domain, as otherwise the resulting average is not representative of the processes occurring at a given point in the porous medium. An excellent discussion of the REV concept for flow and transport phenomena in porous media is given by Bear [363].

Song and Elimelech [345] have introduced the concept of the flux correcting function to describe the effect of surface charge heterogeneity on the dynamics of particle transport and deposition. The flux correcting function is used to characterize the variation in local deposition rate as blocking occurs and the resulting effect on colloid deposition dynamics. In the most general form, the flux correcting function is given by

$$G_0 = \frac{R}{K} = \frac{1}{S}\frac{1}{K}\int_S K(\xi)g(F_0)d\xi \tag{9.3}$$

where K is the average particle transfer rate coefficient obtained by integrating the local particle transfer rate over the entire surface area in the REV. The function $g(F_0)$ describes the relation between the local particle deposition rate and local surface coverage. With the flux correcting function, the colloid transport equation becomes

$$\frac{\partial C}{\partial t} = \nabla\cdot(\boldsymbol{D}_h\cdot\nabla C) - \nabla\cdot(\boldsymbol{V}C) - \frac{f}{\epsilon}KG_0C \tag{9.4}$$

Expressions for the flux correcting function were developed for patchwise and randomly distributed surface charge heterogeneities assuming a linear relationship between $g(F_0)$ and F_0 [345].

Finally, a rate equation for the local surface coverage by retained colloids should be given. The general form of this rate equation is [345]

$$\frac{\partial F_0}{\partial t} = -aK(\xi)g(F_0)C \tag{9.5}$$

where a is the average surface area blocked (excluded) by retained particles. With proper boundary and initial conditions, Eq. (9.4) coupled with the rate equation for surface coverage, Eq. (9.5), can be solved numerically to yield colloidal breakthrough curves or transport fronts of colloids for different time intervals.

9.4. The dynamic blocking function

Adamczyk et al. [332] introduced the dynamic blocking function to characterize the dynamic (transient) nature of the particle deposition rate when blocking occurs. A dynamic deposition rate arises as particles deposit on collector surfaces, thereby excluding a portion of the surface from subsequent particle attachment [200,346]. This results in a declining probability that approaching particles will impact an unoccupied site on the collector surface as deposition proceeds. The dynamic blocking function $B(\theta)$ represents this changing probability as a function of fractional surface coverage θ (note that θ is equivalent to $1-F_0$ used in Eqs. (9.2)–(9.5)). The dynamic blocking function is indeed a special case of the more general function $g(F_0)$ discussed in the previous subsection.

For initially bare (particle-free) collector surfaces, $B(0)=1$. As deposited particles begin to block surface sites from further deposition, $B(\theta)$ decreases until the maximum attainable surface coverage (often called the jamming limit) is reached (i.e. $\theta = \theta_{max}$) at $B(\theta)=0$. Separate mathematical expressions are available for the dynamic blocking function, based on either the Langmuir adsorption model or RSA mechanics.

9.4.1. The Langmuirian dynamic blocking function

The Langmuirian dynamic blocking function is in principle identical to the linear blocking function described in the classic Langmuir molecular adsorption model [364]. It displays a linear dependence on fractional surface coverage θ [200]:

$$B(\theta) = 1 - \beta\theta \tag{9.6}$$

Here β is the excluded area parameter, which is equivalent to the reciprocal of the maximum attainable surface coverage (jamming limit) θ_{max}. The excluded area parameter is a measure of the collector surface area blocked from subsequent deposition by a deposited particle. It is expressed as a

dimensionless quantity determined by the ratio of the blocked surface area to the projected (cross-sectional) area of retained particles (i.e. $\beta = a/\pi a_p^2$). A method for obtaining β from experimental particle breakthrough curves has been recently presented by Johnson and Elimelech [200].

The Langmuirian dynamic blocking function was originally intended to describe surface exclusion of adsorption sites by point-size molecules. Hence, the Langmuirian dynamic blocking function does not adequately describe surface exclusion effects of larger, finite-size colloidal particles [365]. For deposition of colloids, the relationship between blocking and fractional surface coverage is no longer described by a linear function because of surface exclusion effects. A non-linear dynamic blocking function based on RSA mechanics that addresses surface exclusion effects is described below.

9.4.2. The RSA dynamic blocking function

When stable colloidal particles deposit onto oppositely-charged collector surfaces or favorable patches, the following conditions should apply [200,332,346,366]: (1) attachment is irreversible as long as chemical and hydrodynamic conditions do not change; (2) surface diffusion is negligible; and (3) particle–particle contact is prohibited. Under these conditions, the RSA mechanism is directly applicable and may be used to obtain a dynamic blocking function for colloidal particles.

Schaaf and Talbot [365] developed a dynamic blocking function from the RSA mechanism that applies to deposition of non-interacting (hard) spheres onto flat collector surfaces. Their blocking function is based on a virial expansion of excluded area effects to third order in density, and may be used for low and moderate surface coverage:

$$B(\theta) = 1 - 4\theta + \frac{6(3)^{1/2}}{\pi}\theta^2 + \left(\frac{40}{(3)^{1/2}\pi} - \frac{176}{3\pi^2}\right)\theta^3 \tag{9.7}$$

This equation applies only to deposition of "hard" (non-interacting) spheres. A more general expression, applicable to any collector geometry and "soft" particle deposition (i.e. with consideration of lateral double layer repulsion), may be obtained from Eq. (9.6) based on the jamming limit for general cases, θ_{max} [200,346,367]:

$$B(\theta) = 1 - 4\theta_\infty\beta\theta + \frac{6(3)^{1/2}}{\pi}(\theta_\infty\beta\theta)^2 + \left(\frac{40}{(3)^{1/2}\pi} - \frac{176}{3\pi^2}\right)(\theta_\infty\beta\theta)^3 \tag{9.8}$$

where θ_∞ is the hard sphere jamming limit. This generalized expression for the dynamic blocking function applies to surface coverages below $0.8\theta_{max}$. A separate expression is necessary when surface coverage approaches the jamming limit θ_{max}.

As coverage of a flat collector surface approaches θ_{max}, the dynamic blocking function can be expressed as [200,246,368,369]

$$B(\theta) = \frac{(1-\beta\theta)^3}{2m^2\beta^3} \tag{9.9}$$

This modified expression for the dynamic blocking function applies when surface coverage is in excess of $0.8\theta_{max}$. The jamming limit slope m is determined from particle breakthrough curves following the method outlined by Johnson and Elimelech [200].

10. Concluding remarks

To predict the potential susceptibility of an aquifer to colloid-facilitated transport, three important processes must be understood: (1) the generation of colloids; (2) the association of contaminants with colloids; and (3) the transport of colloids. Presently, only the association of contaminants with colloids can be quantitatively predicted with some degree of certainty. Current knowledge of the mechanisms controlling colloid generation and transport is inadequate to accurately predict these processes in natural sediments. Despite great strides in understanding the processes of mobilization and deposition of colloids in model systems, the heterogeneity of natural sediments presents a great obstacle to predictions of the potential for colloid-facilitated transport.

10.1. Colloid mobilization

Field observations indicate that the mobilization of existing colloids by chemical and physical perturbations is the predominant source of colloids in groundwater. Chemical perturbations brought on by contaminant plumes represent the most common form of colloid mobilization. In some instances, natural processes in aquifers can also generate colloids through chemical perturbations.

Chemical perturbations like decreasing ionic strength, increasing pH, and increasing concentrations of surfactants and dissolved organic matter can mobilize colloids. In contaminant plumes, which are frequently characterized by elevated ionic strength and decreased pH, colloid mobilization may not seem likely. However, contaminant plumes often contain other compounds, such as organic acids, organic macromolecules, reductants, and detergents, capable of causing colloid mobilization through reversal of surface charges or dissolution of cementing mineral phases. Prediction of the susceptibility of natural sediments to these changes is a daunting task owing to the heterogeneity of most natural sediments. In model systems, the effects of these chemical perturbations can be predicted qualitatively; however, a quantitative understanding of these processes is hampered by insufficient knowledge of intersurface forces at very small separation distances.

In natural systems, current knowledge of colloid mobilization can be applied only very generally. If detailed characterizations of sediment mineralogy and morphology are made, assessments of the potential for colloid mobilization can be made. For instance, the measurements of colloid mobilization from an iron oxide-coated sand made by Ryan and Gschwend [109] lead to the generalization that the reversal of charge or dissolution of the cementing iron oxide phase will lead to rapid colloid mobilization. More research is required on colloid mobilization in other common surficial sediments to extend these generalizations to a wider range of natural aquifers. Assessments of colloid mobilization tendencies can be made with some basic information that should be readily available, like solution chemistry, pH, mineral composition, mineral pH_{pzc}, and clay-sized content of the sediments.

In fractured media and macroporous soils, physical perturbations are the most common form of colloid mobilization. The increased velocities resulting from flow channeled into fractures and macropores results in colloid mobilization through hydrodynamic shear. Colloid mobilization in fractured media is of great concern in nuclear waste disposal because many of the world's high-level nuclear waste repositories are to be situated in low permeability geological formations in which the only form of transport is through fractures. Colloid mobilization in soil macropores is also a mechanism of colloid generation in groundwater because colloids mobilized in the soil zone may eventually be transported to the water table.

Prediction of the mobilization of colloids by shear is somewhat satisfactory in model systems, with the exception that intersurface forces are poorly understood at very small separation distances. These forces control the adhesion of the attached colloids. Beyond the realm of spherical colloids and flat collector surfaces, however, little is understood about the effect of elevated flow rates on colloid mobilization by shear. Again, the heterogeneity of natural sediments is a problem. Colloids and sediment grains come in different size, shape, and chemical composition, all factors that affect the susceptibility of colloids to hydrodynamic detachment. Fractures and macropores and the flow within are usually poorly characterized. Assessing the potential for colloid mobilization by shear in natural aquifers and soils is still mainly a matter of experimentation.

This situation could be improved by experiments directed toward model systems that better represent natural sediments, by testing the detachment of polydisperse populations of attached particles. In addition, further experiments with natural aquifer materials could be performed under controlled settings by devising appropriate means of isolating these sediments from the field.

10.2. Colloid transport and deposition (filtration)

Field observations of colloidal transport and deposition are rather limited. Much of our current

knowledge comes from field experiments with traceable colloids, most commonly bacteria, viruses, and latex microspheres. These field studies demonstrate substantial attenuation in the number concentration of injected particles as they travel to the monitoring well. The reports in the literature indicate that particles can break through at an earlier or a later time than a conservative tracer. Observations of an earlier breakthrough of particles are most likely attributed to the phenomenon of size-exclusion chromatography, where particles are excluded from the smaller pore spaces and more tortuous flow paths. A substantial early breakthrough relative to a conservative tracer has been observed in several field tests of virus transport and is most likely attributed to virus restriction to fracture flow and diffusion of the tracer into the clay matrix. These physical heterogeneities are difficult to characterize and thus they cannot be incorporated adequately in colloidal transport models.

Recent laboratory studies of colloidal transport and deposition in natural sediments point to the important role of the chemical composition of mineral grains. The presence of iron oxide coatings on mineral grains has been shown to significantly enhance the retention of colloids and thus limit their mobility. Recent theoretical studies emphasize the important role of surface charge heterogeneities in colloid deposition and transport. Future research should focus on development of experimental methods to characterize and quantify the surface chemical heterogeneities of natural sediments. Quantification of the chemical heterogeneity of natural sediments is a key to prediction of colloidal transport in groundwater.

Current filtration theories are adequate for prediction of colloidal deposition under so-called favorable chemical conditions. The failure of filtration theories to predict the capture of colloids in natural sediments under unfavorable chemical conditions is most likely attributed to chemical heterogeneities of colloid and mineral grain surfaces. Recent theoretical studies clearly show that particle deposition rates in heterogeneously charged porous media are much less sensitive to variations in solution ionic strength compared to theoretical predictions within the framework of the DLVO theory, as indeed observed in laboratory experiments. Colloidal transport experiments in well-controlled chemically heterogeneous porous media should be designed in an attempt to test theories of colloid deposition kinetics in heterogeneously charged porous media.

Theoretical and experimental studies demonstrate that the process of particle deposition in heterogeneous porous media is a transient, time-dependent process. Filtration theories are applicable only to the initial stages of filtration where mineral grains are devoid of retained particles. As particles deposit onto mineral surface sites (regions) with charge characteristics favorable for deposition, the particle deposition rate progressively declines due to the phenomenon of blocking. While blocking and its effect on the dynamics of colloid transport and deposition in model systems in fairly well understood, the application of blocking to the subsurface aquatic environment is seriously complicated because of the physical and chemical heterogeneities of natural sediments.

11. Acknowledgments

The authors acknowledge the helpful comments of three anonymous reviewers. J.N.R. acknowledges the financial support of the National Science Foundation (Research Grants BES-9307190 and CTS-9410301) and the National Water Research Institute/US Environmental Protection Agency (Research Grant HRA 699-514-92). M.E. acknowledges the support of the National Science Foundation (Research Grant BCS-9308118) and the W.M. Keck Foundation (Engineering Teaching Excellence Award). The endeavors of past doctoral students, Lianfa Song, Philip Johnson, and Daylin Liu of UCLA, are also greatly appreciated.

List of symbols

A	Cross-sectional area above a flat surface collector
A_{123}	Hamaker constant of interacting media (particle–water–collector)

A_S porosity-dependent parameter used in Happel's model
a average surface area blocked by one retained particle (for a monolayer deposition)
a_c spherical collector radius
a_p spherical particle radius
$B(\theta)$ dynamic blocking function
b radius of the fluid envelope in Happel's model defined by Eq. (6.14)
C particle concentration
C_0 inlet or bulk particle concentration
$\boldsymbol{D}$ particle diffusion tensor
$\boldsymbol{D}_h$ particle hydrodynamic dispersion tensor
D_∞ particle diffusion coefficient in an infinite medium; $D_\infty = k_B T/(6\pi\mu a_p)$
d_c spherical collector diameter
d_p spherical particle diameter
$\boldsymbol{F}$ external force vector
$\boldsymbol{F}_{col}$ colloidal force vector
$\boldsymbol{F}_G$ gravitational force vector
F_A adhesive force due to net DLVO attraction
F_D drag force on attached spherical particle
F_L lift force on attached spherical particle
F_0 local bare (clean) surface fraction
f specific surface area of stationary media (area per unit volume)
G_0 flux-correcting function
g gravitational acceleration
$g(F_0)$ function relating local particle transfer rate to local surface coverage
h surface-to-surface separation distance
I overall particle deposition rate on a spherical collector
$\boldsymbol{J}$ particle flux vector
$J_\perp$ local perpendicular flux of particles
K average particle transfer rate coefficient
$K(\xi)$ local particle transfer rate coefficient
K_d equilibrium sorption distribution coefficient
k proportionality constant in the particle concentration–size relationship; $N = k d_p^{\beta^*}$
k_{att} attachment rate coefficient
k_B Boltzmann's constant (1.3805×10^{-23} J K^{-1})
k_{det} detachment rate coefficient
k_{dif} rate coefficient for colloid diffusion across the diffusion boundary layer
k_F pseudo first order constant used in Eq. (6.16)
L filter (porous medium) depth (length)
l thickness of flow area above a flat collector surface
l_x lever arm for torque due to adhesion
l_y lever arm for torque due to drag
m jamming limit slope
N number concentration of particles at a given particle size interval
N_G dimensionless parameter defined by Eq. (6.22)
N_{LO} dimensionless parameter defined by Eq. (6.20)
N_R aspect ratio defined by Eq. (6.21)
n number of patch types used in Eqs. (8.1) and (8.4)
pH_{iep} isoelectric point
pH_{pzc} point of zero charge
Q source or sink term used in Eq. (6.1)
Q_f volumetric flow rate past flat collector surface
R overall particle transfer rate
S total surface area in the representative elementary volume (REV)
T absolute temperature
T_A torque due to adhesive force
T_D torque due to drag force
t time
t_{dif} characteristic diffusion time for Brownian particle
U approach (superficial) velocity of fluid
U_x tangent pore velocity at distance a_p from the collector surface
U_x^{crit} critical pore velocity for particle detachment by hydrodynamic shear
$\boldsymbol{u}$ particle velocity vector
$\boldsymbol{V}$ interstitial velocity vector
V pore velocity
x axial coordinate
x_0 minimum separation distance between particle and collector surface (m)

Greek letters

α collision (attachment) efficiency
β excluded area parameter used in Eqs. (9.6),

(9.8), and (9.9); or a function defined by Eq. (6.16). These are not related.

β^* exponential constant in particle concentration–size relationship; $N = kd_p^{\beta^*}$

Δ arbitrary point beyond the energy barrier used in Eq. (6.9)

δ separation distance at the primary minimum

δ_{bl} diffusion boundary layer thickness

δ_ϕ interaction boundary layer thickness

ϵ porous medium (filter) porosity

η single collector efficiency

η_0 single collector efficiency in the absence of double layer interaction (favorable)

η_P single collector efficiency of favorable patch

η_R single collector efficiency of unfavorable regions of collector grains

λ surface fraction of favorable patches

μ dynamic viscosity

θ fractional surface coverage

θ_{max} jamming limit

θ_∞ hard sphere jamming limit

ν kinematic viscosity

ρ density of fluid

ρ_b bulk density

ρ_p density of particles

σ standard deviation in surface potential used in Eq. (8.2)

ϕ^{tot} total DLVO potential energy

ϕ^{dl} double layer potential energy

ϕ^{vdW} van der Waals potential energy

ϕ^{det} height of detachment energy barrier, $|\phi_{max} - \phi_{min1}|$

ϕ_{min1} primary minimum in DLVO potential energy

ϕ_{max} primary maximum (energy barrier) in DLVO potential energy

ϕ_{min2} secondary minimum in DLVO potential energy

ψ local or nominal surface potential

ψ_0 mean surface potential

ω velocity gradient

ξ local point on porous medium surface

Abbreviations

DLVO Derjaguin–Landau–Verwey–Overbeek

IFBL Interaction force boundary layer

NOM Natural organic matter

RSA Random sequential adsorption

References

[1] A. Avogadro and G. de Marsily, Mat. Res. Symp. Proc., 26 (1984) 495.

[2] J.F. McCarthy and J.M. Zachara, Environ. Sci. Technol., 23 (1989) 496.

[3] V. Moulin and G. Ouzounian, Appl. Geochem., Suppl. Issue No. 1 (1992) 179.

[4] D.R. Champ, J.L. Young, D.E. Robertson and K.H. Abel, Water Poll. Res. J. Canada, 19 (1984) 35.

[5] R.W. Buddemeier and J.R. Hunt, Appl. Geochem., 3 (1988) 535.

[6] W.R. Penrose, W.L. Polzer, E.H. Essington, D.M. Nelson and K.A. Orlandini, Environ. Sci. Technol., 24 (1990) 228.

[7] M. Magaritz, A.J. Amiel, D. Ronen and M.C. Wells, J. Contam. Hydrol., 5 (1990) 333.

[8] C. Amrhein, P.A. Mosher and J.E. Strong, Soil Sci. Soc. Am. J., 57 (1993) 1212.

[9] L. Airey, Chem. Geol., 55 (1986) 255.

[10] S.A. Short, R.T. Lowson and J. Ellis, Geochim. Cosmochim. Acta, 52 (1988) 2555.

[11] M. Benedetti and J. Boulègue, Geochim. Cosmochim. Acta, 55 (1991) 1539.

[12] P. Vilks, J.J. Cramer, D.B. Bachinski, D.C. Doern and H.G. Miller, Appl. Geochem., 8 (1993) 605.

[13] J.B.F. Champlin, Soc. Petroleum Eng. J., December (1971) 367.

[14] G.G. Eichholz, B.G. Wahlig, G.F. Powell and T.F. Craft, Nucl. Technol., 58 (1982) 511.

[15] J. Torok, L.P. Buckley and B.L. Woods, J. Contam. Hydrol., 6 (1990) 185.

[16] R.W. Puls and R.M. Powell, Environ. Sci. Technol., 26 (1992) 614.

[17] R.W.D. Killey, J.O. McHugh, D.R. Champ, E.L. Cooper and J.L. Young, Environ. Sci. Technol., 18 (1984) 148.

[18] J.P.L. Dearlove, G. Longworth, M. Ivanovich, J.I. Kim, B. Delakowitz and P. Zeh, Radiochim. Acta, 52/53 (1991) 83.

[19] F.M. Dunnivant, P.M. Jardine, D.L. Taylor and J.F. McCarthy, Environ. Sci. Technol., 26 (1992) 360.

[20] W.I. Oden, G.L. Amy and M. Conklin, Environ. Sci. Technol., 27 (1993) 1045.

[21] R.J. Bowell, A.P. Gize and R.P. Foster, Geochim. Cosmochim. Acta, 57 (1993) 4179.

[22] N.A. Marley, J.S. Gaffney, K.A. Orlandini and M.M. Cunningham, Environ. Sci. Technol., 27 (1993) 2456.

[23] A.J.A. Vinten, B. Yaron and P.H. Nye, J. Agric. Food Chem., 31 (1983) 664.

[24] C.G. Enfield and G. Bengtsson, Ground Water, 26 (1988) 64.

[25] A.S. Abdul, T.L. Gibson and D.N. Rai, Environ. Sci. Technol., 24 (1990) 328.
[26] B.R. Magee, L.W. Lion and A.T. Lemley, Environ. Sci. Technol., 25 (1991) 323.
[27] L.R. Johnson-Logan, R.E. Broshears and S.J. Klaine, Environ. Sci. Technol., 26 (1992) 2234.
[28] H. Liu and G. Amy, Environ. Sci. Technol., 27 (1993) 1553.
[29] M.L. Brusseau, X. Wang and Q. Hu, Environ. Sci. Technol., 28 (1994) 952.
[30] D.M. Dohse and L.W. Lion, Environ. Sci. Technol., 28 (1994) 541.
[31] W.P. Johnson and G.L. Amy, Environ. Sci. Technol., 29 (1995) 807.
[32] R.A. Freeze and J.A. Cherry, Groundwater, Prentice Hall, Englewood Cliffs, NJ, p. 404.
[33] L.M. McDowell-Boyer, J.R. Hunt and N. Sitar, Water Resour. Res., 22 (1986) 1901.
[34] C.R. O'Melia, in W. Stumm (Ed.), Aquatic Chemical Kinetics, Wiley, New York, 1990, Chapter 14.
[35] M. Elimelech, J. Gregory, X. Jia and R.A. Williams, Particle Deposition and Aggregation: Measurement, Modeling and Simulation, Butterworth–Heinemann, Oxford, 1995.
[36] V. Gounaris, P.R. Anderson and T.M. Holsen, Environ. Sci. Technol., 27 (1993) 1381.
[37] W.B. Mills, S. Liu and F.K. Fong, Ground Water, 29 (1991) 199.
[38] J.Y. Chung and K.J. Lee, Ann. Nucl. Energy, 19 (1992) 145.
[39] P. Grindrod, J. Contam. Hydrol., 13 (1993) 167.
[40] S. Haber and H. Brenner, J. Colloid Interface Sci., 155 (1993) 226.
[41] S. Jiang and M.Y. Corapcioglu, Colloids Surfaces A, 73 (1993) 275.
[42] P.A. Smith and C. Degueldre, J. Contam. Hydrol., 13 (1993) 143.
[43] J.F. McCarthy and C. Degueldre, in J. Buffle and H.P. van Leeuwen (Eds.), Environmental Particles, Vol. 2, Lewis Publishers, Boca Raton, FL, 1993, Chapter 6.
[44] D. Langmuir, U.S. Geol. Surv. Prof. Pap., 650-C (1969) C224.
[45] J.I. Kim, G. Buchau, F. Baumgärtner, H.C. Moon and D. Lux, Mat. Res. Soc. Symp. Proc., 26 (1984) 31.
[46] P.M. Gschwend and M.D. Reynolds, J. Contam. Hydrol., 1 (1987) 309.
[47] D. Postma and B.S. Brockenhuus-Schack, J. Sed. Petrol., 57 (1987) 1040.
[48] C. Degueldre, B. Baeyens, W. Goerlich, J. Riga, J. Verbist and P. Stadelmann, Geochim. Cosmochim. Acta, 53 (1989) 603.
[49] J.N. Ryan and P.M. Gschwend, Water Resour. Res., 26 (1990) 307.
[50] P.M. Gschwend, D.A. Backhus, J.K. MacFarlane and A.L. Page, J. Contam. Hydrol., 6 (1990) 307.
[51] P. Vilks, H.G. Miller and D.C. Doern, Appl. Geochem., 6 (1991) 565.
[52] D. Ronen, M. Magaritz, U. Weber and A.J. Amiel, Water Resour. Res., 28 (1992) 1279.
[53] R.W. Puls, D.A. Clark, B. Bledsoe, R.M. Powell and C.J. Paul, Haz. Wastes Haz. Mater., 9 (1992) 149.
[54] D.A. Backhus, J.N. Ryan, D.M. Groher, J.K. MacFarlane and P.M. Gschwend, Ground Water, 31 (1993) 466.
[55] N. Kallay, E. Barouch and E. Matijević, Adv. Colloid Interface Sci., 27 (1987) 1.
[56] L.M. McDowell-Boyer, Environ. Sci. Technol., 26 (1992) 586.
[57] J.N. Ryan and P.M. Gschwend, J. Colloid Interface Sci., 164 (1994) 21.
[58] D.I. Kaplan, P.M. Bertsch, D.C. Adriano and W.P. Miller, Environ. Sci. Technol., 27 (1993) 1193.
[59] J.N. Ryan, B.D. Honeyman, R. Murphy and R. Shannon, V.M. Goldschmidt Conf., Geochem. Soc., Penn. State Univ., 1995.
[60] P.M. Kearl, N.E. Korte, M. Stites and J. Baker, Ground Water Monit. Remed., 14(4) (1994) 183.
[61] M.A. Hubbe, Colloids Surfaces, 16 (1985) 249.
[62] M.M. Sharma, H. Chamoun, D.S.H. Sita Rama Sarma and R.S. Schechter, J. Colloid Interface Sci., 149 (1992) 121.
[63] S.K. Das, R.S. Schechter and M.M. Sharma, J. Colloid Interface Sci., 164 (1994) 63.
[64] G. Sposito, The Surface Chemistry of Soils, Oxford University Press, New York, 1984.
[65] W. Stumm, Chemistry of the Solid–Water Interface, Wiley Interscience, New York, 1992.
[66] R.P. Schwarzenbach, P.M. Gschwend and D.M. Imboden, Environmental Organic Chemistry, John Wiley and Sons, New York, 1994.
[67] P. Lafrance, L. Marineau, L. Perreault and J.-P. Villeneuve, Environ. Sci. Technol., 28 (1994) 2314.
[68] F.C. Spurlock and J.W. Biggar, Environ. Sci. Technol., 24 (1990) 736.
[69] A. Saltelli, A. Avogadro and G. Bidoglio, Nucl. Technol., 67 (1984) 245.
[70] C.H. Ho and N.H. Miller, J. Colloid Interface Sci., 113 (1986) 232.
[71] W.W. Wood and G.G. Ehrlich, Ground Water, 16 (1978) 398.
[72] R.W. Harvey, L.H. George, R.L. Smith and D.R. LeBlanc, Environ. Sci. Technol., 23 (1989) 51.
[73] R.W. Harvey and S.P. Garabedian, Environ. Sci. Technol., 25 (1991) 178.
[74] J.J.W. Higgo, G.M. Williams, I. Harrison, P. Warwick, M.P. Gardiner and G. Longworth, Colloids Surfaces A, 73 (1993) 179.
[75] L.D. McKay, J.A. Cherry, R.C. Bales, M.T. Yahya and C.P. Gerba, Environ. Sci. Technol., 27 (1993) 1075.
[76] L.D. McKay, R.W. Gillham and J.A. Cherry, Water Resour. Res., 29 (1993) 3879.
[77] P. Rossi, A. DeCarvalho-Dill, I. Müller and M. Aragno, Environ. Geol., 23 (1994) 192.

[78] B.H. Keswick, D.-S. Wang and C.P. Gerba, Ground Water, 20 (1982) 142.
[79] T.R. Walker, B. Waugh and A.J. Crone, Geol. Soc. Am. Bull., 89 (1976) 19.
[80] J.P. Owens, M.M. Hess, C.S. Denny and E.J. Dwornik, U.S. Geol. Surv. Prof. Pap., 1067-F (1983).
[81] M.L. Passaretti and E.V. Eslinger, J. Sed. Petrol., 57 (1987) 94.
[82] N. Molenaar, J. Sed. Petrol., 56 (1986) 359.
[83] K.S. Matlack, D.W. Houseknecht and K.R. Applin, J. Sed. Petrol., 59 (1989) 77.
[84] M.A.S. Moraes and L.F. De Ros, J. Sed. Petrol., 60 (1990) 809.
[85] K.-M. Yao, M.T. Habibian and C.R. O'Melia, Environ. Sci. Technol., 5 (1971) 1105.
[86] R. Rajagopalan and C. Tien, AIChE J., 22 (1976) 523.
[87] H.R. Von Gunten, U.E. Waber and U. Krähenbühl, J. Contam. Hydrol., 2 (1988) 237.
[88] L. Liang, J.F. McCarthy, L.W. Jolley, J.A. McNabb and T.L. Mehlhorn, Geochim. Cosmochim. Acta, 57 (1993) 1987.
[89] T.W. Muecke, J. Pet. Technol., February (1979) 144.
[90] C. Gruesbeck and R.E. Collins, Soc. Pet. Eng. J., 22 (1982) 847.
[91] K.C. Khilar and H.S. Fogler, Soc. Pet. Eng. J., 23 (1983) 55.
[92] J.P. Quirk and R.K. Schofield, J. Soil Sci., 6 (1955) 163.
[93] B.L. McNeal and N.T. Coleman, Soil Sci. Soc. Am. Proc., 30 (1966) 308.
[94] H. Frenkel, J.O. Goertzen and J.D. Rhoades, Soil Sci. Soc. Am. J., 42 (1978) 32.
[95] T.M. Abu-Sharar, F.T. Bingham and J.D. Rhoades, Soil Sci. Soc. Am. J., 51 (1987) 309.
[96] H.I. Nightingale and W.C. Bianchi, Ground Water, 15 (1977) 146.
[97] C.J. Lind, U.S. Geol. Surv. Prof. Pap., 700-D (1970) D272.
[98] D.L. Brown and W.D. Silvey, U.S. Geol. Surv. Prof. Paper, 939 (1977).
[99] L.C. Goldenberg, J. Hydrol., 78 (1985) 183.
[100] L.C. Goldenberg, M. Magaritz, A.J. Amiel and S. Mandel, J. Hydrol., 70 (1984) 329.
[101] L.C. Goldenberg, M. Magaritz and S. Mandel, Water Resour. Res., 19 (1983) 77.
[102] C.S. Land and O.C. Baptist, Petrol. Trans., Oct. (1965) 1213.
[103] G.A. Parks, in W. Stumm (Ed.), Equilibrium Concepts in Natural Water Systems, Adv. Chem. Ser. 67, American Chemical Society, Washington, DC, 1967, Chapter 6.
[104] K.A. Morris and C.M. Sheppard, Clay Min., 17 (1982) 41.
[105] D.L. Suarez, J.D. Rhoades, R. Lavado and C.M. Grieve, Soil Sci. Soc. Am. J., 48 (1984) 50.
[106] A.S. Abdul, T.L. Gibson and D.N. Rai, Ground Water, 24 (1990) 920.
[107] B. Allred and G.O. Brown, Ground Water Monitor. Remed., Spring (1994) 174.
[108] J.N. Ryan and P.M. Gschwend, Geochim. Cosmochim. Acta, 56 (1992) 1507.
[109] J.N. Ryan and P.M. Gschwend, Environ. Sci. Technol., 28 (1994) 1717.
[110] D.A. Backhus, P.M. Gschwend and M.D. Reynolds, EOS Trans. Am. Geophys. Union, 67 (1986) 954.
[111] J.N. Ryan, M.S. Thesis, Massachusetts Institute of Technology, Cambridge, MA, 1988, 250 pp.
[112] M.A. Hubbe, Colloids Surfaces, 16 (1985) 227.
[113] T. Shiga, M. Sekiya, N. Maeda and S. Oka, J. Colloid Interface Sci., 107 (1985) 194.
[114] U.S.E.P.A., Ground Water Sampling: A Workshop Summary, U.S. Environmental Protection Agency, Rep. EPA/600/R-94/205, 1995.
[115] T.F. Rees, J. Contam. Hydrol., 1 (1987) 425.
[116] T.F. Rees, Water Resour. Res., 26 (1990) 2777.
[117] C. Degueldre, G. Longworth, V. Moulin, P. Vilks, C. Ross, G. Bidoglio, A. Cremers, J. Kim, J. Pieri, J. Ramsay, B. Salbu and U. Viorinen, Paul Scherrer Institut, PSI-Bericht Nr. 39, Würenlingen und Villigen, Switzerland, 1989.
[118] H. Bader, J. Geophys. Res., 75 (1970) 2822.
[119] A. Lerman, K.L. Carder and P.R. Betzer, Earth Planet. Sci. Lett., 37 (1977) 61.
[120] W. Stumm and J.J. Morgan, Aquatic Chemistry, 2nd edn., Wiley-Interscience, New York, 1981.
[121] I.N. McCave, Deep-Sea Res., 31 (1984) 329.
[122] J.R. Hunt, in M.C. Kavanaugh and J.O. Leckie (Eds.), Particulates in Water, Adv. Chem. Ser. 189, American Chemical Society, Washington, DC, 1980, p. 243.
[123] B.V. Derjaguin and L. Landau, Acta Physicochim. URSS, 14 (1941) 633.
[124] E.J.W. Verwey and J.Th.G. Overbeek, Theory of the Stability of Lyophobic Colloids, Elsevier, Amsterdam, 1948.
[125] E. Ruckenstein and D.C. Prieve, AIChE J., 22 (1976) 276.
[126] J.N. Israelachvili, Intermolecular and Surface Forces, 2nd edn., Academic Press, New York, 1992.
[127] J.Th.G. Overbeek, Adv. Colloid Interface Sci., 16 (1982) 17.
[128] N.H.G. Penners and L.K. Koopal, Colloids Surfaces, 28 (1987) 67.
[129] M. Elimelech and C.R. O'Melia, Langmuir, 6 (1990) 1153.
[130] R.J. Hunter, Zeta Potential in Colloid Science, Academic Press, New York, 1981.
[131] G.A. Parks, Chem. Rev., 65 (1965) 177.
[132] H. van Olphen, An Introduction to Clay Colloid Chemistry, 2nd. edn., John Wiley and Sons, New York, 1977.
[133] J.A. Davis and D.B. Kent, in M.F. Hochella, Jr. and A.F. White (Eds.), Mineral Water Interface Geochemistry, Mineral Society of America, Washington, DC, 1990, p. 177.
[134] D.A. Dzombak and F.M.M. Morel, Surface Complexation Modeling, Hydrous Ferric Oxide, John Wiley and Sons, New York, 1990.

[135] W.G. Eversole and W.W. Boardman, J. Chem. Phys., 9 (1941) 789.
[136] R.J. Hunter and A.E. Alexander, J. Colloid Sci., 18 (1963) 820.
[137] J.Th.G. Overbeek, in H.R. Kruyt (Ed.), Colloid Science, Vol. I, Elsevier, Amsterdam, 1952, p. 200.
[138] J.N. Israelachvili and G.E. Adams, J. Chem. Soc., Faraday Trans. I, 74 (1978) 975.
[139] R.M. Pashley and J.N. Israelachvili, J. Colloid Interface Sci., 101 (1984) 511.
[140] D.E. Yates, S. Levine and T.W. Healy, J. Chem. Soc., Faraday Trans. I, 70 (1974) 1807.
[141] J.A. Davis, R.O. James and J.O. Leckie, J. Colloid Interface Sci., 63 (1978) 480.
[142] D.E. Yates and T.W. Healy, J. Chem. Soc., Faraday Trans. I, 76 (1980) 9.
[143] H.J. van den Hul, J. Colloid Interface Sci., 92 (1983) 217.
[144] P.F. Low, Soil Sci. Soc. Am. J., 40 (1976) 500.
[145] H. Hühnerfuss, J. Colloid Interface Sci., 126 (1988) 384.
[146] M.A. Cohen Stuart and J.W. Mulder, Colloids Surfaces, 15 (1985) 49.
[147] J.N. Israelachvili, Adv. Colloid Interface Sci., 16 (1982) 31.
[148] J.N. Israelachvili and P.M. McGuiggan, Science, 241 (1988) 795.
[149] P.F. Luckham and B.A. de L. Costello, Adv. Colloid Interface Sci., 44 (1993) 183.
[150] E. Barouch, E. Matijević and T.H. Wright, Chem. Eng. Commun., 55 (1987) 29.
[151] R.M. Pashley, J. Colloid Interface Sci., 80 (1981) 153.
[152] V.E. Shubin and P. Kékicheff, J. Colloid Interface Sci., 155 (1993) 108.
[153] R.M. Pashley, J. Colloid Interface Sci., 102 (1984) 23.
[154] R.M. Pashley and J.N. Israelachvili, J. Colloid Interface Sci., 97 (1984) 446.
[155] D. Henderson and M. Lozada-Cassou, J. Colloid Interface Sci., 114 (1986) 180.
[156] J. Marra, J. Colloid Interface Sci., 107 (1985) 446.
[157] J. Marra, J. Colloid Interface Sci., 109 (1986) 11.
[158] J. Marra, J. Phys. Chem., 92 (1988) 6044.
[159] J.M. Berg, P.M. Claesson and R.D. Neuman, J. Colloid Interface Sci., 161 (1993) 182.
[160] G. Vigil, Z. Xu, S. Steinberg and J. Israelachvili, J. Colloid Interface Sci., 165 (1994) 367.
[161] W.A. Ducker and T.J. Senden, Langmuir, 8 (1992) 1831.
[162] H. Kihira and E. Matijević, Adv. Colloid Interface Sci., 42 (1992) 1.
[163] S.G. Flicker, J.L. Tipa and S.G. Bike, J. Colloid Interface Sci., 158 (1993) 317.
[164] Y.Q. Li, N.J. Tao, J. Pan, A.A. Garcia and S.M. Lindsay, Langmuir, 9 (1993) 637.
[165] G. Frens and J.Th.G. Overbeek, J. Colloid Interface Sci., 38 (1972) 376.
[166] J.E. Kolakowski and E. Matijević, J. Chem. Soc., Faraday Trans. I, 75 (1979) 65.
[167] R.J. Kuo and E. Matijević, J. Chem. Soc., Faraday Trans. I, 75 (1979) 2014.
[168] R.J. Kuo and E. Matijević, J. Colloid Interface Sci., 78 (1980) 407.
[169] D.L. Feke, N.D. Prabhu, J.A. Mann, Jr. and J.A. Mann, III, J. Phys. Chem., 88 (1984) 5735.
[170] D.D. Fitts, Ann. Rev. Phys. Chem., 17 (1966) 59.
[171] E. Ruckenstein and D.C. Prieve, J. Chem. Soc., Faraday Trans. II, 69 (1973) 1522.
[172] L.A. Spielman and S.K. Friedlander, J. Colloid Interface Sci., 46 (1974) 22.
[173] M. Elimelech, Water Res., 26 (1992) 1.
[174] H.C. Hamaker, Recl. Trav. Chem., 56 (1937) 3.
[175] B. Dahneke, J. Colloid Interface Sci., 50 (1975) 194.
[176] T.J. Murphy and J.L. Aguirre, J. Chem. Phys., 57 (1972) 2098.
[177] V.G. Levich, Physicochemical Hydrodynamics, Prentice-Hall, Englewood Cliffs, NJ, 1962.
[178] R.B. Bird, W.E. Stewart and E.N. Lightfoot, Transport Phenomena, Wiley, New York, 1960.
[179] P.C. Hiemenz, Principles of Colloid and Surface Chemistry, Marcel Dekker, New York, 1986.
[180] J. Visser, in E. Matijević (Ed.), Surface and Colloid Science, Wiley, New York, 1976, Chapter 8.
[181] J. Visser, J. Colloid Interface Sci., 34 (1970) 26.
[182] A.J. Goldman, R.G. Cox and H. Brenner, Chem. Eng. Sci., 22 (1967) 653.
[183] M.E. O'Neill, Chem. Eng. Sci., 23 (1968) 1293.
[184] P.G. Saffman, J. Fluid Mech., 22 (1965) 385.
[185] B. Dahneke, J. Colloid Interface Sci., 40 (1972) 1.
[186] J. Visser, J. Colloid Interface Sci., 55 (1976) 664.
[187] M.A. Hubbe, Colloids Surfaces, 12 (1984) 151.
[188] E.J. Clayfield and E.C. Lumb, Discuss. Faraday Soc., 42 (1966) 285.
[189] E. Barouch, E. Matijević, T.A. Ring and M.J. Finlan, J. Colloid Interface Sci., 70 (1979) 400.
[190] R. Hogg, T.W. Healy and D.W. Fuerstenau, Trans. Faraday Soc., 62 (1966) 1638.
[191] N. Kallay and E. Matijević, J. Colloid Interface Sci., 83 (1981) 289.
[192] J.D. Nelligan, N. Kallay and E. Matijević, J. Colloid Interface Sci., 89 (1982) 9.
[193] G. Thompson, N. Kallay and E. Matijević, Chem. Eng. Sci., 39 (1984) 1271.
[194] N. Kallay, M. Tomic, B. Biškup, I. Kunjašic and E. Matijević, Colloids Surfaces, 28 (1987b).
[195] S.F. Kia, H.S. Fogler and M.G. Reed, J. Colloid Interface Sci., 118 (1987) 158.
[196] C.M. Cerda, Colloids Surfaces, 27 (1987) 219.
[197] C.M. Cerda, Clays Clay Miner., 36 (1988) 491.
[198] R.N. Vaidya and H.S. Fogler, Colloids Surfaces, 50 (1990) 215.
[199] N. Kallay, B. Biškup, M. Tomic and E. Matijević, J. Colloid Interface Sci., 114 (1986) 357.
[200] P.R. Johnson and M. Elimelech, Langmuir, 11 (1995) 801.
[201] D. Liu, P.R. Johnson and M. Elimelech, Environ. Sci. Technol., in press.

[202] K.C. Khilar and H.S. Fogler, J. Colloid Interface Sci., 101 (1984) 214.
[203] P. Somasundaran, T.W. Healy and D.W. Fuerstenau, J. Phys. Chem., 68 (1964) 3562.
[204] L. Liang and J.J. Morgan, Aquatic Sci., 52 (1990) 32.
[205] E.J. Clayfield and A.L. Smith, Environ. Sci. Technol., 4 (1970) 413.
[206] H. Krupp, Adv. Colloid Interface Sci., 1 (1967) 111.
[207] H. Krupp, G. Walter, W. Kling and H. Lange, J. Colloid Interface Sci., 28 (1968) 170.
[208] M.A. Hubbe, Colloids Surfaces, 25 (1987) 311.
[209] M.A. Hubbe, Colloids Surfaces, 25 (1987) 325.
[210] J.Th.G. Overbeek, J. Colloid Interface Sci., 58 (1977) 408.
[211] R.H. Ottewill, J. Colloid Interface Sci., 58 (1977) 357.
[212] T.W. Healy, Pure Appl. Chem., 52 (1980) 1207.
[213] J. Lyklema, Pure Appl. Chem., 52 (1980) 1221.
[214] J. Kijlstra and H.P. van Leeuwen, J. Colloid Interface Sci., 160 (1993) 424.
[215] K. Gotoh, T. Inoue and M. Tagawa, Colloid Polymer Sci., 262 (1984) 982.
[216] K. Gotoh, M. Iriya, A. Mitsui and M. Tagawa, Colloid Polymer Sci., 261 (1983) 805.
[217] A. Amirtharajah and P. Raveendran, Colloids Surfaces A: Physicochem. Eng. Aspects, 73 (1993) 211.
[218] G.A. Truskey and T.L. Proulx, Biotechnol. Progr., 6 (1990) 513.
[219] G.A. Truskey and T.L. Proulx, Biomater., 14 (1993) 243.
[220] G.A. Truskey and J.S. Pirone, J. Biomed. Mater. Res., 24 (1990) 1333.
[221] B.H. Keswick and C.P. Gerba, Environ. Sci. Technol., 14 (1980) 1290.
[222] R.W. Harvey, in C.J. Hurst (Ed.), Modeling the Environmental Fate of Microorganisms, American Society for Microbiology, Washington, DC, 1991, p. 89.
[223] R.W. Harvey, Curr. Opinion Biotechnol., 4 (1993) 312.
[224] G. Bitton and R.W. Harvey, in R. Mitchell (Ed.), Environmental Microbiology, Wiley–Liss, New York, 1992, p. 103.
[225] H. Small, J. Colloid Interface Sci., 48 (1974) 147.
[226] C. Horvath and H.-J. Lin, J. Chromatogr., 126 (1976) 401.
[227] D.C. Prieve and P.M. Hoysan, J. Colloid Interface Sci., 76 (1978) 201.
[228] A.J. McHugh, Crit. Rev. Anal. Chem., 15 (1984) 63.
[229] H. Gvirtzman and S.M. Gorelick, Nature, 352 (1991) 793.
[230] R.W. Harvey, N.E. Kinner, A. Bunn, D. MacDonald and D.W. Metge, Appl. Environ. Microbiol., 61 (1995) 209.
[231] H.C. Folks and F.F. Riecken, Soil Sci. Soc. Am. Proc., 20 (1956) 575.
[232] J.C. Dijkerman, M.G. Cline and G.W. Olson, Soil Sci., 104 (1967) 7.
[233] W.J. Bond, Soil Sci. Soc. Am. J., 50 (1986) 265.
[234] Z. Adamczyk, T. Dabros, J. Czarnecki and T.G.M. van de Ven, Adv. Colloid Interface Sci., 19 (1983) 183.
[235] T.G.M. van de Ven, Colloidal Hydrodynamics, Academic Press, London, 1989.
[236] W.B. Russel, D.A. Saville and W.R. Schowalter, Colloidal Dispersions, Cambridge University Press, Cambridge, 1989.
[237] X. Jia and R.A. Williams, Chem. Eng. Commun., 91 (1990) 127.
[238] D. Gupta and M.H. Peters, J. Colloid Interface Sci., 104 (1985) 375.
[239] B.V. Ramaro and C. Tien, in R.P. Chabra and D. DeKey (Eds.), Transport Processes in Bubbles, Drops and Particles, Hemisphere, New York, 1991, p. 191.
[240] M.H. Peters and R. Ying, Chem. Eng. Commun., 108 (1991) 165.
[241] C. Tien, Granular Filtration of Aerosols and Hydrosols, Butterworth, Stoneham, MA, 1989.
[242] M. Elimelech, Sep. Technol., 4 (1994) 186.
[243] S.W. Swanton, Adv. Colloid Interface Sci., 54 (1995) 129.
[244] C. Tien and A.C. Payatakes, AIChE J., 25 (1979) 737.
[245] D.C. Prieve and E. Ruckenstein, AIChE J., 20 (1974) 1178.
[246] Z. Adamczyk, T. Dabros, J. Czarnecki and T.G.M. van de Ven, J. Colloid Interface Sci., 97 (1984) 91.
[247] L. Song and M. Elimelech, J. Chem. Soc., Faraday Trans., 89 (1993) 3443.
[248] M.V. Smoluchowski, Z. Phys. Chem., 92 (1917) 129.
[249] Z. Adamczyk, J. Colloid Interface Sci., 78 (1980) 559.
[250] Z. Adamczyk and T.G.M. van de Ven, J. Colloid Interface Sci., 80 (1981) 340.
[251] T. Dabros and T.G.M. van de Ven, Colloid Polym. Sci., 261 (1983) 694.
[252] K. Chari and R. Rajagopalan, J. Chem. Soc., Faraday Trans. 2, 81 (1985) 1345.
[253] J. Happel and H. Brenner, Low Reynolds Number Hydrodynamics, Prentice Hall, NJ, 1963.
[254] E. Ruckenstein, Chem. Eng. Sci., 19 (1964) 131.
[255] C.R. O'Melia, Environ. Sci. Technol., 14 (1980) 1052.
[256] J.E. Tobiason and C.R. O'Melia, J. Am. Water Works Assoc., 80 (1988) 54.
[257] C.R. O'Melia, Colloids Surfaces, 39 (1989) 255.
[258] M. Elimelech and C.M. O'Melia, Environ. Sci. Technol., 24 (1990) 1528.
[259] H.C. Brinkman, Appl. Sci. Res., A1 (1947) 27.
[260] J. Happel, AIChE J., 4 (1958) 197.
[261] S. Kuwabara, J. Phys. Soc. Jpn., 14 (1959) 527.
[262] L.A. Spielman and J.A. FitzPatrick, J. Colloid Interface Sci., 42 (1973) 607.
[263] J.E. Tobiason, Colloids Surfaces, 39 (1989) 53.
[264] M. Elimelech, J. Colloid Interface Sci., 146 (1991) 337.
[265] R.C. Bales, S. Li, K.M. Maguire, M.T. Yahya and C.P. Gerba, Water Resour. Res., 29 (1993) 957.
[266] G.M. Hornberger, A.L. Mills and J.S. Herman, Water Resour. Res., 28 (1992) 915.
[267] J.E. Saiers, G.M. Hornberger and L. Liang, Water Resour. Res., 30 (1994) 2499.
[268] A.C. Payatakes, R. Rajagapolan and C. Tien, J. Colloid Interface Sci., 49 (1974) 321.

[269] L. Song and M. Elimelech, J. Colloid Interface Sci., 153 (1992) 294.
[270] F.J. Onorato and C. Tien, Chem. Eng. Commun., 7 (1980) 363.
[271] J. Gregory and A.J. Wishart, Colloids Surfaces, 1 (1980) 313.
[272] J.S. Kim and R. Rajagopalan, Colloids Surfaces, 4 (1982) 17.
[273] Z. Wang, Ph.D. Dissertation, The Johns Hopkins University, Baltimore, MD, 1986.
[274] M. Shapiro, H. Brenner and D.C. Guell, J. Colloid Interface Sci., 136 (1990) 552.
[275] G.M. Litton and T.M. Olson, Environ. Sci. Technol., 27 (1993) 185.
[276] B. Dahneke, J. Colloid Interface Sci., 48 (1974) 520.
[277] D.C. Prieve and E. Ruckenstein, J. Colloid Interface Sci., 57 (1976) 547.
[278] R. Rajagopalan, C. Tien, R. Pfeffer and G. Tadros, AIChE J. Letter to the Editor, 28 (1982) 871.
[279] J.E. Tobiason, Ph.D. Dissertation, The Johns Hopkins University, Baltimore, MD, 1987.
[280] L.A. Spielman, Ann. Rev. Fluid Mech., 9 (1977) 297.
[281] M. Elimelech, J. Colloid Interface Sci., 164 (1994) 190.
[282] C.R. O'Melia, in W. Stumm (Ed.), Aquatic Surface Chemistry, Wiley-Interscience, New York, 1987.
[283] N. Kallay, J.D. Nelligan and E. Matijević, J. Chem. Soc., Faraday Trans. I, 79 (1983) 65.
[284] J.A. FitzPatrick and L.A. Spielman, J. Colloid Interface Sci., 43 (1973) 350.
[285] R. Vaidyanathan and C. Tien, Chem. Eng. Sci., 46 (1991) 967.
[286] Z. Adamczyk, B. Siwek, M. Zembala and P. Warszynski, J. Colloid Interface Sci., 130 (1989) 578.
[287] L. Song, P.R. Johnson and M. Elimelech, Environ. Sci. Technol., 28 (1994) 1164.
[288] R. Rajagopalan and R.Q. Chu, J. Colloid Interface Sci., 86 (1982) 299.
[289] D.C. Prieve and M.M. Lin, J. Colloid Interface Sci., 76 (1980) 32.
[290] X. Jia, R.A. Williams and M. Green, Chem. Eng. Commun., 91 (1990) 199.
[291] D.C. Prieve and E. Ruckenstein, J. Colloid Interface Sci., 73 (1980) 539.
[292] R.Y. Ofoli, Ph.D. Dissertation, Carnegie Mellon University, Pittsburgh, PA, 1994.
[293] R. Vaidyanathan, M.S. Thesis, Syracuse University, Syracuse, NY, 1986.
[294] M. Jaroniec and R. Madey, Physical Adsorption on Heterogeneous Solids, Elsevier, Amsterdam, 1988.
[295] T. Hiemstra, W.H. Van Riemsdijk and G.H. Bolt, J. Colloid Interface Sci., 133 (1989) 91.
[296] T. Hiemstra, J.C.M. De Wit and W.H. van Riemsdijk, J. Colloid Interface Sci., 133 (1989) 105.
[297] M. Hull and J.A. Kitchener, Trans. Faraday Soc., 65 (1969) 3093.
[298] B.D. Bowen and M. Epstein, J. Colloid Interface Sci., 72 (1979) 81.
[299] H. Kihira and E. Matijević, J. Chem. Soc., Faraday Trans., 88 (1992) 2379.
[300] H. Kihira and E. Matijević, Langmuir, 8 (1992) 2855.
[301] J. Czarnecki, Adv. Colloid Interface Sci., 24 (1986) 283.
[302] H. Reerink and J.Th.G. Overbeek, Discuss. Faraday Soc., 18 (1954) 74.
[303] S.Y. Shulepov and G. Frens, J. Colloid Interface Sci., 170 (1995) 44.
[304] J.K. Marshall and J.A. Kitchener, J. Colloid Interface Sci., 22 (1966) 342.
[305] S.S. Dukhin and J. Lyklema, Langmuir, 3 (1987) 94.
[306] H.P. van Leeuwen and J. Lyklema, Ber. Bunsenges. Phys. Chem., 91 (1987) 288.
[307] S.S. Dukhin and J. Lyklema, Faraday Discuss. Chem. Soc., 90 (1990) 261.
[308] S.Y. Shulepov, S.S. Dukhin and J. Lyklema, J. Colloid Interface Sci., 171 (1995) 340.
[309] A. Kotera, K. Furusawa and K. Kudo, Kolloid Z. Z. Polym., 240 (1970) 837.
[310] K. Takamura, H.L. Goldsmith and S.G. Mason, J. Colloid Interface Sci., 82 (1981) 175.
[311] P. Ludwig and G. Peschel, Progr. Colloid Polym. Sci., 77 (1988) 146.
[312] G.R. Wiese and T.W. Healy, Trans. Faraday Soc., 66 (1970) 490.
[313] R. Hogg and K.C. Yang, J. Colloid Interface Sci., 56 (1976) 573.
[314] A. Marmur, J. Colloid Interface Sci., 72 (1979) 41.
[315] M.W. Hahn, Ph.D. Dissertation, The Johns Hopkins University, Baltimore, MD, 1995.
[316] G.M. Litton and T.M. Olson, J. Colloid Interface Sci., 165 (1994) 522.
[317] R.M. Taylor, M. Raupach and C.J. Chartres, Clay Miner., 25 (1990) 375.
[318] R. Kretzschmar, W.P. Robarge and A. Amoozegar, Environ. Sci. Technol., 28 (1994) 1907.
[319] M. Schnitzer and S.U. Khan, Humic Substances in the Environment, Marcel Dekker, New York, 1972.
[320] W. Stumm, Colloids Surfaces A: Physicochem. Eng. Aspects, 73 (1993) 1.
[321] J.B. Peri, J. Phys. Chem., 69 (1965) 220.
[322] G.G. Armistead, A.J. Tyler, F.H. Hambleton, S.A. Mitchell and J.A. Hockey, J. Phys. Chem., 73 (1969) 3947.
[323] P. Jones and J.A. Hockey, Trans. Faraday Soc., 67 (1971) 2679.
[324] R.L. Prafitt, R.J. Atkinson and R.C.S. Smart, Soil Sci. Soc. Am. Proc., 39 (1975) 837.
[325] L.K. Koopal and S.S. Dukhin, Colloids Surfaces A: Physicochem. Eng. Aspects, 73 (1993) 201.
[326] J.L. Riccardo, M.A. Chade, V.D. Pereyra and G. Zgrablich, Langmuir, 8 (1992) 1518.
[327] W.J. Wnek, D. Gidaspow and D.T. Wasan, Chem. Eng. Sci., 30 (1975) 1035.
[328] J.L. Darby and D.F. Lawler, Environ. Sci. Technol., 24 (1990) 1069.

[329] V. Privman, H.L. Frisch, N. Ryde and E. Matijević, J. Chem. Soc., Faraday Trans., 87 (1991) 1371.
[330] N. Ryde, N. Kallay and E. Matijević, J. Chem. Soc., Faraday Trans., 87 (1991) 1377.
[331] L. Song and M. Elimelech, Colloids Surfaces A: Physicochem. Eng. Aspects, 73 (1993) 49.
[332] Z. Adamczyk, B. Siwek, M. Zembala and P. Belouschek, Adv. Colloid Interface Sci., 48 (1994) 151.
[333] N. Ryde and E. Matijević, J. Colloid Interface Sci., 169 (1995) 468.
[334] R. Kretzschmar, W.P. Robarge and A. Amoozegar, Water Resour. Res., 31 (1995) 435.
[335] C.R. O'Melia and W. Ali, Progr. Water Technol., 10 (1978) 167.
[336] C.E. Billings, Ph.D. Dissertation, California Institute of Technology, Pasadena, CA, 1966.
[337] C.N. Davies, Air Filtration, Academic Press, Orlando, FL, 1973.
[338] A.C. Payatakes and C. Tien, J. Aerosol Sci., 7 (1976) 85.
[339] C. Tien, C.S. Wang and D.T. Barot, Science, 196 (1977) 983.
[340] C.S. Wang, M. Beizaie and C. Tien, AIChE J., 23 (1977) 879.
[341] A.C. Payatakes, H.Y. Park and J. Petrie, Chem. Eng. Sci., 36 (1981) 1319.
[342] H.W. Chiang and C. Tien, AIChE J., 31 (1985) 1349.
[343] J.E. Tobiason and B. Vigneswaran, Water Res., 28 (1994) 335.
[344] M.A. Scholl, A.L. Mills, J.S. Herman and G.M. Hornberger, J. Contam. Hydrol., 6 (1990) 321.
[345] L. Song and M. Elimelech, J. Colloid Interface Sci., 167 (1994) 301.
[346] P.R. Johnson, Ph.D. Dissertation, University of California, Los Angeles, CA, 1995.
[347] J.P. Loveland, J.N. Ryan, G.L. Amy and R.W. Harvey, Colloids Surfaces A: Physicochem. Eng. Aspects, 107 (1996) 205–221.
[348] M.A. Scholl and R.W. Harvey, Environ. Sci. Technol., 26 (1992) 1410.
[349] D.G. Lewis, Adv. Chem. Ser. 73, American Chemical Society, Washington, DC, 1968, p. 337.
[350] E.A. Jenne, Adv. Chem. Ser. 73, American Chemical Society, Washington, DC, 1968, p. 337.
[351] J. Vuceta and J.J. Morgan, Environ. Sci. Technol., 12 (1978) 1302.
[352] D.E. Fontes, A.L. Mills, G.M. Hornberger and J.S. Herman, Appl. Environ. Microbiol., 57 (1991) 2473.
[353] A.L. Mills, J.S. Herman, G.M. Hornberger and T.H. DeJesus, Appl. Environ. Microbiol., 60 (1994) 3300.
[354] D. Liu, Ph.D. Dissertation, University of California, Los Angeles, CA, 1994.
[355] Z. Adamczyk, B. Siwek, L. Szyk and M. Zembala, Bull. Pol. Acad. Sci. (Chem.), 41 (1993) 41.
[356] T. Dabros and T.G.M. van de Ven, J. Colloid Interface Sci., 149 (1992) 493.
[357] M.Y. Corapcioglu and S. Jiang, Water Resour. Res., 29 (1993) 2215.
[358] A. Abdel-Salem and C.V. Chrysakopoulos, Adv. Water Resour., 17 (1994) 283.
[359] E.J. Bouwer and B.E. Rittmann, Environ. Sci. Technol., 26 (1992) 401.
[360] R. Lindqvist, J.S. Cho and C.G. Enfield, Water Resour. Res., 30 (1994) 3291.
[361] Y. Tan, J.T. Cannon, P. Baveye and M. Alexander, Water Resour. Res., 30 (1994) 3243.
[362] M.Y. Corapcioglu and A. Haridas, J. Hydrol., 72 (1984) 149.
[363] J. Bear, Dynamics of Fluids in Porous Media, Elsevier, Amsterdam, 1972.
[364] I. Langmuir, J. Am. Chem. Soc., 40 (1918) 1361.
[365] P. Schaaf and J. Talbot, Phys. Rev. Lett., 62 (1989) 175.
[366] B. Widom, J. Chem. Phys., 44 (1966) 3888.
[367] Z. Adamczyk, B. Siwek and M. Zembala, Colloids Surfaces, 62 (1992) 119.
[368] Y. Pomeau, J. Phys. A: Math. Gen., 13 (1980) L193.
[369] E.L. Hinrichsen, J. Feder and T. Jossang, J. Stat. Phys., 44 (1986) 793.